

AEDC-TR-79-57

C-2

OCT 12 1979
JAN 18 1980



IR Optical Properties of Thin H_2O , NH_3 , and CO_2 Cryofilms

J. A. Roux, B. E. Wood, and A. M. Smith
ARG, Inc.

September 1979

Final Report for Period October 1, 1977 – March 15, 1979

Approved for public release; distribution unlimited.

PROPERTY OF U.S. AIR FORCE
AEDC TECHNICAL LIBRARY

Property of U. S. Air Force
AEDC LIBRARY
F41500-77-C-0003

**ARNOLD ENGINEERING DEVELOPMENT CENTER
ARNOLD AIR FORCE STATION, TENNESSEE
AIR FORCE SYSTEMS COMMAND
UNITED STATES AIR FORCE**

NOTICES

When U. S. Government drawings, specifications, or other data are used for any purpose other than a definitely related Government procurement operation, the Government thereby incurs no responsibility nor any obligation whatsoever, and the fact that the Government may have formulated, furnished, or in any way supplied the said drawings, specifications, or other data, is not to be regarded by implication or otherwise, or in any manner licensing the holder or any other person or corporation, or conveying any rights or permission to manufacture, use, or sell any patented invention that may in any way be related thereto.

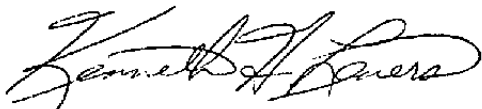
Qualified users may obtain copies of this report from the Defense Documentation Center.

References to named commercial products in this report are not to be considered in any sense as an indorsement of the product by the United States Air Force or the Government.

This report has been reviewed by the Information Office (OI) and is releasable to the National Technical Information Service (NTIS). At NTIS, it will be available to the general public, including foreign nations.

APPROVAL STATEMENT

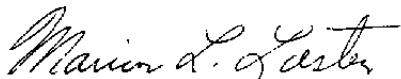
This report has been reviewed and approved.



KENNETH H. LENERS, Captain, USAF
Research Division
Directorate of Technology

Approved for publication:

FOR THE COMMANDER



MARION L. LASTER
Director of Technology
Deputy for Operations

UNCLASSIFIED

REPORT DOCUMENTATION PAGE		READ INSTRUCTIONS BEFORE COMPLETING FORM															
1. REPORT NUMBER AEDC-TR-79-57	2. GOVT ACCESSION NO.	3. RECIPIENT'S CATALOG NUMBER															
4. TITLE (and Subtitle) IR OPTICAL PROPERTIES OF THIN H₂O, NH₃, AND CO₂ CRYOFILMS	5. TYPE OF REPORT & PERIOD COVERED Final Report - October 1, 1977 - March 15, 1979																
	6. PERFORMING ORG. REPORT NUMBER																
7. AUTHOR(s) J. A. Roux, B. E. Wood, and A. M. Smith, ARO, Inc., a Sverdrup Corporation Company	8. CONTRACT OR GRANT NUMBER(s)																
9. PERFORMING ORGANIZATION NAME AND ADDRESS Arnold Engineering Development Center/DOTR Air Force Systems Command Arnold Air Force Station, Tennessee 37389	10. PROGRAM ELEMENT, PROJECT, TASK AREA & WORK UNIT NUMBERS Program Element 65807F																
11. CONTROLLING OFFICE NAME AND ADDRESS Arnold Engineering Development Center/DOS Air Force Systems Command Arnold Air Force Station, Tennessee 37389	12. REPORT DATE September 1979																
	13. NUMBER OF PAGES 108																
14. MONITORING AGENCY NAME & ADDRESS (if different from Controlling Office)	15. SECURITY CLASS. (of this report) UNCLASSIFIED																
	15a. DECLASSIFICATION/DOWNGRADING SCHEDULE N/A																
16. DISTRIBUTION STATEMENT (of this Report) Approved for public release; distribution unlimited.																	
17. DISTRIBUTION STATEMENT (of the abstract entered in Block 20, if different from Report)																	
18. SUPPLEMENTARY NOTES Available in DDC																	
19. KEY WORDS (Continue on reverse side if necessary and identify by block number) <table style="width: 100%; border: none;"> <tr> <td style="width: 33%;">optical properties</td> <td style="width: 33%;">germanium</td> <td style="width: 33%;">vapor pressure</td> </tr> <tr> <td>thin films</td> <td>substrates</td> <td>refractive index</td> </tr> <tr> <td>cryopumping</td> <td>Fourier spectrometers</td> <td></td> </tr> <tr> <td>infrared spectrometers</td> <td>Fourier transformation</td> <td></td> </tr> <tr> <td>infrared transmitters</td> <td>vapor deposition</td> <td></td> </tr> </table>			optical properties	germanium	vapor pressure	thin films	substrates	refractive index	cryopumping	Fourier spectrometers		infrared spectrometers	Fourier transformation		infrared transmitters	vapor deposition	
optical properties	germanium	vapor pressure															
thin films	substrates	refractive index															
cryopumping	Fourier spectrometers																
infrared spectrometers	Fourier transformation																
infrared transmitters	vapor deposition																
20. ABSTRACT (Continue on reverse side if necessary and identify by block number) <p>The infrared spectral transmittance of cryofilms formed by H₂O, NH₃, CO₂, and mixtures of these constituents in an N₂ matrix were measured. These 0.25- to 14-μm-thick films were cryopumped onto 20 and 77°K germanium substrates; the deposition pressure for the films deposited at 20°K and that for the 77°K films was approximately 2 x 10⁻⁶ torr. Transmission spectra were obtained for the 500- to 3,700-cm⁻¹ wave number range with a Fourier</p>																	

UNCLASSIFIED

UNCLASSIFIED

20. ABSTRACT (Continued)

transform spectrometer. Values of the complex index of refraction ($\bar{n} = n - ik$) for the H_2O , NH_3 , and CO_2 cryodeposits were derived from the experimental data using an analytical model and the nonlinear least-squares method. The analytical model treats the germanium as a thick noninterfering film and the deposit as a thin film. Results from the least-squares method are compared with a Kramers-Kronig determination of the real part of the index of refraction. The optical properties (n , k) of such cryofilms are essential for predicting the degradation of contaminated cryocooled optical surfaces.

PREFACE

The work reported herein was conducted by the Arnold Engineering Development Center (AEDC), Air Force Systems Command (AFSC). The results of this research were obtained by ARO, Inc., AEDC Division (a Sverdrup Corporation Company), operating contractor for the AEDC, AFSC, Arnold Air Force Station, Tennessee. The work was performed under ARO Project Numbers V32S-R1, V32K-13A, and P32K-13A. Dr. H. E. Scott was the Air Force project manager. The manuscript was submitted for publication on July 3, 1979.

CONTENTS

	<u>Page</u>
1.0 INTRODUCTION	7
2.0 INSTRUMENTATION	7
3.0 PROCEDURE	9
4.0 RESULTS	
4.1 NH ₃	11
4.2 CO ₂	13
4.3 H ₂ O	14
4.4 Mixtures Containing H ₂ O	14
5.0 OPTICAL PROPERTIES DETERMINATION	
5.1 NH ₃ Optical Constants	23
5.2 CO ₂ Optical Constants	24
5.3 H ₂ O Optical Constants	25
6.0 SUMMARY	25
REFERENCES	26

ILLUSTRATIONS

Figure

1. Schematic of the Infrared Optical Transmission Chamber (IROTIC) with Fourier Transform Spectrometer	29
2. Plan and Elevation Views of Cryogenically Cooled Window Holder	30
3. Gas Deposition System	31
4. Transmittance of 0.231- μ m-Thick Solid NH ₃ on 80°K Germanium	32
5. Transmittance of 1.38- μ m-Thick Solid NH ₃ on 80°K Germanium	32
6. Transmittance of 14.1- μ m-Thick Solid NH ₃ on 80°K Germanium	33
7. Transmittance of 0.238- μ m-Thick Solid NH ₃ on 20°K Germanium	33
8. Transmittance of 1.43- μ m-Thick Solid NH ₃ on 20°K Germanium	34
9. Transmittance of 4.97- μ m-Thick Solid NH ₃ /N ₂ Mixture (20 percent/80 percent) on 20°K Germanium	34
10. Transmittance of 4.97- μ m-Thick Solid NH ₃ /N ₂ Mixture (20 percent/80 percent) After Warmup from 20 to 59°K on Germanium	35
11. Transmittance of 0.231- μ m-Thick Solid CO ₂ on 80°K Germanium	35
12. Transmittance of 1.39- μ m-Thick Solid CO ₂ on 80°K Germanium	36
13. Transmittance of 12.7- μ m-Thick Solid CO ₂ on 80°K Germanium	36
14. Transmittance of 0.259- μ m-Thick Solid CO ₂ on 20°K Germanium	37

Figure	Page
15. Transmittance of 1.55- μm -Thick Solid CO_2 on 20°K Germanium	37
16. Transmittance of 3.88- μm -Thick Solid CO_2 on 20°K Germanium	38
17. Transmittance of 4.74- μm -Thick Solid CO_2/N_2 Mixture (20 percent/80 percent) on 20°K Germanium	38
18. Transmittance of 0.25- μm -Thick Solid H_2O on 80°K Germanium	39
19. Transmittance of 1.50- μm -Thick Solid H_2O On 80°K Germanium	39
20. Transmittance of 6.25- μm -Thick Solid H_2O on 80°K Germanium	40
21. Transmittance of 0.25- μm -Thick Solid H_2O on 50°K Germanium	40
22. Transmittance of 1.51- μm -Thick Solid H_2O on 50°K Germanium	41
23. Transmittance of 2.51- μm -Thick Solid H_2O on 50°K Germanium	41
24. Transmittance of 0.25- μm -Thick Solid H_2O on 20°K Germanium	42
25. Transmittance of 1.00- μm -Thick Solid H_2O on 20°K Germanium	42
26. Transmittance of 6.78- μm -Thick Solid $\text{N}_2/\text{H}_2\text{O}/\text{CO}_2$ Mixture (86 percent/13 percent/1 percent) on 20°K Germanium	43
27. Transmittance of 6.78- μm -Thick Solid $\text{N}_2/\text{H}_2\text{O}/\text{CO}_2$ Mixture (86 percent/13 percent/1 percent) after Warmup from 20 to 35°K on Germanium	43
28. Transmittance of 6.78- μm -Thick Solid $\text{N}_2/\text{H}_2\text{O}/\text{CO}_2$ Mixture (86 percent/13 percent/1 percent) After Warmup from 20 to 64°K on Germanium	44
29. Transmittance of 5.75- μm -Thick Solid $\text{Ar}/\text{H}_2\text{O}$ Mixture (93 percent/6 percent) on 20°K Germanium	44
30. Transmittance of 3.63- μm -Thick Solid $\text{CO}_2/\text{H}_2\text{O}$ Mixture (91 percent/9 percent) on 20°K Germanium	45
31. Transmittance of 3.63- μm -Thick Solid $\text{CO}_2/\text{H}_2\text{O}$ Mixture (91 percent/9 percent) After Warmup from 20 to 102°K on Germanium	45
32. Transmittance of 3.49- μm -Thick Solid $\text{H}_2\text{O}/\text{CO}_2/\text{N}_2$ Mixture (61 percent/36 percent/2 percent) on 20°K Germanium	46
33. Transmittance of 3.49- μm -Thick Solid $\text{H}_2\text{O}/\text{CO}_2/\text{N}_2$ Mixture (61 percent/36 percent/2 percent) After Warmup from 20 to 128°K on Germanium	46
34. Transmittance of 3.49- μm -Thick Solid $\text{H}_2\text{O}/\text{CO}_2/\text{N}_2$ Mixture (61 percent/36 percent/2 percent) After Warmup from 20 to 153°K on Germanium	47
35. Geometry Depicting Analytical Model for a Thin Film Formed on a Thick Film	47
36. Optical Properties of NH_3 Condensed on 80°K Germanium	48

<u>Figure</u>	<u>Page</u>
37. Optical Properties for NH ₃ Condensed on 20°K Germanium	49
38. Effect of Substrate Temperature on NH ₃ Optical Properties (20 and 80°K)	50
39. Comparison of Theory and Data for 80°K Solid NH ₃ for Three Different Wavenumbers	51
40. Comparison of Theory and Data for 20°K Solid NH ₃ for Three Different Wavenumbers	52
41. Comparison of Results at 80°K with Those of Ref. 14 at 190°K	53
42. Comparison of Results at 20°K with Those of Ref. 15 at 30°K	54
43. Comparison of Results at 80°K with Those of Ref. 1 at 80°K	55
44. Optical Properties of CO ₂ Condensed on 80°K Germanium	56
45. Optical Properties of CO ₂ Condensed on 20°K Germanium	57
46. Effect of Substrate Temperature on CO ₂ Optical Properties (20 and 80°K)	58
47. Comparison of Theory and Data for 80°K Solid CO ₂ for Three Different Wavenumbers	59
48. Comparison of Theory and Data for 20°K Solid CO ₂ for Three Different Wavenumbers	60
49. Optical Properties for H ₂ O Condensed on 80°K Germanium	61
50. Optical Properties for H ₂ O Condensed on 50°K Germanium	62
51. Optical Properties for H ₂ O Condensed on 20°K Germanium	63
52. Effect of Substrate Temperature on H ₂ O Optical Properties (20, 50, and 80°K)	64
53. Comparison of Theory and Data for 80°K Solid H ₂ O for Three Different Wavenumbers	65
54. Comparison of Theory and Data for 50°K Solid H ₂ O for Three Different Wavenumbers	66
55. Comparison of Theory and Data for 20°K Solid H ₂ O for Three Different Wavenumbers	67
56. Comparison of Results at 20°K with Those of Ref. 4 at 30°K	68
57. Comparison of Results at 80°K with Those of Ref. 9 at 100°K	69

TABLES

1. Molecular Bands in NH ₃ (cm ⁻¹)	70
2. Molecular Bands in CO ₂ (cm ⁻¹)	70
3. Molecular Bands in H ₂ O (cm ⁻¹)	70
4. Solid NH ₃ Optical Properties at 80°K	71
5. Solid NH ₃ Optical Properties at 20°K	79

<u>Table</u>	<u>Page</u>
6. Solid CO ₂ Optical Properties at 80°K	87
7. Solid CO ₂ Optical Properties at 20°K	92
8. Solid H ₂ O Optical Properties at 80°K	97
9. Solid H ₂ O Optical Properties at 50°K	101
10. Solid H ₂ O Optical Properties at 20°K	105

1.0 INTRODUCTION

The requirements for observation of infrared radiation sources at long distances have created severe design problems for infrared optical systems. These systems must often function at cryogenic temperatures; thus, contamination of optical surfaces by atmospheric and rocket exhaust plume gases is a serious problem. Upon contact with cold optical surfaces, these gases condense and degrade system performance through thin film interference and vibrational band absorption. Two of the most common exhaust products from bipropellant engines [monomethyl hydrazine (MMH)/nitrogen tetroxide (N_2O_4)] and atmospheric constituents are carbon dioxide (CO_2) and water (H_2O). Ammonia (NH_3) is also a common exhaust constituent from monopropellant [hydrazine (N_2H_4)] engines.

To better identify and account for the effects from possible contamination by MMH/ N_2O_4 and N_2H_4 engines, the infrared (IR) spectra of H_2O , CO_2 , NH_3 , and of mixtures of these constituents in a nitrogen (N_2) matrix were measured. The normal transmittance spectra were measured using 20 and 77°K germanium as a substrate material. Germanium is one of the most commonly employed substrates for cryocooled optical components because of its higher thermal conductivity as compared to that of pure dielectrics, the Irtrans, or polycrystals. Also, germanium has a flat transmittance rate of 47 percent between 2 and 10 μm .

Complete experimental details have been given elsewhere (see Ref. 1); thus, only a basic description of the chamber and apparatus is presented here. The absolute transmittances of thin solid films ranging in thickness up to 14 μm are presented. Finally, a theoretical model of window plus film transmission is derived and is subsequently used, along with the experimental results, to determine the complex refractive index ($\bar{n} = n - ik$) of each of the contaminants. The subtractive Kramers-Kronig method for calculation of the film refractive index has also been applied, and results are compared to those of the least-squares determination.

2.0 INSTRUMENTATION

Figure 1 gives a plan view schematic of the experimental apparatus showing the IR interferometer (Digilab Model FTS-14), the high vacuum chamber containing the cryocooled substrate, and the IR source location. The chamber is an all-stainless-steel cell equipped with a liquid-nitrogen (LN_2)-cooled liner. A water-vapor-free vacuum of 10^{-8} torr can be routinely obtained. The substrate holder can be actively cooled with either LN_2 (80°K) or gaseous helium (GHe) (20°K). The three platinum resistors located on the window holder yielded temperature measurements accurate to within 0.5°K.

The 4-mm-thick germanium window was mounted for cryocooling as shown by Fig. 2. To ensure that the germanium windows did not act as an optical stop in any manner, a stop was located in the "back-of-window" gas baffle. This stop was 1.50 in. in diameter; the clear aperture of the germanium was 2.0 in. in diameter.

The spectral resolution of the interferometer system could be selected between 16.0 and 0.5 cm^{-1} , but 4 cm^{-1} resolution was found sufficient for all work reported herein. The wavelength accuracy of the interferometer is near 0.02 cm^{-1} since the interferogram sampling interval is governed by an auxiliary helium-neon (He-Ne) laser interferometer. Transmittance data were recorded in the 500- to 3,700- cm^{-1} wavenumber range. Transmittance measurements were performed by rotating the germanium out of the beam and recording and storing a reference power spectrum. Generally, as many as 16 interferograms were co-added to improve the signal-to-noise ratio before execution of the Fourier transform. Next, the window was rotated into the beam and the process repeated. The reference file was then divided into the sample file and plotted by a digital incremental plotter, producing the final data record on a linear ordinate scale of 0- to 100-percent transmittance.

Controlled contamination of the cryocooled germanium window was accomplished with the gas induction system shown schematically in Fig. 3. A toroidal header with thirty-six 1/16-in.-diam orifices spaced 10 deg apart directed the gas toward the germanium window. The upstream pressure was determined by the vapor pressure of the liquid, and the gas flow rate was regulated by the variable leak valve. The chamber pressure rose from 1×10^{-8} to 2×10^{-7} or 2×10^{-6} torr, respectively, during deposition at 20 and 77°K, thus indicating good cryopumping by the liner and window. Gas was prevented from condensing on the back of the germanium window by a gas baffle positioned close to the back of the window holder. (This baffle also held the optical stop mentioned earlier.) The gas induction system, though quite simple, worked well: The deposition rate could be easily controlled, and the final thin-film thickness was uniform across the exposed 2-in.-diam window area. Film uniformity and absolute thickness are two important parameters since the objective of the experiment was to determine the complex refractive index of the thin film, a quantity derived by comparison of experimental transmittance data with theoretical model thickness data. Any error in absolute film thickness is directly introduced into the film complex refractive index results. A dual-angle laser interference technique (Ref. 2) was used for monitoring the film thickness and the film refractive index at $\lambda = 0.6328 \mu\text{m}$.

Basically, two He-Ne laser beams are specularly reflected off the germanium window for two different, accurately measured incidence angles. As the gas is condensed, two interference patterns of different periods are monitored in the reflected laser light. If the

ratio of pattern periods is termed β , then the refractive index of the film, n , is given by

$$n = \frac{(\sin^2 \theta_b - \beta^2 \sin^2 \theta_a)^{1/2}}{(1 - \beta^2)^{1/2}} \quad (1)$$

where θ_a and θ_b (typically 18 and 68 deg) are the two laser beam incidence angles. Once n has been established, the thickness of the film, d_1 , is readily calculated from $m_a \lambda = 2nd_1 [1 - (\sin^2 \theta_a / n^2)]^{1/2}$, where m_a is the order of the interference maxima for incidence angle θ_a . The dual-angle laser beam thickness monitor yielded thin-film refractive index values accurate to within two percent. A quartz crystal microbalance (QCM) was used in conjunction with the dual-angle laser beam interference technique to determine the density of each contaminant. The QCM was adjacent to and just above the germanium window (Fig. 3) so that the mass deposition rate would equal that of the germanium window. The surface density (in gm/cm²) was determined from the QCM, and the film thickness determined from the interference patterns. From these two values the film density was calculated. The QCM operates on the principle that the crystal vibration frequency changes linearly with changes in the mass deposited on the crystal.

3.0 PROCEDURE

The chamber was initially pumped down to approximately 1.0×10^{-7} torr using the diffusion pump and the LN₂ liner. Chamber pressures in the low 10^{-8} torr range were obtained when the germanium substrate, holder, and transfer lines were cooled to approximately 20°K with the cryostat (2-kw capacity).

Samples of research grade CO₂ and NH₃ were obtained from lecture bottles to be introduced into the chamber. A special gas addition system was used to introduce water vapor into the chamber to be cryopumped. Before the water vapor was introduced, the distilled water was boiled under vacuum while being pumped with a mechanical pump to remove gases absorbed in the water. The gas mixtures were made based on partial pressures and were checked for mole fractions by the Arnold Engineering Development Center (AEDC) Chemical Laboratory.

Deposition of the gas on the cold germanium window was monitored using the two He-Ne laser beams with the two-angle interference technique. Transmittance measurements were made upon reaching the interference maxima, at which points the gas flow was shut off. Upon completion of the transmittance measurements, the gas flow was again started, and deposition occurred until a film thickness corresponding to the next interference

maxima was reached, and so on. In some instances in which very strong absorption bands were observed, transmittance measurements were made for each interference minimum and maximum. This was done since accurate determination of n 's and k 's required as many thicknesses as possible.

After completion of a series of transmittance measurements for all the thicknesses, the cryogenic flow rate to the germanium substrate was turned off, and the substrate and deposited film were allowed to warm up. Transmittance measurements were made at intervals during warmup. Two to three minutes were required for the interferometer to scan the sample (a total of 16 scans); a similar time was required for the reference beam scans. With the additional time required for obtaining the Fourier transform and for the plotting of the data, this resulted in 10-min intervals between measurements. Note that the temperature given on each warmup data plot is the temperature at the end of the sample interferometer scan.

The objective was to obtain transmittance measurements for as many thicknesses as possible during an experiment on each gas. The number of thicknesses obtained depended considerably on the particular gas. For "well-behaved" deposits, 16 to 25 thicknesses (interference maxima or minima) were obtained, whereas in some cases only a few thickness measurements could be made. The "fracture" or "shattering" effect was the main problem. For both H_2O and NH_3 , only a very small thickness could be formed at $20^\circ K$ before the entire deposit fractured or shattered; at this point the film became highly scattering. At $77^\circ K$ an H_2O deposit $30\ \mu m$ thick was formed; this deposit was so clear that it could not be detected with the naked eye. However, because of the shattering effect, at $20^\circ K$ a $3\text{-}\mu m$ thickness could be seen easily.

4.0 RESULTS

Transmittance measurements were made of thin films of gases condensed on the cryogenically cooled germanium window. These measurements were multiples of the thickness determined from the film interference equation for maxima:

$$r = \frac{m\lambda}{2n \sqrt{1 - \frac{\sin^2 \theta}{n^2}}} \quad (2)$$

where $m = 1, 2, 3 \dots$ and θ is the incidence angle measured from the normal.

The first thickness (or interference maxima) is given by

$$\tau = \lambda/2n \left(1 - \frac{\sin^2 \theta}{n^2} \right)^{1/2} \quad (3)$$

for $m = 1$, and other thicknesses are given by

$$\tau = (2) \lambda/2n \left(1 - \frac{\sin^2 \theta}{n^2} \right)^{-1/2} \quad (4)$$

for $m = 2$, and

$$\tau = (3) \lambda/2n \left(1 - \frac{\sin^2 \theta}{n^2} \right)^{-3/2} \quad (5)$$

for $m = 3$, and so forth, with the differential between successive maxima equivalent to that given by Eq. (3).

In each case, the refractive index, n , had to be measured before a thickness could be calculated. This measurement of n has been described previously (Ref. 3); it involves using Eq. (2) for two different incidence angles — approximately 18 and 68 deg in this study. In this study, thickness is based on interference maxima for 18-deg incidence.)

4.1 NH₃

Thin films of NH₃ gas were deposited on the germanium window cooled to 80 and 20°K. The refractive indices at these two temperatures (for $\lambda = 0.6328 \mu\text{m}$) were 1.41 and 1.37, respectively. These refractive indices correspond to thickness increments of $0.231 \mu\text{m}$ for interference maxima for 80°K and $0.238 \mu\text{m}$ for 20°K. The densities were 0.87 gm/cm^3 at 77°K and 0.76 gm/cm^3 at 20°K. The spectra obtained for NH₃ condensed at these temperatures are shown in Figs. 4 through 6 and Figs. 7 and 8, respectively. Figures 4 and 5 are for the first and sixth interference maxima. The absorption band locations and assignments are given in Table 1, which shows comparisons with other investigations. By comparing 80°K NH₃ (Fig. 5) with 20°K NH₃ (Fig. 8) for approximately the same thickness, it can be seen that the major difference lies in broadening of the bands in Fig. 8. This has been pointed out earlier in Refs. 1 and 4. The complicated structure between $1,340 \text{ cm}^{-1}$ and $1,700 \text{ cm}^{-1}$ and centered at $1,650 \text{ cm}^{-1}$ for the 77°K is seen as only one distinct band (ν_4) located at $1,625 \text{ cm}^{-1}$ for 20°K (Fig. 8). The band located at $3,300 \text{ cm}^{-1}$ for 77°K is much less significant for 20°K and must be assigned to be the $2\nu_4$ band. However, a band observed at $3,220 \text{ cm}^{-1}$ for 20°K is noticeably weaker at 80°K. This band is believed to be primarily due to the ν_1 vibration, with a possible contribution by the $2\nu_4$ band as suggested by Wolff et al.

(Ref. 5). The bands observed at $3,385\text{ cm}^{-1}$ for 77°K films and at $3,380\text{ cm}^{-1}$ for 20°K are assigned to the ν_3 vibration band. For 77°K (Fig. 6) the ν_4 band is located at $1,650\text{ cm}^{-1}$, and the band located at $3,300\text{ cm}^{-1}$ is, therefore, assumed to be the $2\nu_4$ band. At 20°K , however, the band is located at $1,625\text{ cm}^{-1}$, but no band is observed at $3,250\text{ cm}^{-1}$, which would correspond to the $2\nu_4$ band. The only other band in the vicinity is that at $3,215\text{ cm}^{-1}$ which, although relatively weak, was observed for 77°K (see Figs. 5 and 6). The lattice band at 525 cm^{-1} in Fig. 8 for 20°K was also observed at 77°K (Figs. 5 and 6). This band was not observed at 20°K in either Ref. 1 or Ref. 4; this disappearance was explained by the fact that amorphous NH_3 — which would not have a lattice band — was formed at 20°K . The descriptions in Refs. 1 and 4 of the physical appearance of the films during deposition correspond to our observations: The films formed at 20°K were more scattering (or had a milkier appearance) than the clear films observed at 77°K . This result (Refs. 1 and 4) is inconsistent with what is normally observed for H_2O : clear-glassy deposits that are amorphous and crystalline deposits that are more scattered. It appears that, for the present measurements, showing the band at 525 cm^{-1} would indicate at least a small amount of crystallinity in the condensed films. Deposition of NH_3 at 20°K was more difficult than at 77°K as far as getting a good clear deposit is concerned. Shattering or fracture often occurred; at such times, the thin-film interference technique for measuring thickness was inapplicable. The band at $1,890\text{ cm}^{-1}$ observed in Figs. 4 through 6 for 77°K NH_3 is believed to be due to the combination band $\nu_4 + \nu_5$ where ν_5 is a torsional mode (Ref. 6). The band at $1,890\text{ cm}^{-1}$ was not observed for the 20°K films.

A mixture of 20-percent NH_3 and 80-percent N_2 was prepared and deposited as a thin film as was done previously. Figure 9 shows the transmittance of a film $4.97\text{ }\mu\text{m}$ thick whose refractive index was measured and found to be 1.25 at $\lambda = 0.6328\text{ }\mu\text{m}$. Since the film is predominantly N_2 with NH_3 included in the matrix, only weak absorption is observed. The channel spectra are evident. The lattice band at 530 cm^{-1} is not observed for this thickness, and the ν_2 band, previously observed as the $1,060\text{--}1,070\text{ cm}^{-1}$ band, is unlike the spectra observed previously at 80 or 20°K . The ν_2 band for the mixture occurs at approximately $1,030\text{ cm}^{-1}$ with two weaker bands on the low wavenumber side occurring at 975 and 985 cm^{-1} with the broader irregular ν_1 band observed from $3,300$ to $3,540\text{ cm}^{-1}$. A very sharp and In the higher wavenumber absorption region ($3,200$ to $3,400\text{ cm}^{-1}$), four distinct bands are observed at $3,210$, $3,240$, $3,305$, and $3,380\text{ cm}^{-1}$, all of the same general order of magnitude in strength. Note again that the ν_4 band at $1,620\text{ cm}^{-1}$ correlates with the $2\nu_4$ band at $3,240\text{ cm}^{-1}$. The ν_3 band is still located at $3,380\text{ cm}^{-1}$. The ν_1 band, observed at $3,215\text{ cm}^{-1}$ in the NH_3/N_2 mixture (Fig. 9) and at $3,220\text{ cm}^{-1}$ for NH_3 at 20°K (Fig. 8), is more intense than those for the films condensed at 77°K (Figs. 5 and 6).

After warmup to 59°K , the film transmittance (Fig. 10) changed considerably. Presumably, most of the N_2 had already sublimated, leaving only the NH_3 behind. None of

the channel spectra remained. The absorption bands, though still weak, are seen at 1,060, 1,630, and 3,380 cm^{-1} .

4.2 CO_2

Thin films of CO_2 were condensed on both 77 and 20°K germanium substrates and were also studied. The refractive indices at $\lambda = 0.6328 \mu\text{m}$ were found to be 1.41 at 77°K and 1.28 at 20°K. The CO_2 refractive index showed the greatest change with temperature of all the gases condensable at both 77 and 20°K that were studied. For an incidence angle of approximately 19 deg, this yields a film thickness of 0.231 μm between interference maxima at 77°K and a thickness of 0.259 μm between maxima for films at 20°K. The densities of the films at 77 and 20°K were measured using the film thickness and the surface density from the QCM; values of 1.67 and 1.08 gm/cm^3 were obtained, respectively, for the 77°K and 20°K films.

Transmittance spectra of 77°K films are shown in Figs. 11 through 13 for film thicknesses of 0.231, 1.39, and 12.7 μm , which correspond to the 1st, the 6th, and the 55th interference maxima. The identification of the bands is shown in Table 2, which compares the results of the present experiments with those of Refs. 1 and 4. In addition to the bands listed in Table 2, very weak bands can be seen at 760, 2,045, 2,415, and 2,425 cm^{-1} (Fig. 13) for the largest deposit thickness. The bands at 755, 2,270, 2,320, and 3,635 cm^{-1} are unidentified. The $\nu_1 + \nu_3$ band, not shown in Figs. 11 through 13, was observed at 3,710 cm^{-1} in the mixture data.

Transmittance spectra of CO_2 films deposited on 20°K germanium are shown in Figs. 14, 15, and 16 for film thicknesses of 0.259, 1.55, and 3.88 μm (the 1st, 6th, and 15th laser interference maxima for $\lambda = 0.6328 \mu\text{m}$). The spectral band locations agree with the values observed for the 77°K spectra. The bands at 20°K are somewhat broader than those observed at 77°K. This is most easily seen by comparing corresponding absorption bands in Figs. 11 and 14. The band at 2,340 cm^{-1} seems to be much sharper at 77°K than that at 20°K, as can be seen by comparing Figs. 13 and 16, even though Fig. 13 is for a considerably thicker film.

A CO_2/N_2 mixture (25-percent CO_2 /75-percent N_2) was deposited at 20°K; the spectra obtained are shown in Fig. 17 for a film thickness of 4.74 μm (18th interference maxima) and for a refractive index of 1.25 at $\lambda = 0.6328 \mu\text{m}$. In contrast to other gases contained within an N_2 matrix, the location and shape of the spectral absorption line was essentially unchanged from that in the pure state. Mixtures of CO_2 with H_2O will be discussed later.

4.3 H₂O

H₂O films were condensed on the cryogenically cooled germanium substrate at temperatures of 80, 50, and 20°K. The spectra for 80°K are shown in Figs. 18 through 20 for the 1st, 6th, and 25th interference maxima, which correspond to film thicknesses of 0.25, 1.50, and 6.25 μm , where $n = 1.32$ at $\lambda = 0.6328 \mu\text{m}$. Films deposited at 50°K for thicknesses of 0.25, 1.51, and 2.51 μm are shown in Figs. 21 through 23. Figures 24 and 25 show data for films 0.25 and 1.00 μm thick formed at 20°K. Essentially no differences were observed for the refractive index of H₂O at $\lambda = 0.6328 \mu\text{m}$ for these three temperatures.

Four absorption bands or regions were seen for H₂O; they all were quite broad in contrast to those of the gases previously studied. These bands are summarized in Table 3. Observing these bands in Figs. 18 through 20 makes it obvious that the band locations are too broad to be designated by a number as given in the above table. Therefore, the numbers refer to the approximate centers of the broad bands. The ν_1 band at 3,260 to 3,300 cm^{-1} is observed to be deeper at the higher temperature. For a thickness of 0.25 μm (first interference maxima) the transmission varies for the ν_1 band from 30 percent at 80°K, to 32 percent at 50°K, and finally to 34 percent at 20°K. Thus, the depth of the absorption band increases with increasing temperature. For a film thickness of 1.50 μm , the transmission is reduced to zero for the ν_1 band. It also appears that the location of the band shifts to higher wavenumbers with *decreasing* temperature. (The central location for the 77°K film was 3,255 cm^{-1} , whereas it was 3,300 cm^{-1} for 20°K.) This trend agrees with warmup data for H₂O films studied in Ref. 4. The libration band, ν_L , observed in the solid at 825 cm^{-1} at 77°K, was observed at 800 cm^{-1} for the 20°K films, a shift toward the opposite direction from the ν_1 band. The ν_2 band at 1,665 cm^{-1} was independent of temperature, whereas the 2,245 cm^{-1} band at 77°K shifted to 2,220 cm^{-1} at 20°K, illustrating the same trend observed for the libration band. The spectral location of this latter band agrees with Ref. 9 but is shifted at least 30 cm^{-1} from the 2,190 cm^{-1} value observed by Ref. 4. The band at 2,220 cm^{-1} has been assigned as a combination of the ν_2 and librational band ($\nu_2 + \nu_L$) by Ockman (Ref. 10); this band is expected to be temperature dependent as is the ν_L band.

4.4 MIXTURES CONTAINING H₂O

The following mixtures containing H₂O condensed at 20°K were analyzed: (1) 86-percent N₂/13-percent H₂O/1-percent CO₂ - ($n = 1.24$); (2) 93-percent Ar/6 percent H₂O - ($n = 1.25$); (3) 91-percent CO₂/9-percent H₂O - ($n = 1.26$); and (4) 36-percent CO₂/61-percent H₂O/2-percent N₂ - ($n = 1.31$). The films were much more transparent than were the pure gases condensed at 20°K. As seen above, most of the mixtures had refractive indices (at $\lambda = 0.6328 \mu\text{m}$) between 1.24 and 1.26.

4.4.1 86-percent N_2 /13-percent H_2O /1-percent CO_2

The transmission spectrum observed for a 26 interference maxima thick ($\tau = 6.78 \mu m$) film is shown in Fig. 26. There are some distinct differences between the spectra for H_2O in a mixture and the pure H_2O spectra. For example, the ν_1 band observed previously at $1,665 \text{ cm}^{-1}$ is split into two bands at $1,610$ and $1,635 \text{ cm}^{-1}$. The librational band ν_L previously observed at 800 to 825 cm^{-1} is missing as is the combination ν_2 librational band at approximately $2,245 \text{ cm}^{-1}$. The region between $3,200$ and $3,700 \text{ cm}^{-1}$ differed substantially from those of the other mixtures containing H_2O . A well-defined band is observed at $3,230 \text{ cm}^{-1}$ with the broader irregular ν_1 band observed from $3,300$ to $3,540 \text{ cm}^{-1}$. A very sharp and strong band observed at $3,695 \text{ cm}^{-1}$ is believed to be the ν_3 fundamental band that was not observed in pure H_2O . Figures 27 and 28 show the same deposit as Fig. 26 but after warmup to 35 and $64^\circ K$, respectively. Notice in Fig. 27 that the ν_2 band has changed with the strongest band still at $1,635 \text{ cm}^{-1}$ but a lobe is now on the wavenumber high side, occurring at about $1,660 \text{ cm}^{-1}$. The well-defined bands near $3,300 \text{ cm}^{-1}$ have now essentially merged into a single broad band, but the sharp ν_3 band previously observed at $3,695 \text{ cm}^{-1}$ is now located at $3,675 \text{ cm}^{-1}$, a shift of about 20 cm^{-1} to the lower wavenumbers. At this temperature ($35^\circ K$), the film still exhibits channel spectra (interference).

Figure 28, for a warmup to $64^\circ K$, shows further changes. Now the film does not exhibit channel spectra, and the ν_2 band is quite broad and centered at $1,650 \text{ cm}^{-1}$. The CO_2 band at $2,345 \text{ cm}^{-1}$ shows appreciable change in the absorption band shape with the shape in Fig. 28 closely resembling the anomalous dispersion in the refractive index versus wavenumber curve. The behavior also agrees with the expected trend in transmission as a strong absorption band is approached. The peak in transmission at $2,350 \text{ cm}^{-1}$ is the result of the refractive index approaching zero as the center of the absorption band is approached from the wavenumber high end. Notice also in Fig. 28 that the H_2O ν_3 band that was previously observed at about $3,690 \text{ cm}^{-1}$ is completely gone, but the libration band in the vicinity of 780 cm^{-1} is beginning to appear.

4.4.2 93-percent Ar/6-percent H_2O /Trace of CO_2 (< 0.05 percent)

Figure 29 shows a spectral transmission curve similar to that previously presented but for H_2O condensed within an argon matrix at $20^\circ K$. The film is $5.75 \mu m$ thick and has a refractive index of 1.26 . The ν_2 band is again split with absorption peaks at $1,595$ and $1,625 \text{ cm}^{-1}$ both shifted by about 10 cm^{-1} from that observed in the N_2 matrix. The band located at $3,230 \text{ cm}^{-1}$ in N_2 is split into two weaker bands at $3,200$ and $3,220 \text{ cm}^{-1}$ in argon. The broad, irregular ν_1 band extends on out to about $3,600 \text{ cm}^{-1}$. The ν_3 band is observed at $3,700 \text{ cm}^{-1}$. Beyond $3,700 \text{ cm}^{-1}$, the data are meaningless in this spectrum as the interferometer noise was

considerably greater than usual for this series of measurements. Upon warmup to 60°K, the spectrum was essentially the same as that seen in Fig. 28 in which the absorption bands in the vicinity of 3,300 cm^{-1} all merged into a single strong and broad absorption centered at 3,240 cm^{-1} .

4.4.3 91-percent CO_2 /9-percent H_2O Mixture

Figure 30 presents the transmission of a 3.63- μm -thick film of $\text{CO}_2/\text{H}_2\text{O}$ mixture with $n = 1.26$ at 20°K. The ν_2 band is observed at 1,615 and 1,635 cm^{-1} , essentially the same as the ν_2 band observed for H_2O in the N_2 matrix. The ν_3 band of H_2O is not observed, but a band was detected at 3,715 cm^{-1} (this is not shown in the figure because of the noise buildup), which is some 15 to 20 cm^{-1} higher than that observed in the other mixtures. The band at 3,600 cm^{-1} is the $2\nu_2 + \nu_3$ CO_2 band. Figure 31 shows the same film after warmup to 102°K. As can be seen, much of the CO_2 has already sublimated. Again there is a slight depression in the transmission curve around 1,640 cm^{-1} (the H_2O , ν_2 band), and the broad ν_1 band is centered at 3,260 cm^{-1} . The CO_2 band at 2,345 cm^{-1} is much less intense than previously since much of the CO_2 has left the surface. Measurements made at intermediate temperatures were not shown due to their similarity to Fig. 30.

4.4.4 61-percent H_2O /36-percent CO_2 /2-percent N_2

Whereas the previously discussed mixture was predominantly CO_2 , this mixture contains more H_2O than CO_2 . Figure 32 shows the transmission of the germanium at 20°K with a 3.49- μm -thick film condensed on it. The refractive index of this film at $\lambda = 0.6328 \mu\text{m}$ was found to be 1.31. This is significantly higher than the value obtained for the film that was predominantly CO_2 . At 20°K it was observed that the refractive index of CO_2 (1.28) was less than that for H_2O (1.31), whereas CO_2 had the higher refractive index for films condensed at 77°K. In Fig. 32 there is only a single band at 1,660 cm^{-1} instead of two observed previously in the other mixtures (Fig. 30). Again the ν_1 band is broad and strong, but it is now centered at 3,340 cm^{-1} , which is a shift from the center previously seen. Again there are two sharp bands located at 3,660 and 3,700 cm^{-1} . The relative strengths of these two bands have varied considerably in these mixtures. The CO_2 band locations at 660, 2,345, and 3,600 cm^{-1} have not shown any variation.

Warmup transmission spectra are presented in Figs. 33 and 34. Figure 33 shows that, after warmup to 128°K, the H_2O band centered at 830 cm^{-1} is much more pronounced than it was in the previous figure, but, in contrast, the ν_2 band at 1,660 cm^{-1} is less pronounced. The strong ν_1 band previously centered at 3,340 cm^{-1} is now deeper and broader, and the center of the band has shifted to approximately 3,240 cm^{-1} — a shift of 100 cm^{-1} . The two bands

previously seen at 3,660 and at 3,700 cm^{-1} are barely distinguishable from the noise. At 128°K some of the CO_2 has already evaporated as the CO_2 bands are not nearly as strong as they were previously. CO_2 normally sublimates at about 100°K (at 10^{-6} torr), but, in this case, it is trapped by the H_2O matrix. Even at a temperature of 153°K (Fig. 34) there is still some CO_2 left as shown by the presence of the CO_2 bands at 660 and 2,340 cm^{-1} . The ν_3 band normally observed at 2,345 cm^{-1} splits into two bands — at 2,340 and 2,355 cm^{-1} — the only time this was observed. The behavior of the water absorption bands observed in Fig. 31 is similar to that in Fig. 33 with the Fig. 33 band at 840 cm^{-1} being deeper and its ν_2 band at 1,640 cm^{-1} being broader than those of Fig. 31, and its bands at 3,660 and 3,700 cm^{-1} disappearing completely. The Fig. 33 band around 3,300 cm^{-1} becomes even broader, and the center shifts perhaps even more to the lower wavenumbers.

5.0 OPTICAL PROPERTIES DETERMINATION

To account for the influence of these constituents as contaminants it is necessary to know the solid-condensed-phase optical properties. These properties are necessary to compute the reflectance change of a surface or of the transmittance change of an optical component. Incorporating the effects of these properties can help correct for or predict the anticipated effects of condensed constituents on an actual surface. The optical properties desired are the refractive index, n , and the absorption index, k .

In order to determine the complex refractive index ($\tilde{n} = n - ik$) of the thin solid film from the transmittance versus thickness data for wavenumbers between 700 to 3,700 cm^{-1} , an analytical model of film plus substrate transmission was developed (Refs. 11 and 12). It was assumed that the germanium window acted as a thick film and that, thus, there was no phase coherence between multiple internal reflected rays. Moreover, the real part of the germanium complex index, n_g , is known and given by Ref. 13:

$$n_g = A + BL + CL^2 + D\lambda^2 + E\lambda^4 \quad (6)$$

where

$$L = (\lambda^2 - 0.028)^{-1}$$

$$A = 3.99931,$$

$$B = 0.391707,$$

$$C = 0.163492,$$

$$D = 0.000006, \text{ and}$$

$$E = 0.000000053.$$

The geometry describing the transmittance is shown in Fig. 35. For convenience the different layers have been subscripted 0, 1, 2, and 3; subscripts 0 and 3 are vacuum, and 1 and 2 are, respectively, the thin condensed film and the thick germanium substrate. The model used to fit the experimental results is for normal incidence only. As shown in Fig. 35, E_0^+ is the amplitude of the incident radiation, which undergoes an infinite number of multiple reflections after passing into the thin film. Following multiple reflections, the total amplitude of reflected and transmitted radiation is given by B1 and E_2^+ , respectively. E_2^+ reflects internally from the back of the germanium window, becomes A1, C1, and again undergoes thin-film multiple reflection in medium 1. This results in the rays B2 and A2, and so on. Analytically, the relationships between the amplitudes of the various waves are the following:

$$\begin{aligned}
 E_2^+ &= t_{012} E_0^+ \\
 A2 &= A1 r_{210} \\
 A4 &= A3 r_{210} \\
 A6 &= A5 r_{210}
 \end{aligned} \tag{7}$$

with

$$\begin{aligned}
 A1 &= E_2^+ r_2 \\
 A3 &= A2 r_2 \\
 A5 &= A4 r_2
 \end{aligned} \tag{8}$$

with

$$\begin{aligned}
 C1 &= t_2 E_2^+ \\
 C2 &= t_2 A2 \\
 C3 &= t_2 A4
 \end{aligned} \tag{9}$$

and with

$$\begin{aligned}
 B1 &= r_{012} E_0^+ \\
 B2 &= A1 t_{210} \\
 B3 &= A3 t_{210} \\
 B4 &= A5 t_{210}
 \end{aligned} \tag{10}$$

where t_2 designates the amplitude transmittance of light traveling from medium 2 to medium 3, r_2 designates the amplitude reflection of light incident upon medium 3 from medium 2, r_{012} designates the amplitude reflection of light that is incident from medium 0 and is reflected back into medium 0 after undergoing thin-film interference in medium 1, r_{210} designates the amplitude reflection of light that is incident from medium 2 and is reflected back into medium 2 after undergoing thin-film interference in medium 1, t_{012} designates the amplitude transmittance of light incident from medium 0 and transmitted into medium 0 after undergoing thin-film interference in medium 1, and t_{210} designates the amplitude transmittance of light incident from medium 2 and transmitted into medium 0 after undergoing thin-film interference in medium 1.

The power transmitted through the thin-film/thick-film combination is given by

$$\xi = n_3 |C1|^2 + n_3 |C2|^2 + n_3 |C3|^2 + \dots \quad (11)$$

where $n_3 = n_0$ since medium 3 and medium 0 are both considered as vacuum and with the constant $c/4\pi$ (c = the speed of light in vacuum) omitted for convenience since this constant will be lost in the division process for determining the overall transmittance.

Substituting Eq. (9) into Eq. (11) yields the transmitted power as

$$\xi = n_0 |t_2|^2 \left(|E_2^+|^2 + |A2|^2 + |A4|^2 + |A6|^2 + \dots \right) \quad (12)$$

Next, combining Eqs. (7) and (8) yields

$$\begin{aligned} |A2|^2 &= R_2 R_{210} |E_2^+|^2 \\ |A4|^2 &= R_2^2 R_{210}^2 |E_2^+|^2 \\ |A6|^2 &= R_2^3 R_{210}^3 |E_2^+|^2 \end{aligned} \quad (13)$$

where

$$R_2 = |r_2|^2 \quad (14)$$

$$R_{210} = |r_{210}|^2 \quad (15)$$

$$T_2 = |t_2|^2 \quad (16)$$

Inserting Eq. (13) into Eq. (12) results in the transmitted power given by

$$\xi = n_o T_2 |E_2|^2 \left(1 + R_2 R_{210} + R_2^2 R_{210}^2 + R_2^3 R_{210}^3 + \dots \right) \quad (17)$$

where the infinite sum converges to the closed-form expression,

$$\xi = \frac{n_o T_2 |E_2^+|^2}{1 - R_2 R_{210}} \quad (18)$$

The transmittance is defined as the transmitted power divided by the incident power. The incident power is given by

$$\xi_o = n_o |E_o^+|^2 \quad (19)$$

and the expression for the overall transmittance is obtained by ratioing Eq. (18) to Eq. (19):

$$T = \frac{\xi}{\xi_o} = \frac{T_2 |E_2^+|^2}{\left(1 - R_2 R_{210} \right) |E_o^+|^2} \quad (20)$$

But from Eq. (7)

$$\frac{|E_2^+|^2}{|E_o^+|^2} = |t_{012}|^2 = T_{012} \quad (21)$$

and the final result for the overall normal transmittance is given by

$$T = \frac{T_2 T_{012}}{\left(1 - R_2 R_{210} \right)} \quad (22)$$

The result in Eq. (22) is valid only when the substrate is a nonabsorbing medium. If the substrate is also absorbing (i.e., if the imaginary part of the complex refractive index of the substrate is nonzero), then Eq. (22) becomes

$$T = \frac{T_2 T_{012} e^{-\alpha_g D}}{1 - R_2 R_{210} e^{-2\alpha_g D}} \quad (23)$$

where

D = the thickness of the substrate (germanium),

$\alpha_g = \frac{4\pi k_g}{\lambda}$ is the absorption coefficient of the substrate (germanium),

k_g = imaginary component of complex refractive index of the substrate (germanium), and

λ = wavelength in vacuum.

Since Eq. (23), the normal transmittance of a thin film deposited upon a thick partially transmitting film, has been developed, it is now necessary to define the expressions T_2 , T_{012} , R_2 , and R_{210} in terms of the optical constants of the thin film, the substrate, and wavelength. The derivation of these quantities is straightforward but tedious; it is outlined in detail in Ref. 12. The expressions required to evaluate Eq. (23) are listed below:

$$R_2 = |r_2|^2 = \left| \frac{\bar{n}_2 - n_o}{\bar{n}_2 + n_o} \right|^2 \quad (24)$$

$$T_2 = |t_2|^2 = \left| \frac{2\bar{n}_2}{(n_o + \bar{n}_2)} \right|^2 \quad (25)$$

The expressions for T_{012} and R_{210} are somewhat more complicated to evaluate and will be considered apart from those for R_2 and T_2 . The expressions for T_{012} and R_{210} , based on Ref. 12, are given by

$$T_{012} = \frac{|t_a|^2 |t_b|^2 e^{-2b}}{\left\{ 1 + |r_a|^2 |r_b|^2 e^{-4b} + 2e^{-2b} \left[\operatorname{Re} (r_a r_b) \cos 2a + \operatorname{Im} (r_a r_b) \sin 2a \right] \right\}} \quad (26)$$

and

$$R_{210} = \frac{\left\{ |r_a|^2 + |r_b|^2 e^{-4b} + 2e^{-2b} \left[\operatorname{Re} (r_b r_a^*) \cos 2a + \operatorname{Im} (r_b r_a^*) \sin 2a \right] \right\}}{\left\{ 1 + |r_a|^2 |r_b|^2 e^{-4b} + 2e^{-2b} \left[\operatorname{Re} (r_a r_b) \cos 2a + \operatorname{Im} (r_a r_b) \sin 2a \right] \right\}} \quad (27)$$

where

$$r_a = \frac{\bar{n}_2 - \bar{n}_1}{\bar{n}_2 + \bar{n}_1} \quad (28)$$

$$r_b = \frac{\bar{n}_1 - \bar{n}_0}{\bar{n}_1 + \bar{n}_0} \quad (29)$$

$$t_a = \frac{2\bar{n}_1}{\bar{n}_1 + \bar{n}_2} \quad (30)$$

$$t_b = \frac{2\bar{n}_0}{\bar{n}_0 + \bar{n}_1} \quad (31)$$

$$\bar{n}_1 = n_1 - ik_1 = n - ik = \bar{n} \quad (32)$$

$$\bar{n}_2 = n_g - ik_g \quad (33)$$

$$a = \frac{2\pi d_1 n_1}{\lambda} \quad (34)$$

$$b = \frac{2\pi d_1 k_1}{\lambda} \quad (35)$$

d_1 = cryodeposit thickness and * denotes the complex conjugate. The optical constants of the cryopumped constituents were determined by using this analytical transmission model in conjunction with a nonlinear least-squares convergence routine. Also, the subtractive Kramers-Kronig relation between n and k was used in conjunction with (for 20°K NH₃ and H₂O) and in comparison with (for 20°K CO₂ and 80°K H₂O, CO₂, and NH₃) the nonlinear least-squares determination of n . The subtractive Kramers-Kronig relation is given by

$$n(\nu) - n(\nu_m) = \frac{2}{\pi} P \int_0^\infty \left[\frac{k(\nu') \nu' - k(\nu) \nu}{(\nu')^2 - \nu^2} - \frac{k(\nu') \nu' - k(\nu_m) \nu_m}{(\nu')^2 - \nu_m^2} \right] d\nu' \quad (36)$$

where ν_m is a reference frequency and P indicates the Cauchy principal value of the integral. Integration was performed by using the simple trapezoidal rule; the $\nu(\nu')$ values used in Eq. (37) were those determined by the nonlinear least-squares technique.

Transmittance data recorded for all deposits discussed here were digitized every 2 cm^{-1} . The optical properties were computed every 10 cm^{-1} except in regions of strong absorption in which computations were performed every 2 cm^{-1} . The optical properties were initially computed by the nonlinear least-squares determination using Eq. (23). However, in some instances, the program did not appear to converge upon a unique value of n . This usually occurred in regions of strong absorption or low wavenumber or for cases in which it was possible to form only a few thin deposit thicknesses. The n value appears to be primarily defined by the period of the transmission versus thickness curve at each wavenumber. At small thicknesses, or high absorption, or low wavenumbers, the transmission versus thickness (for each wavenumber) curve is not well defined; i.e., the period of the interference as a function of thickness is not well defined. The k value, which is primarily defined by the magnitude of the transmittance, did not have this difficulty and was well defined over the whole spectral region (700 to $3,700\text{ cm}^{-1}$). Thus, to determine n , the k values were used with the subtractive Kramers-Kronig relationship; these new n values were then used in the analytical model (along with the k values) to see whether good agreement occurred with the transmittance data. For all wavenumbers, the Kramers-Kronig n 's along with the least-squares k 's yielded good agreement when the analytical model and transmittance data were compared.

Generally the nonlinear least-squares results (thin-film model) did converge, and a comparison of the Kramers-Kronig and thin-film results is shown for each species investigated. The values listed in the tables are the Kramers-Kronig n 's along with the thin-film k 's.

5.1 NH_3 OPTICAL CONSTANTS

The optical constants for NH_3 at 80°K and at 20°K were determined using both the nonlinear least-squares technique and the Kramers-Kronig method. The results are shown in Figs. 36 and 37, respectively; the tabulated results are given, respectively, in Tables 4 and 5. For both temperatures the agreement between the Kramers-Kronig method and nonlinear least-squares technique is very good. The slanted dashed line on the k versus ν plots represents the minimum imaginary refractive index values that can be determined because of the error limits on the film-substrate transmission measurements. Values below the dashed line are shown but should not be considered accurate. The anomalous dispersion at the two strong NH_3 bands is clearly seen in the n versus ν plots of Figs. 36 and 37. Shown in Fig. 38 is the effect of temperature on the NH_3 optical properties. The n values are higher at 80°K than at 20°K as was the density. Also the k values at the two major absorptions bands are greater at 80°K than at 20°K .

Figures 39 and 40 show the excellent agreement between theory and data at a variety of wavenumbers. This shows how well the analytical model describes the physical phenomena. In Fig. 39 the results at 1,000 and 2,100 cm^{-1} show very slight attenuation (small k); at $\nu = 3,370 \text{ cm}^{-1}$ the transmittance is seen to decrease sharply because of the large k value (absorption band). Similar results are shown in Fig. 40 at 20°K. The n and k determination was done using absolute transmission measurements at the 15th interference thickness for 80°K and at the 12th interference thicknesses for 20°K NH_3 .

The data given in Figs. 41, 42, and 43 are a comparison of the results of this work with those of others. The results in Ref. 14 (Fig. 41) were obtained by solidifying liquid ammonia. The Lambert absorption coefficient was determined using thicknesses in the range from 0.50 to 20 μm . Interference effects were not even mentioned for these small thicknesses. The n values were then determined using the subtractive Kramers-Kronig method. Data in Ref. 14 were obtained at 190°K, whereas the present data were obtained at 80°K. However, the agreement for the n values is very good, and the agreement for k is generally good. (Results were limited to $\nu > 950 \text{ cm}^{-1}$ in Ref. 14 because of the use of CaF_2 windows.)

Shown in Fig. 42 is a comparison of the present data at 20°K to the Ref. 15 data at 30°K. Data in Ref. 15 were obtained by using basically the same approach as used in the present tests except that thin-film reflection data were recorded. In general the agreement is good, but the results of the present work yielded higher values for both n and k . The results in Ref. 15 were only shown to 2,400 cm^{-1} .

The results shown in Fig. 43 illustrate the comparison with the results in Ref. 1. The agreement is excellent. The same techniques were used in both the present work and in Ref. 1. The same research cell was also used except that the present work employs a new sample holder that allows much better film thickness determination. In addition, the analytical model convergence routine has been improved by about two orders of magnitude. These two data sets were recorded about two years apart.

5.2 CO_2 OPTICAL CONSTANTS

The optical constants for CO_2 at 80 and 20°K were determined and are shown in Figs. 44 and 45, respectively; tabulated results for these constants for CO_2 at 80 and 20°K are shown in Tables 6 and 7, respectively. Again, results of the nonlinear least-squares technique and the Kramers-Kronig method are in good agreement. As before, values of k below the dashed line should not be considered accurate because of error limits on the film-substrate transmission measurements. Figure 46 shows the effect of temperature on the CO_2 optical properties. As was true for NH_3 , the higher temperatures yielded higher values for n and k as well as for the density.

Determination of n and k for CO_2 at 80°K was done using transmittance measurements at 25 thicknesses; at 20°K , 14 thicknesses were used. The agreement between theory and data is shown in Figs. 47 and 48 for 80 and 20°K , respectively. After the n and k values were determined, they were used in the analytical model to generate the theoretical curves.

No n or k values in the wavenumber range of interest were found in existing studies to which the present work could be compared. Possibly these n and k values are unique in the literature.

5.3 H_2O OPTICAL CONSTANTS

The optical constants for H_2O at 80 , 50 , and 20°K are shown in Figs. 49, 50, and 51, respectively; tabulated results are contained in Tables 8, 9, and 10, respectively. In Figs. 49, 50, and 51, where the nonlinear least-squares technique is not shown, the agreement with the Kramers-Kronig was not good. In these regions the nonlinear least squares did not converge on a unique value of n . Therefore, the k values from the least squares were used with the Kramers-Kronig method to generate n values. Then the least-squares k values and Kramers-Kronig n values were compared with the data as shown in Figs. 53, 54, and 55. All of the k values in Figs. 49, 50, and 51 were above the error line and thus should be considered as accurate values. Figure 52 shows the effect of temperature on the H_2O optical properties. The k values display the same behavior with temperature as was discussed earlier (Section 4.3). Figures 53, 54, and 55 show the very good agreement between theory and data. The n and k values were determined using absolute transmittance measurements at 25 thicknesses for 80°K ; for 50°K , 17 thicknesses were used; for 20°K , 8 thicknesses were used. At 50°K only 17 thicknesses could be formed ($\approx 2.7 \mu\text{m}$) before shattering occurred; at 20°K only 8 thicknesses ($\approx 1.0 \mu\text{m}$) could be formed before shattering occurred.

Figures 56 and 57 show comparisons of the present work with the results in Refs. 4 and 9, respectively. In Fig. 56 the deposition temperature was 30°K and the pressure was about 10^{-6} torr. (As mentioned earlier, the results of Ref. 4 were obtained through a thin-film reflectance analysis.) For results in Ref. 9 (Fig. 47) the data were obtained at 100°K , but the deposition pressure was not given.

6.0 SUMMARY

Experimentally determined transmittance measurements of condensed gases on a cryogenically cooled germanium window were made. Thin films of NH_3 , CO_2 , H_2O , and mixtures were deposited at 20 and 80°K . The infrared spectral transmission was studied over the 500 - to $3,700\text{-cm}^{-1}$ wavenumber range (the 2.70 - to $20.0\text{-}\mu\text{m}$ wavelength range). The film

thickness was accurately determined using a two-angle laser-interference technique. The densities of the films were determined by using quartz-crystal microbalances (QCM's) and by calculating the refractive index at $0.6328\ \mu\text{m}$ to allow accurate thickness measurement. Some fracture and shattering effects were observed for the films condensed at 20°K .

From the transmission data, the optical properties n and k were determined for the 700-to $3,700\text{-cm}^{-1}$ wavenumber range. These results are presented in graphical and tabular form for a wavenumber interval of 2 cm^{-1} . The optical properties presented are important for calculating the effects of possible deposits upon cryogenically cooled surfaces. Such surfaces as cryogenically cooled sensor optics and telescopes function in the wavenumber region investigated. The interpretation of information from these types of thin-film-contaminated instruments requires knowledge of n and k spectra.

REFERENCES

1. Pipes, J. G., Roux, J. A., Smith, A. M., and Scott, H. E. "Infrared Transmission of Contaminated Cryocooled Optical Windows." *AIAA Journal*, Vol. 16, No. 9, September 1978, pp. 984-990.
2. Tempelmeyer, K. E. and Mills, D. W., Jr. "Refractive Index of Carbon Dioxide Cryodeposit." *Journal of Applied Physics*, Vol. 16, No. 6, May 1968, pp. 2968-2969.
3. Smith, A. M., Tempelmeyer, K. E., Müller, P. R., and Wood, B. E. "Angular Distribution of Visible and Near IR Radiation Reflected from CO_2 Cryodeposits." *AIAA Journal*, Vol. 7, No. 12, December 1969, pp. 2274-2280.
4. Thompson, S. B., Arnold, F., Sanderson, R. B., and Mantz, A. W. "Optical Properties of Cryodeposits on Low Scatter Mirrors." *Progress in Aeronautics and Astronautics*, Vol. 35 — *Thermophysics and Spacecraft Thermal Control*. Ed. R. G. Hering. Copyright © 1974 Massachusetts Institute of Technology, Cambridge, Mass., pp. 229-248.
5. Wolff, H., Rollar, H.-G., and Wolff, E. "Infrared Spectra and Vapor Pressure Isotope Effect of Crystallized Ammonia and its Deuterium Derivatives." *Journal of Chemical Physics*, Vol. 55, No. 3, August 1971, pp. 1373-1378.
6. Reding, F. P. and Hornig, D. F. "The Vibrational Spectra of Molecules and Complex Ions in Crystals. V. Ammonia and Deutero-Ammonia." *The Journal of Chemical Physics*, Vol. 19, No. 5, May 1951, pp. 594-601.
7. Herzberg, G. *Infrared and Raman Spectra of Polyatomic Molecules*, D. Van Nostrand Co., Inc., Princeton, N. J., 1954.

8. Osberg, W. E. and Hornig, D. F. "The Vibrational Spectra of Molecules and Complex Ions and Crystal. VI. Carbon Dioxide." *The Journal of Chemical Physics*, Vol. 20, No. 9, September 1952, pp. 1345-1357.
9. Bertie, J. E., Labbe, H. J., and Whalley, E. "Absorptivity of Ice I in the Range 4000-30 cm^{-1} ." *The Journal of Chemical Physics*, Vol. 50, No. 10, May 1969, pp. 4501-4520.
10. Ockman, Nathan. "The Infrared and Raman Spectra of Ice." *Advances in Physics*, Vol. 7, 1957, p. 199.
11. Vašíček, A. *Optics of Thin Films*. Trans. Mrs. H. Watney-Kaczér. Interscience Publishers, New York, 1960.
12. Heavens, O. S. *Optical Properties of Thin Films*. Dover Publications, Inc., New York, 1965.
13. Herzberger, M. and Salzberg, C. D. "Refractive Indices of Infrared Optical Materials and Color Correction of Infrared Lenses." *Journal of the Optical Society of America*, Vol. 52, No. 4, April 1962, pp. 420-426.
14. Robertson, C. W., Downing, H. D., Curnutte, B., and Williams, D. "Optical Constants of Solid Ammonia in the Infrared." *Journal of the Optical Society of America*, Vol. 65, No. 4, April 1975, pp. 432-435.

1. Pyroelectric detector and collection optics.
2. Stainless steel high vacuum chamber, 85 cm tall by 70 cm in diameter (33.5 in. by 27.5 in. in diameter).
3. Cryogenically cooled infrared window; germanium, 4 mm thick by 70 mm square (0.158 in. by 2.76 in.) and QCM.
4. Helium-neon laser (0.6328 μm) beam (one of two shown) employed to measure cryofilm thickness.
5. Infrared beam, 38 mm in diameter (1.5 in.).
6. 2-mw He-Ne laser.
7. Michelson interferometer.
8. Infrared source and collimator mirror.

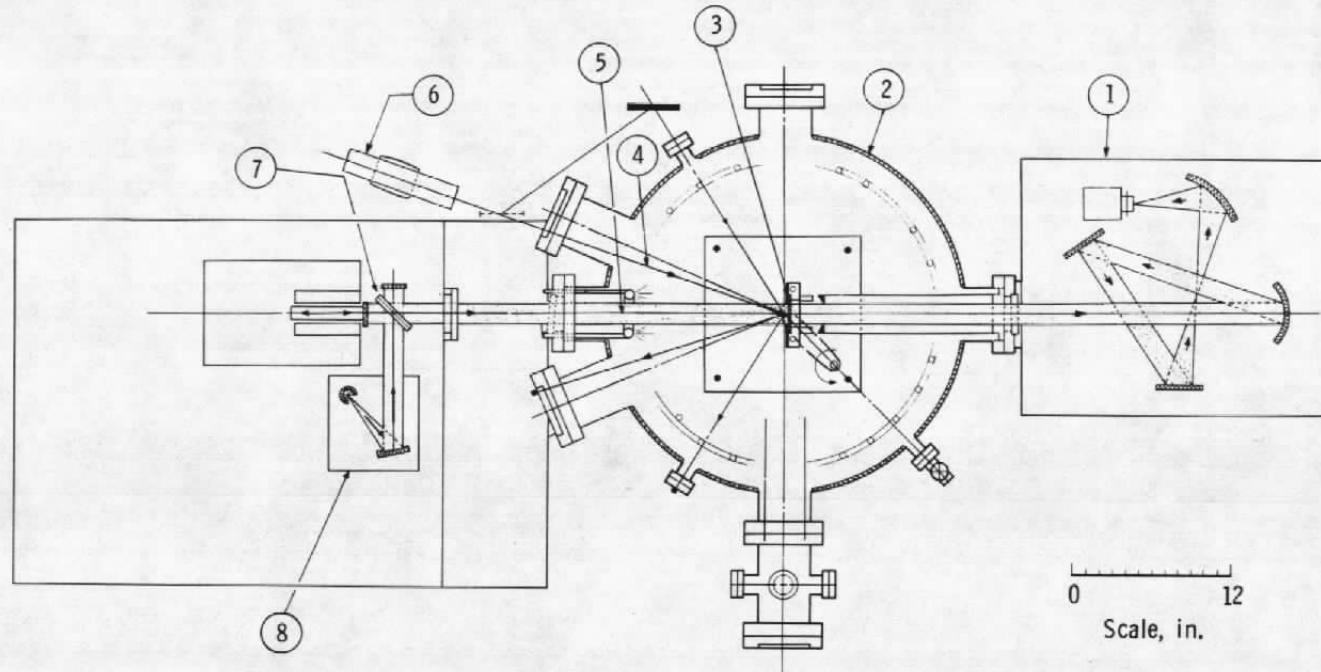


Figure 1. Schematic of the Infrared Optical Transmission Chamber (IROT) with Fourier transform spectrometer.

1. Infrared beam, 38-mm-diameter (1.5 in.).
2. Optical stop required to underfill cryocooled window with infrared beam. Also, this stop is supported by a 3-in. -ID pipe that prevents gas added to chamber from cryopumping on rear of window.
3. Aluminum holder with cryogenic passageways.
4. Germanium window heat sunk with an indium gasket to the aluminum holder.
5. Cover plate.
6. Gaseous helium or liquid nitrogen inlet.
7. Gaseous helium or liquid nitrogen outlet.
8. Crosshatched area illustrates area of window heat sunk to holder. Clear diameter is 50.7 mm (2 in.) while infrared beam diameter is 38 mm (1.5 in.).
9. QCM heat sunk with indium gasket to aluminum holder.

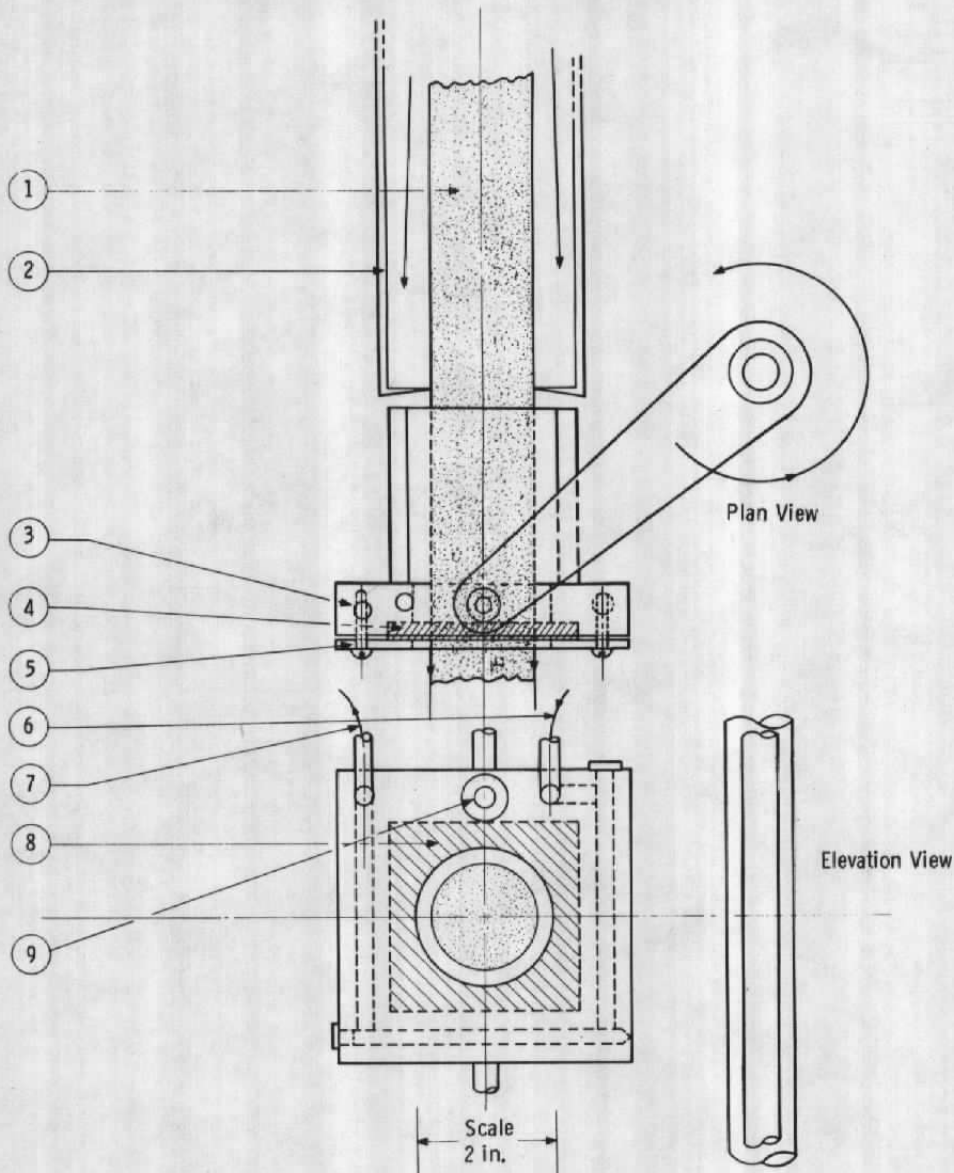


Figure 2. Plan and elevation views of cryogenically cooled window holder.

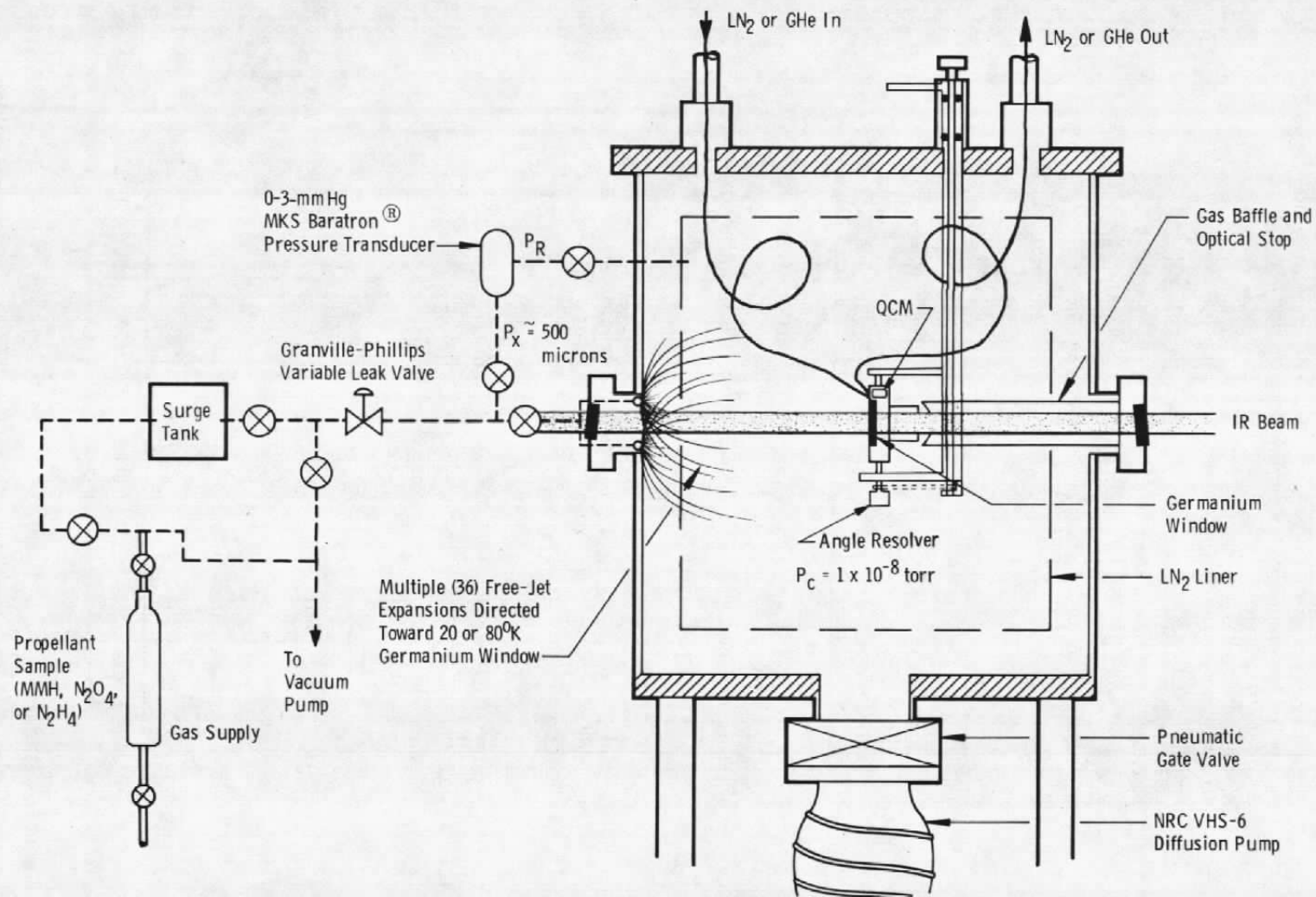


Figure 3. Gas deposition system.

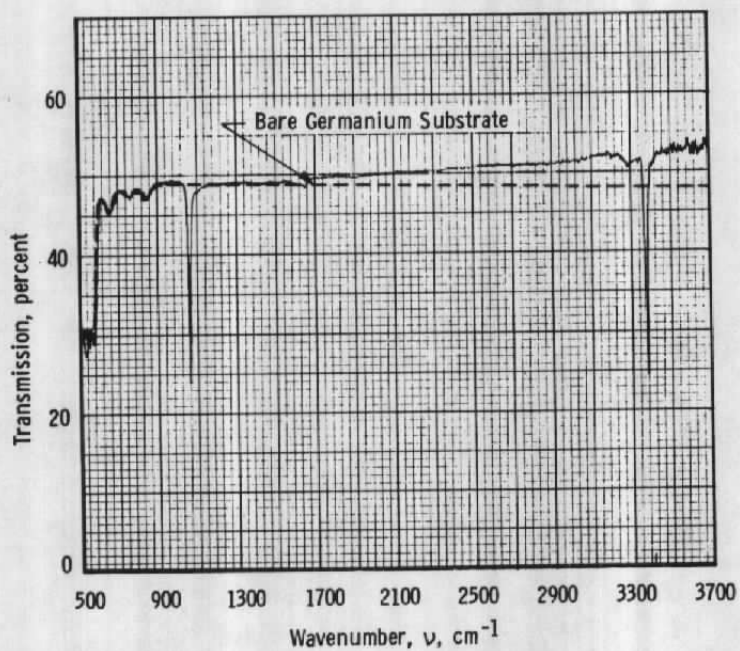


Figure 4. Transmittance of 0.231- μm -thick solid NH_3 on 80°K germanium.

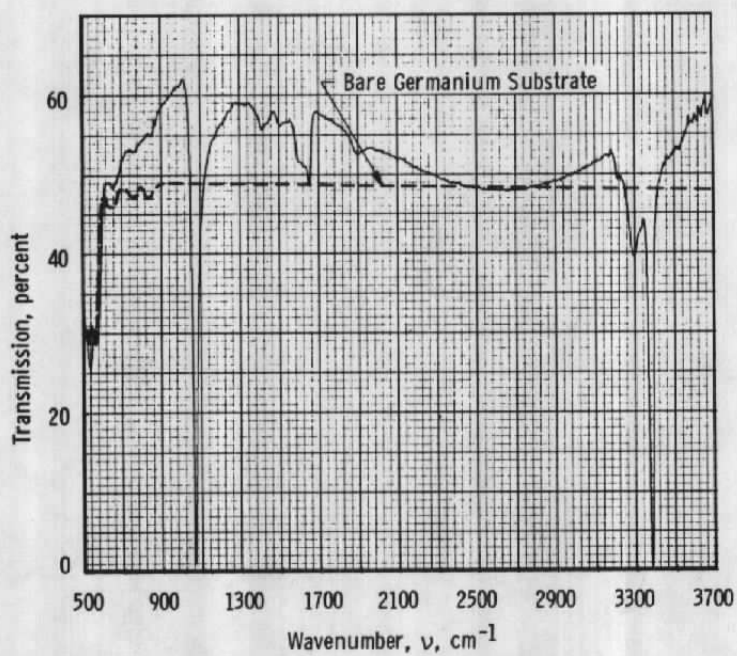


Figure 5. Transmittance of 1.38- μm -thick solid NH_3 on 80°K germanium.

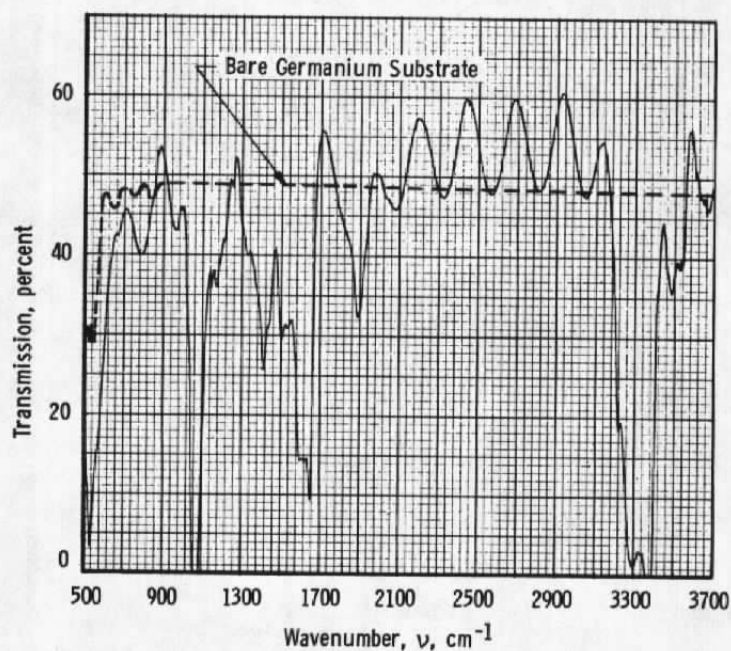


Figure 6. Transmittance of 14.1- μm -thick solid NH_3 on 80°K germanium.

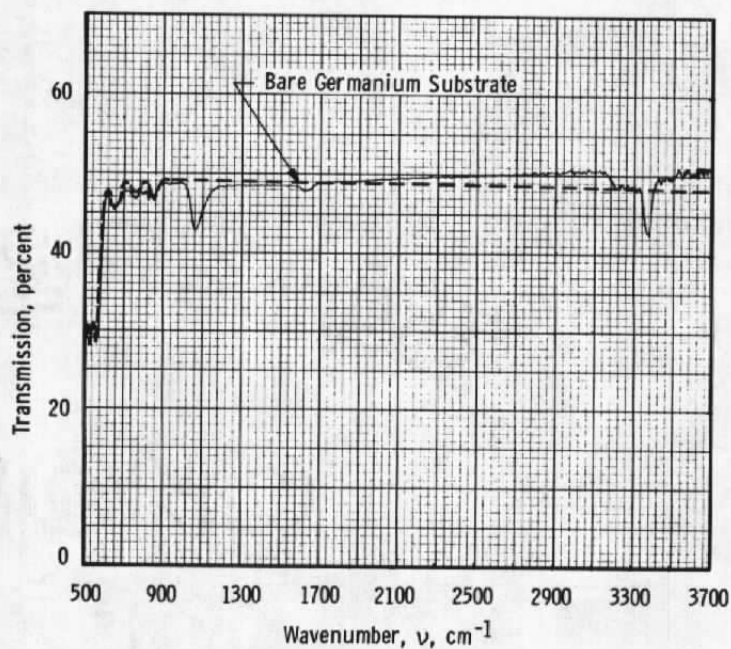


Figure 7. Transmittance of 0.238- μm -thick solid NH_3 on 20°K germanium.

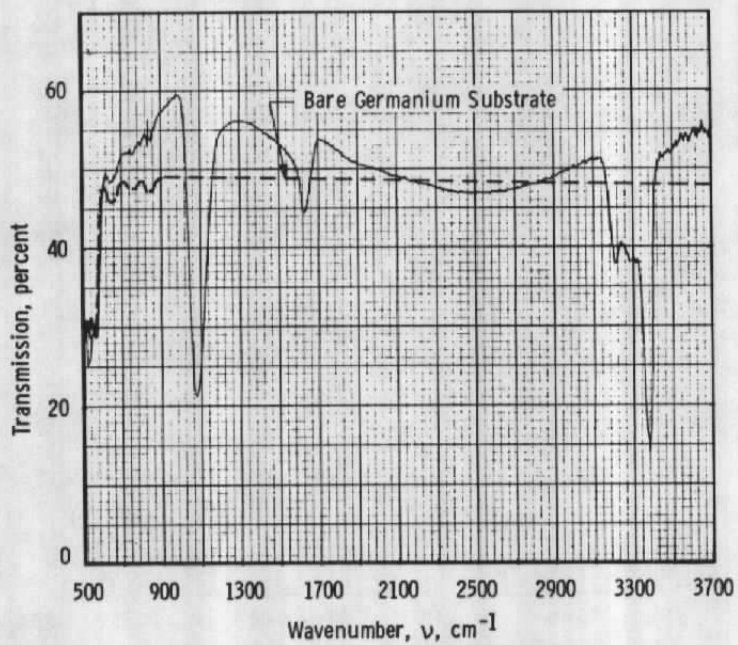


Figure 8. Transmittance of 1.43- μm -thick solid NH_3 on 20°K germanium.

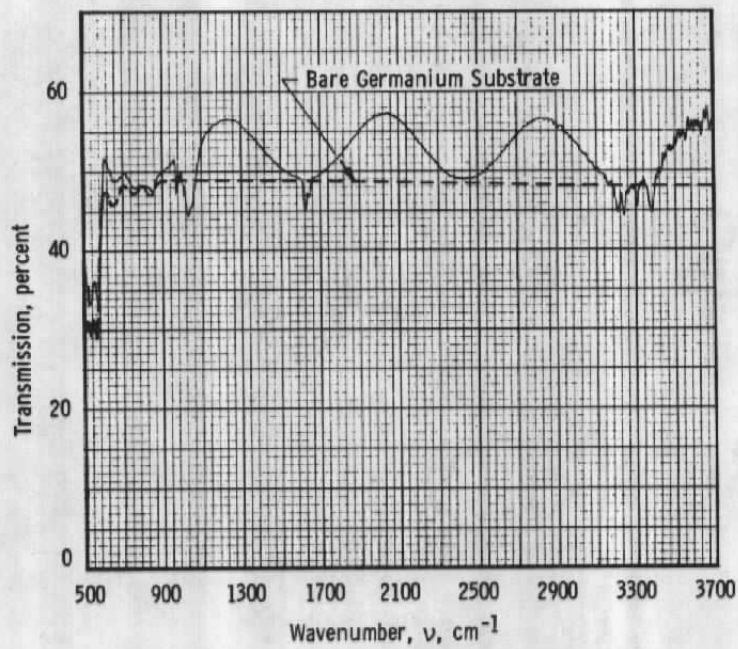


Figure 9. Transmittance of 4.97- μm -thick solid NH_3/N_2 mixture (20 percent/80 percent) on 20°K germanium.

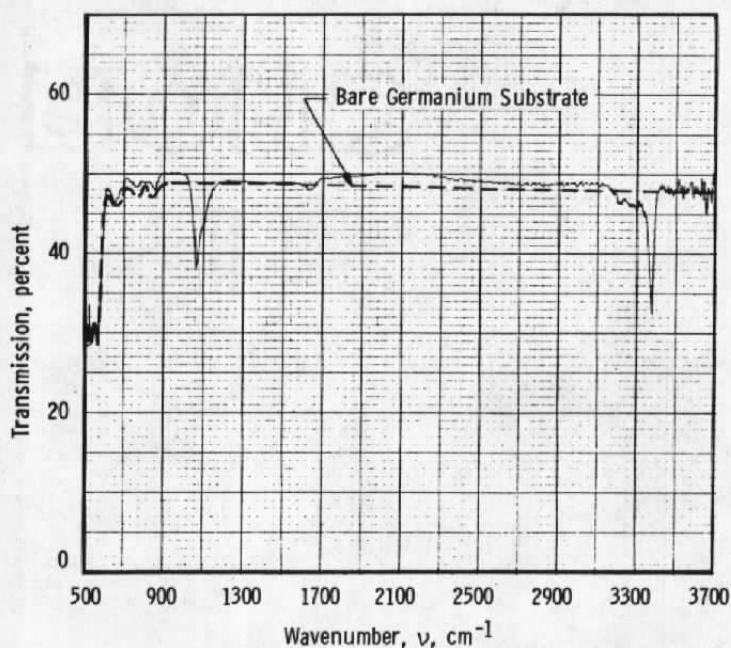


Figure 10. Transmittance of 4.97- μm -thick solid NH_3/N_2 mixture (20 percent/80 percent) after warmup from 20 to 59°K on germanium.

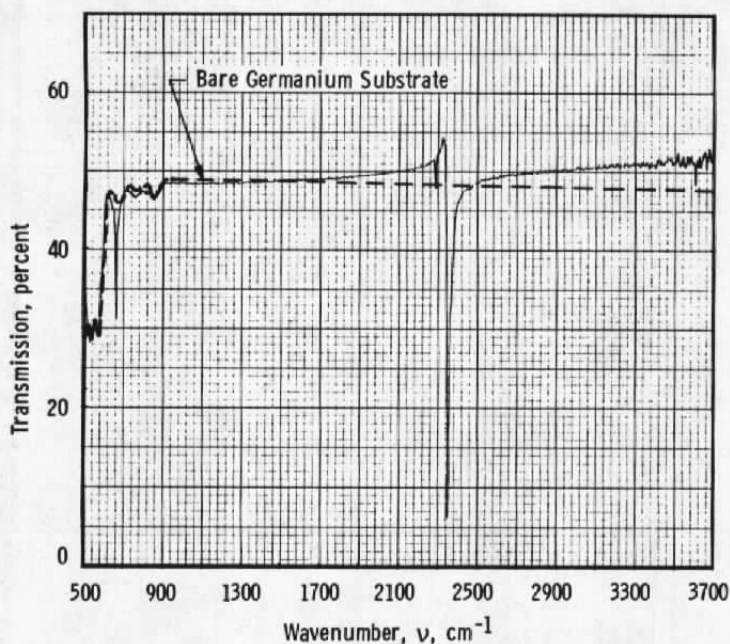


Figure 11. Transmittance of 0.231- μm -thick solid CO_2 on 80°K germanium.

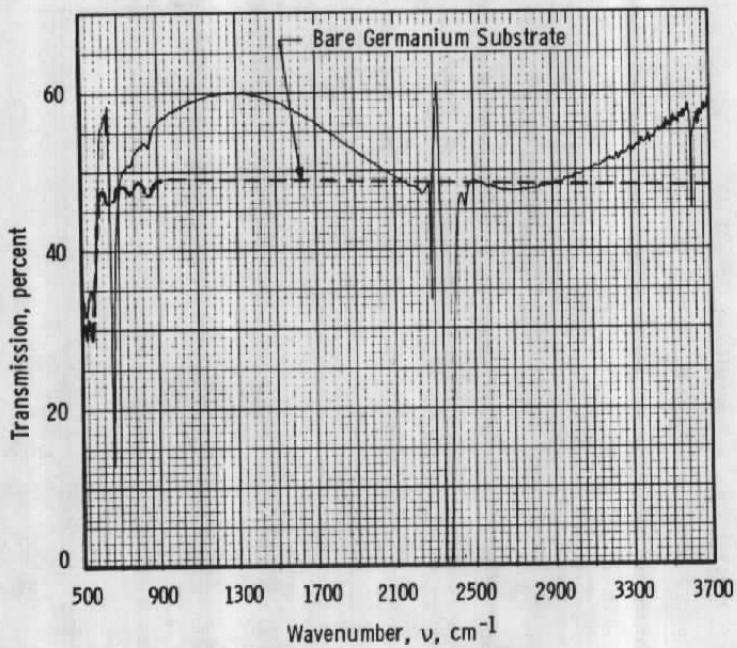


Figure 12. Transmittance of 1.39- μ m-thick solid CO₂ on 80°K germanium.

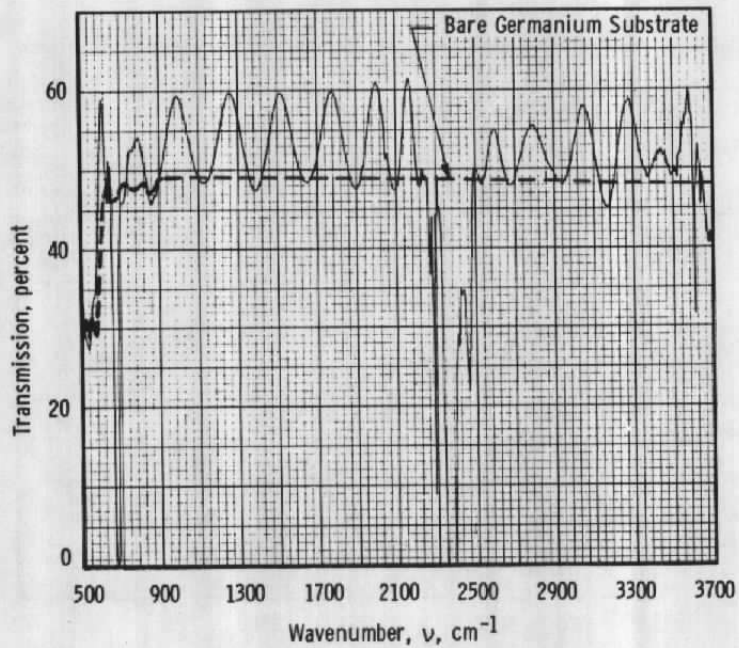


Figure 13. Transmittance of 12.7- μ m-thick solid CO₂ on 80°K germanium.

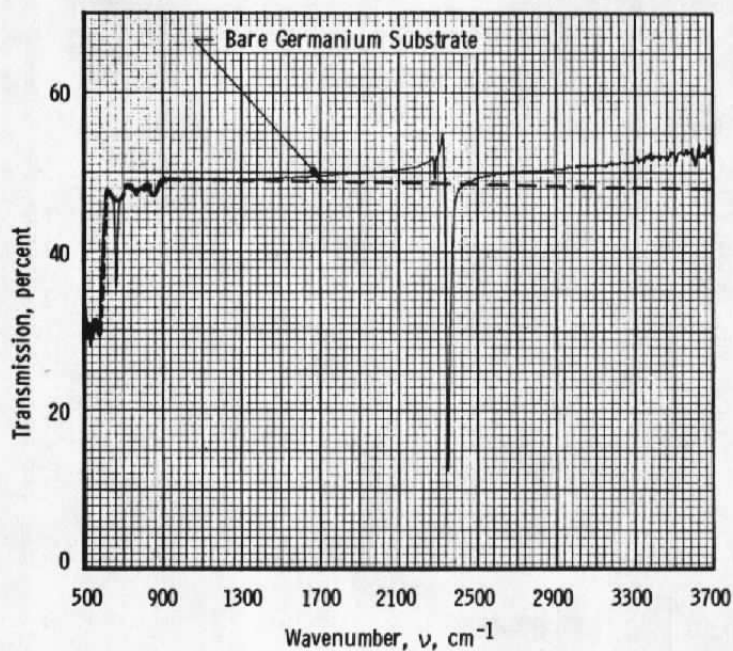


Figure 14. Transmittance of 0.259- μm -thick solid CO_2 on 20°K germanium.

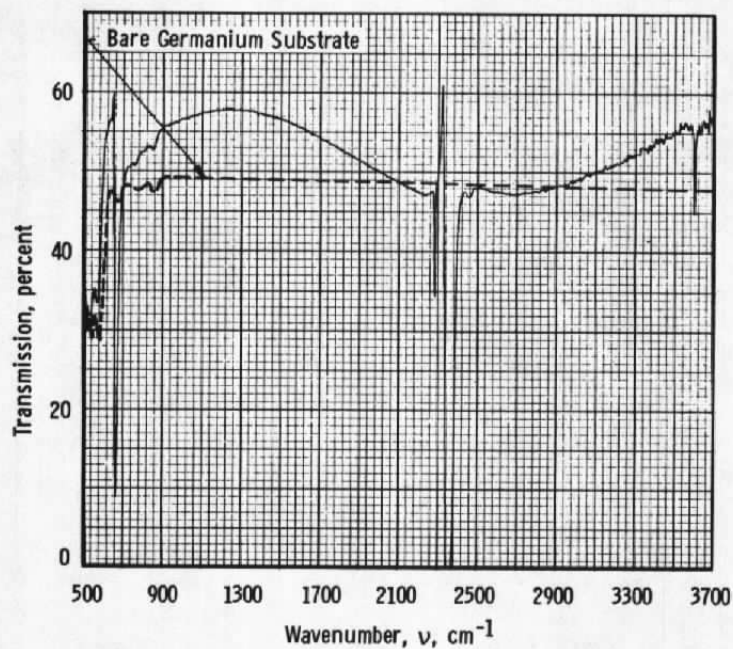


Figure 15. Transmittance of 1.55- μm -thick solid CO_2 on 20°K germanium.

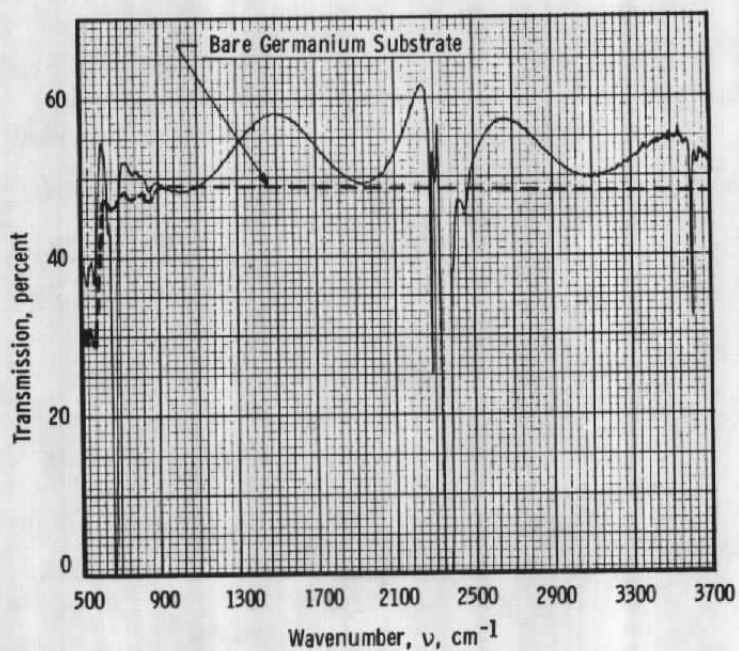


Figure 16. Transmittance of 3.88- μm -thick solid CO_2 on 20°K germanium.

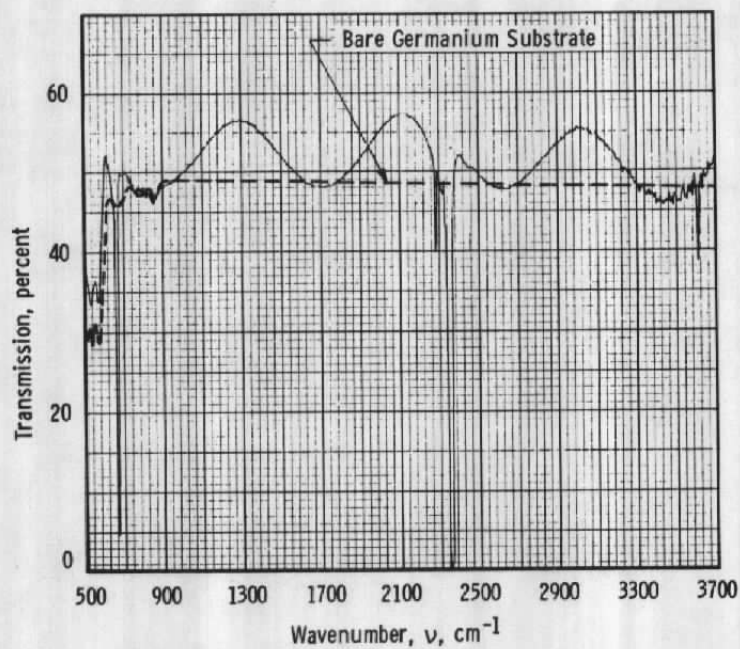


Figure 17. Transmittance of 4.74- μm -thick solid CO_2/N_2 mixture (20 percent/80 percent) on 20°K germanium.

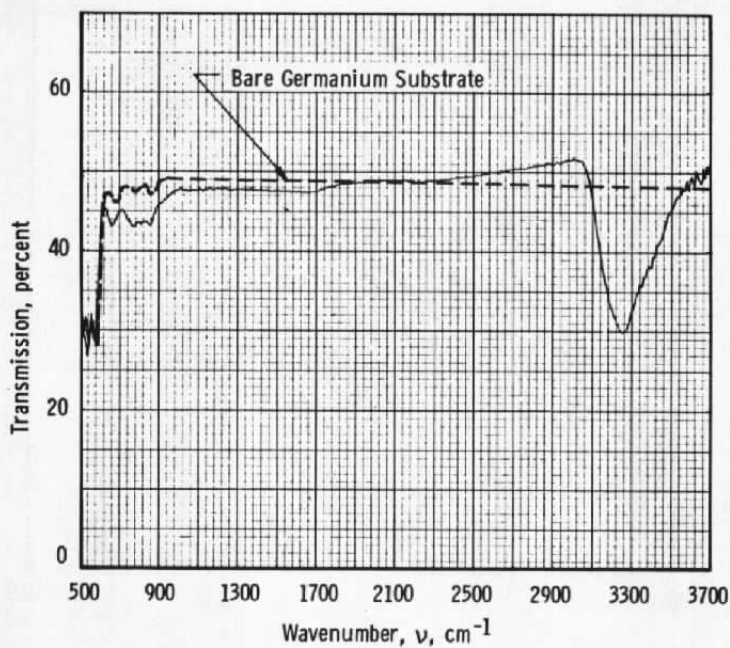


Figure 18. Transmittance of 0.25- μ m-thick solid H₂O on 80°K germanium.

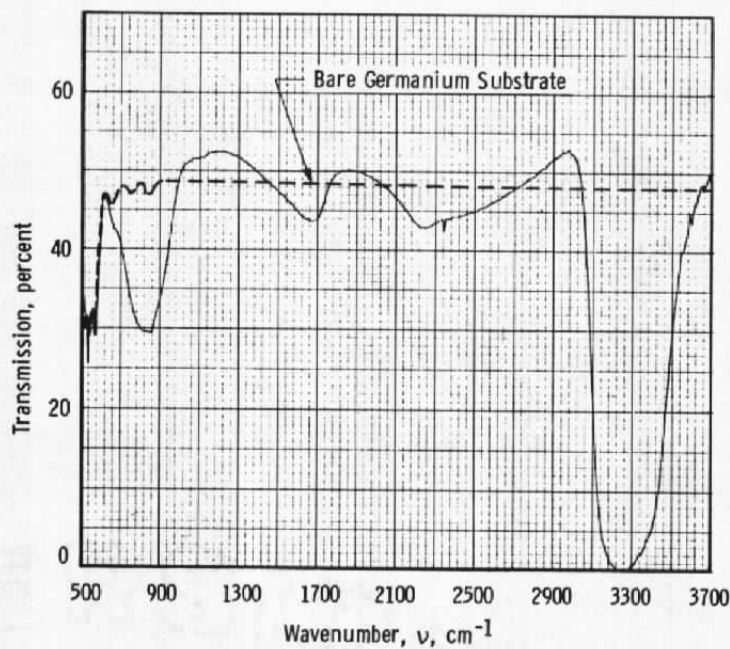


Figure 19. Transmittance of 1.50- μ m-thick solid H₂O on 80°K germanium.

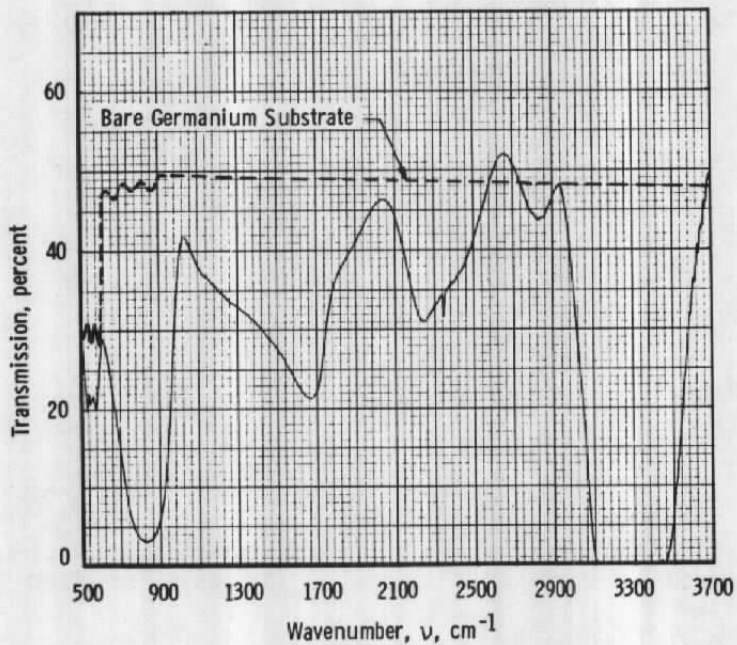


Figure 20. Transmittance of 6.25- μm -thick solid H_2O on 80°K germanium.

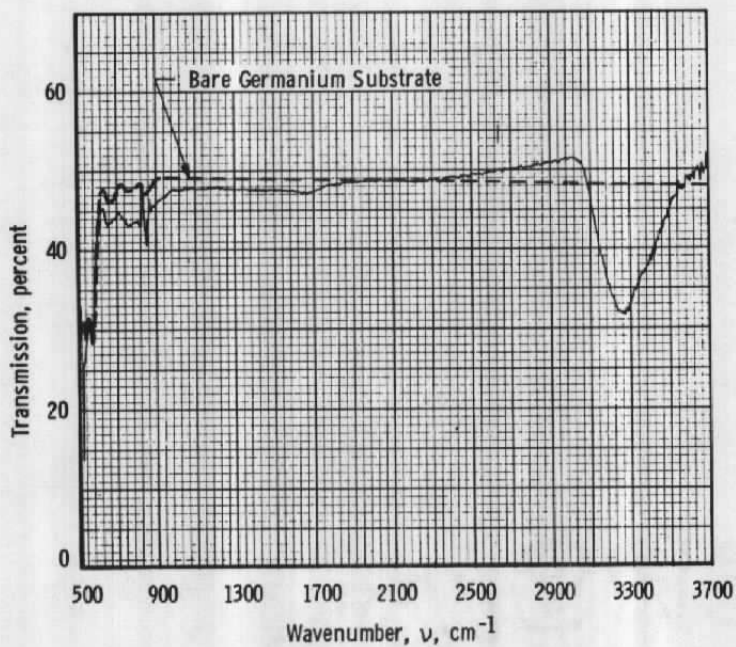


Figure 21. Transmittance of 0.25- μm -thick solid H_2O on 50°K germanium.

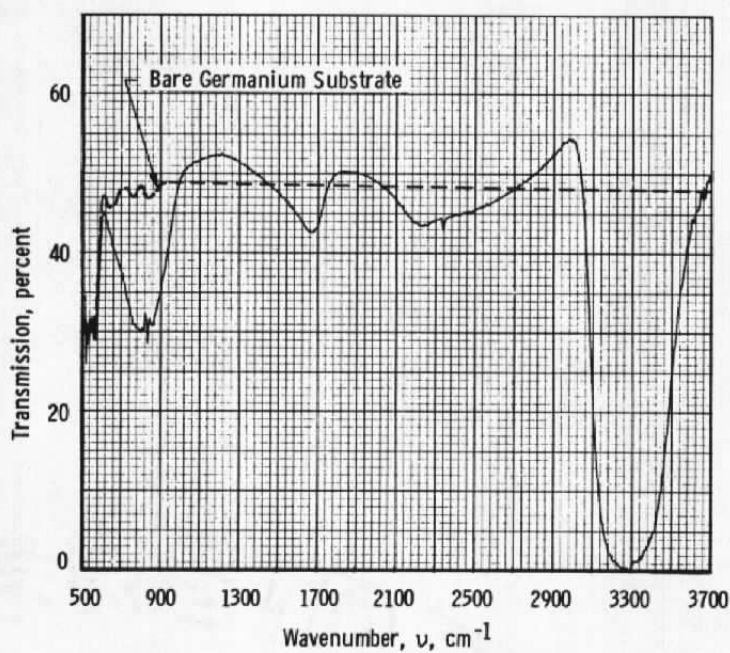


Figure 22. Transmittance of 1.51- μm -thick solid H_2O on 50°K germanium.

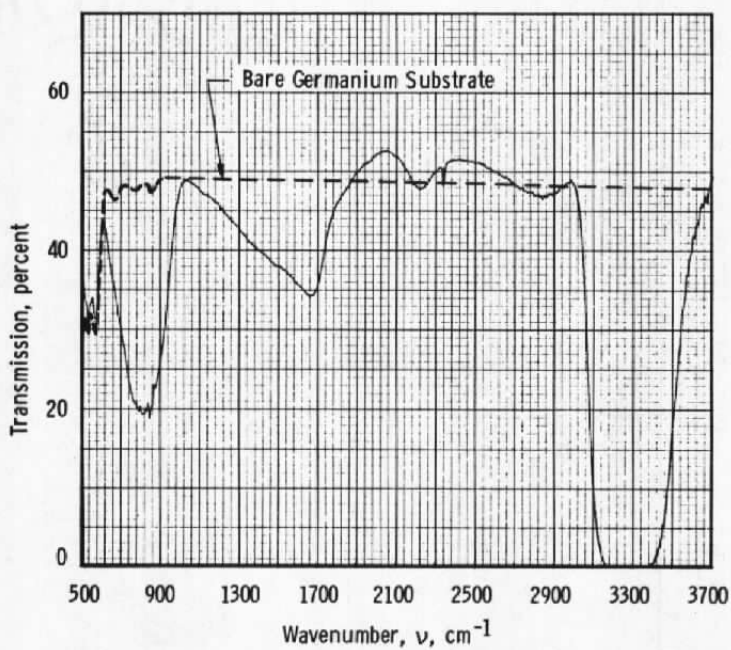


Figure 23. Transmittance of 2.51- μm -thick solid H_2O on 50°K germanium.

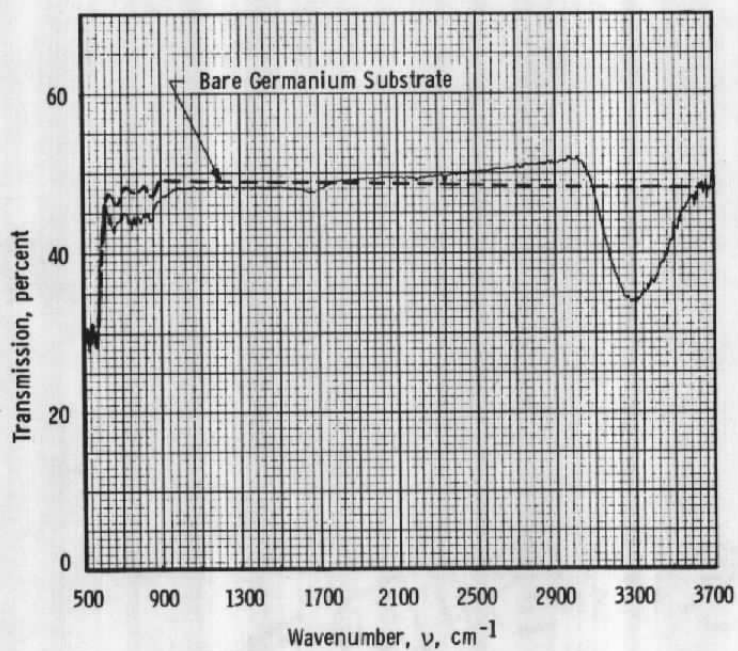


Figure 24. Transmittance of 0.25- μ m-thick solid H₂O on 20°K germanium.

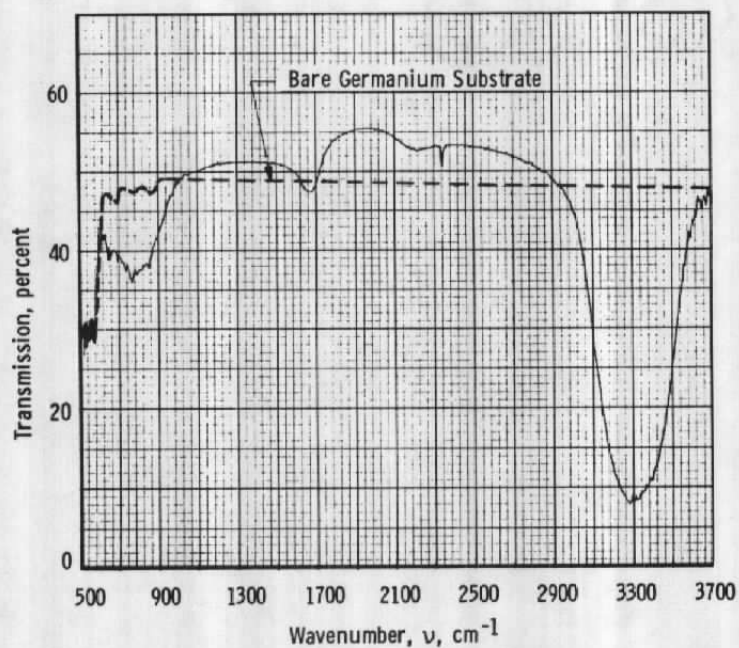


Figure 25. Transmittance of 1.00- μ m-thick solid H₂O on 20°K germanium.

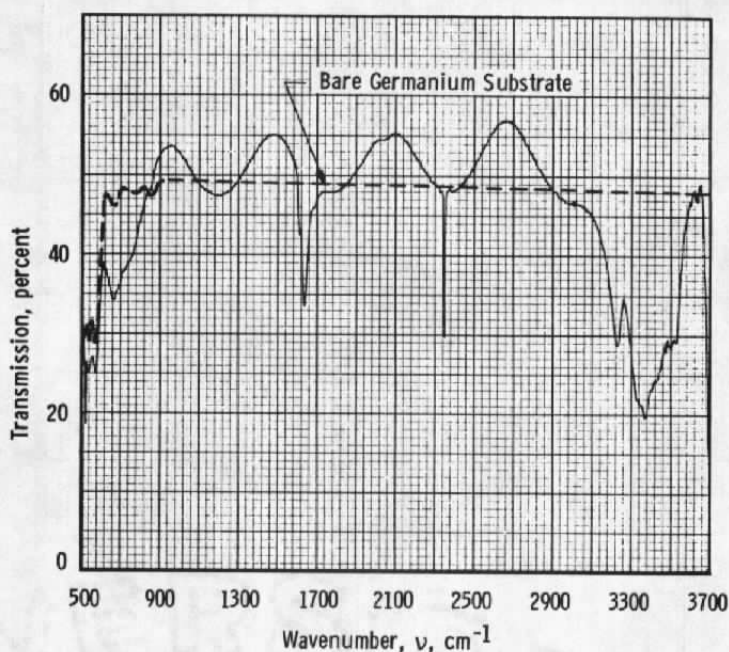


Figure 26. Transmittance of 6.78- μm -thick solid $\text{N}_2/\text{H}_2\text{O}/\text{CO}_2$ mixture (86 percent/13 percent/1 percent) on 20°K germanium.

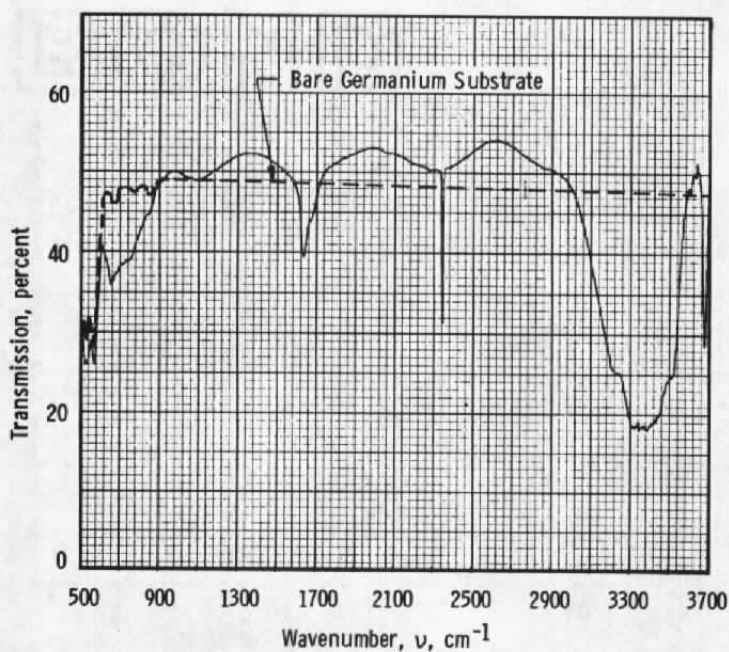


Figure 27. Transmittance of 6.78- μm -thick solid $\text{N}_2/\text{H}_2\text{O}/\text{CO}_2$ mixture (86 percent/13 percent/1 percent) after warmup from 20 to 35°K on germanium.

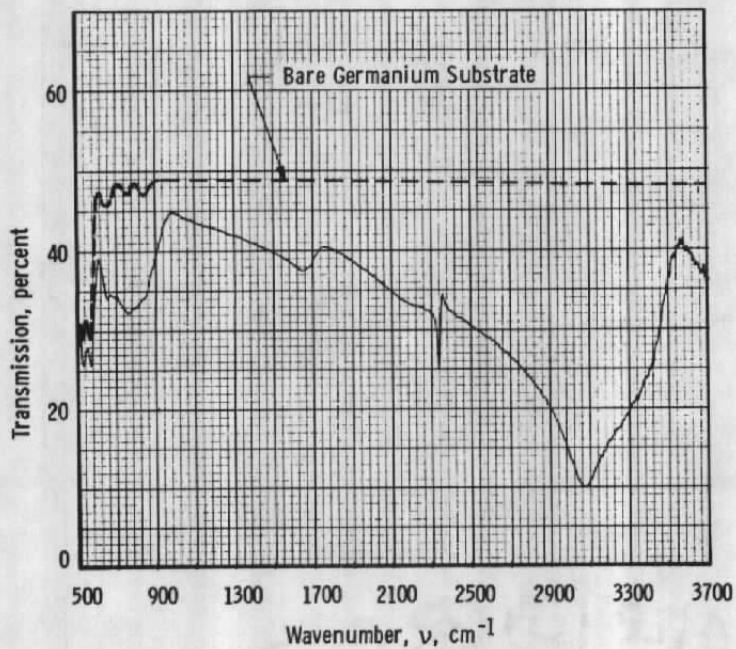


Figure 28. Transmittance of 6.78- μm -thick solid $\text{N}_2/\text{H}_2\text{O}/\text{CO}_2$ mixture (86 percent/13 percent/1 percent) after warmup from 20 to 64°K on germanium.

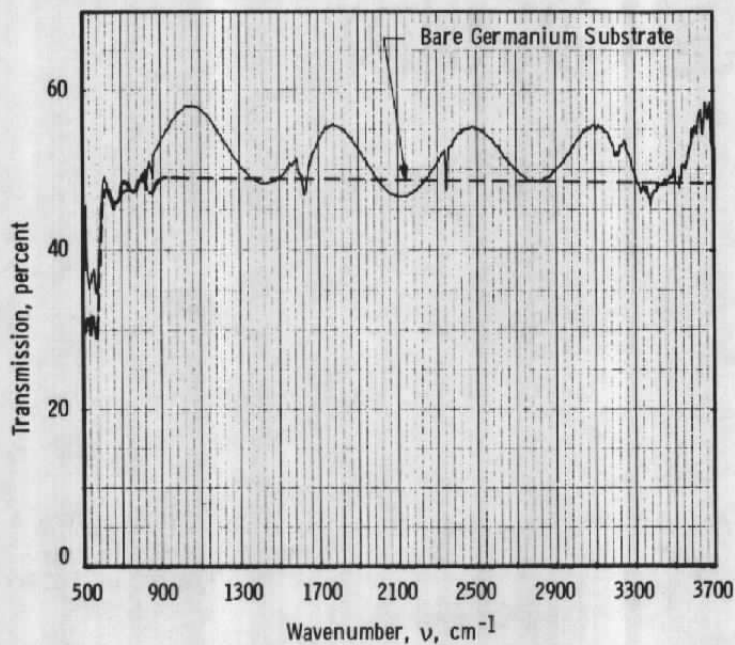


Figure 29. Transmittance of 6.78- μm -thick solid $\text{Ar}/\text{H}_2\text{O}$ mixture (93 percent/6 percent) on 20°K germanium.

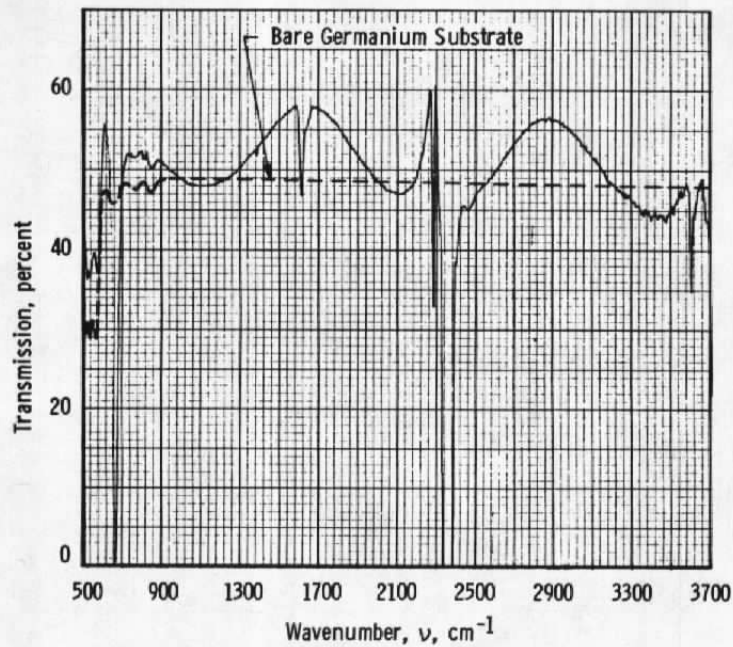


Figure 30. Transmittance of 3.63- μm -thick solid $\text{CO}_2/\text{H}_2\text{O}$ mixture (91 percent/9 percent) on 20°K germanium.

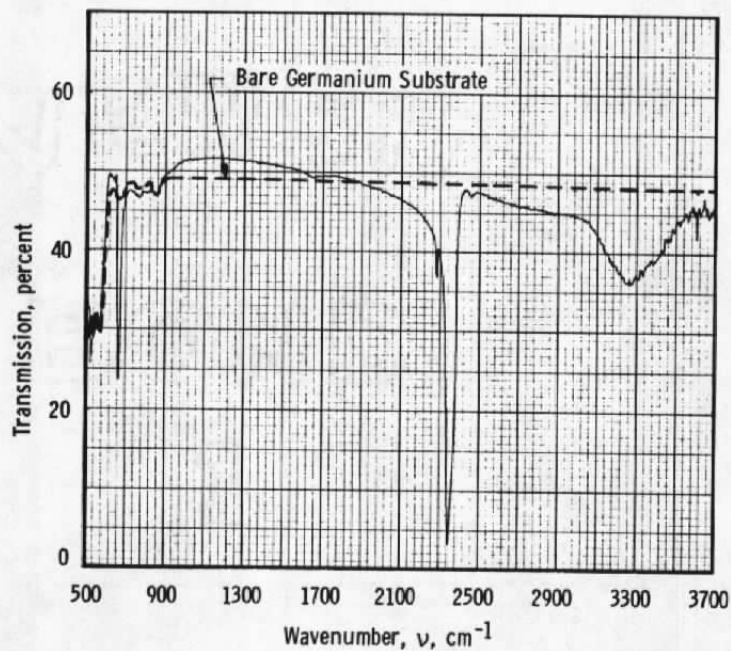


Figure 31. Transmittance of 3.63- μm -thick solid $\text{CO}_2/\text{H}_2\text{O}$ mixture (91 percent/9 percent) after warmup from 20 to 102°K on germanium.

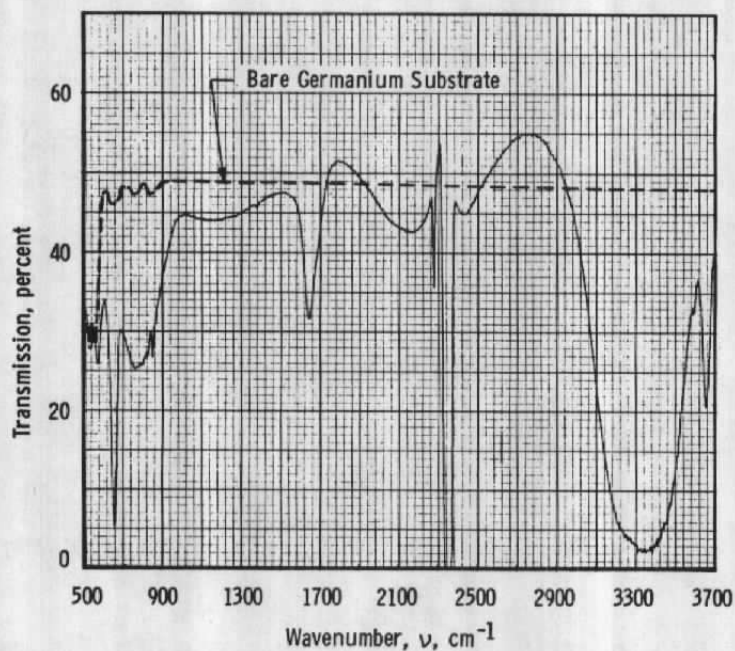


Figure 32. Transmittance of 3.49- μm -thick solid $\text{H}_2\text{O}/\text{CO}_2/\text{N}_2$ mixture (61 percent/36 percent/2 percent) on 20°K germanium.

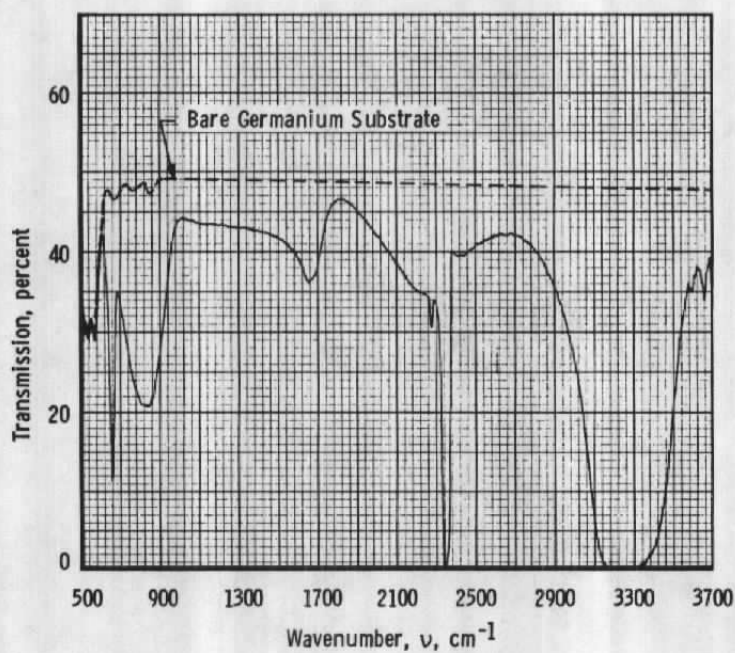


Figure 33. Transmittance of 3.49- μm -thick solid $\text{H}_2\text{O}/\text{CO}_2/\text{N}_2$ mixture (61 percent/36 percent/2 percent) after warmup from 20 to 128°K germanium.

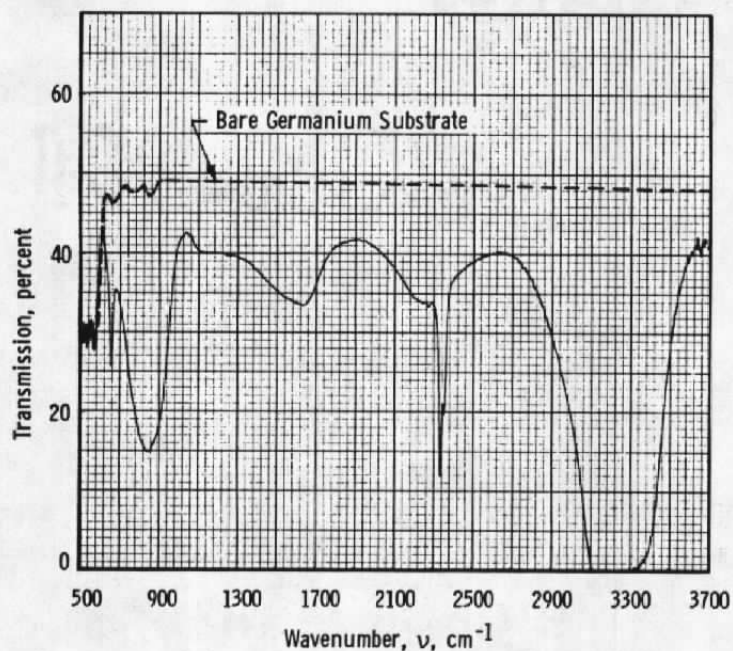


Figure 34. Transmittance of 3.49- μm -thick solid $\text{H}_2\text{O}/\text{CO}_2/\text{N}_2$ mixture (61 percent/36 percent/2 percent) after warmup from 20 to 153°K on germanium.

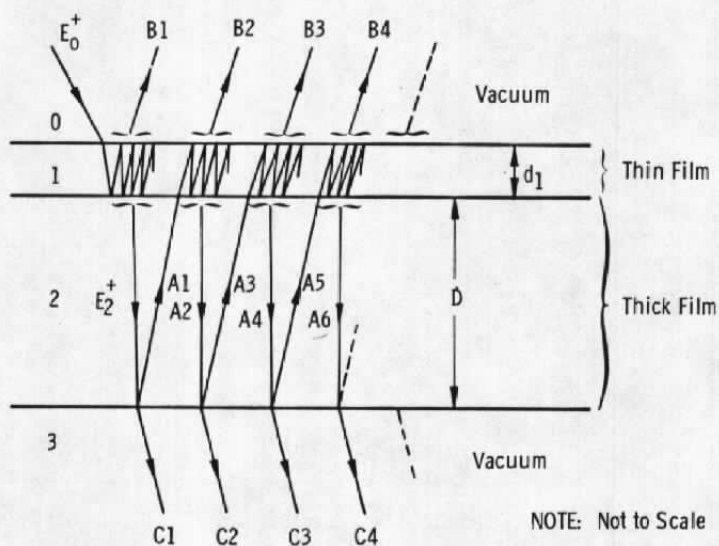


Figure 35. Geometry depicting analytical model for a thin film formed on a thick film.

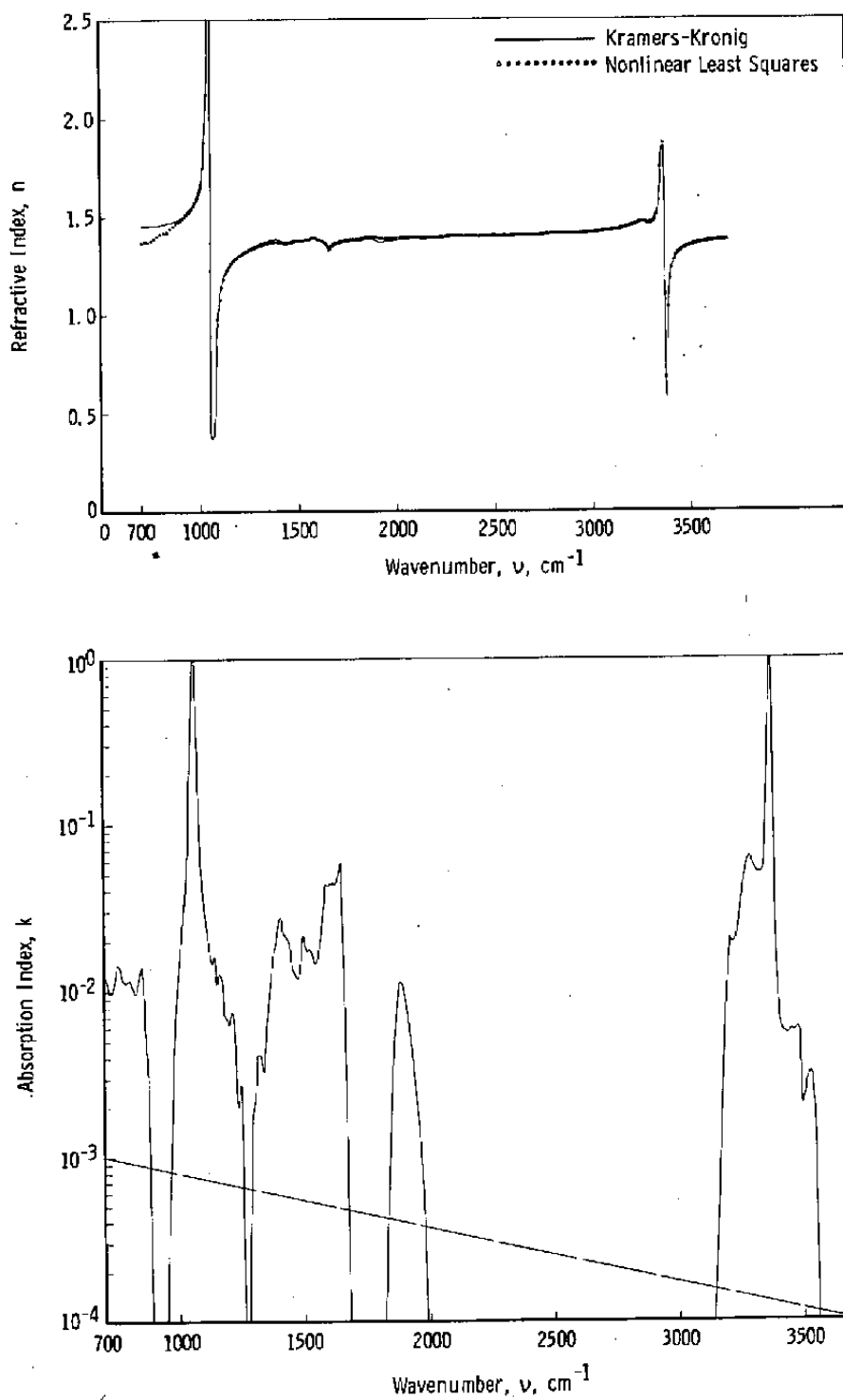


Figure 36. Optical properties of NH_3 condensed on 80°K germanium.

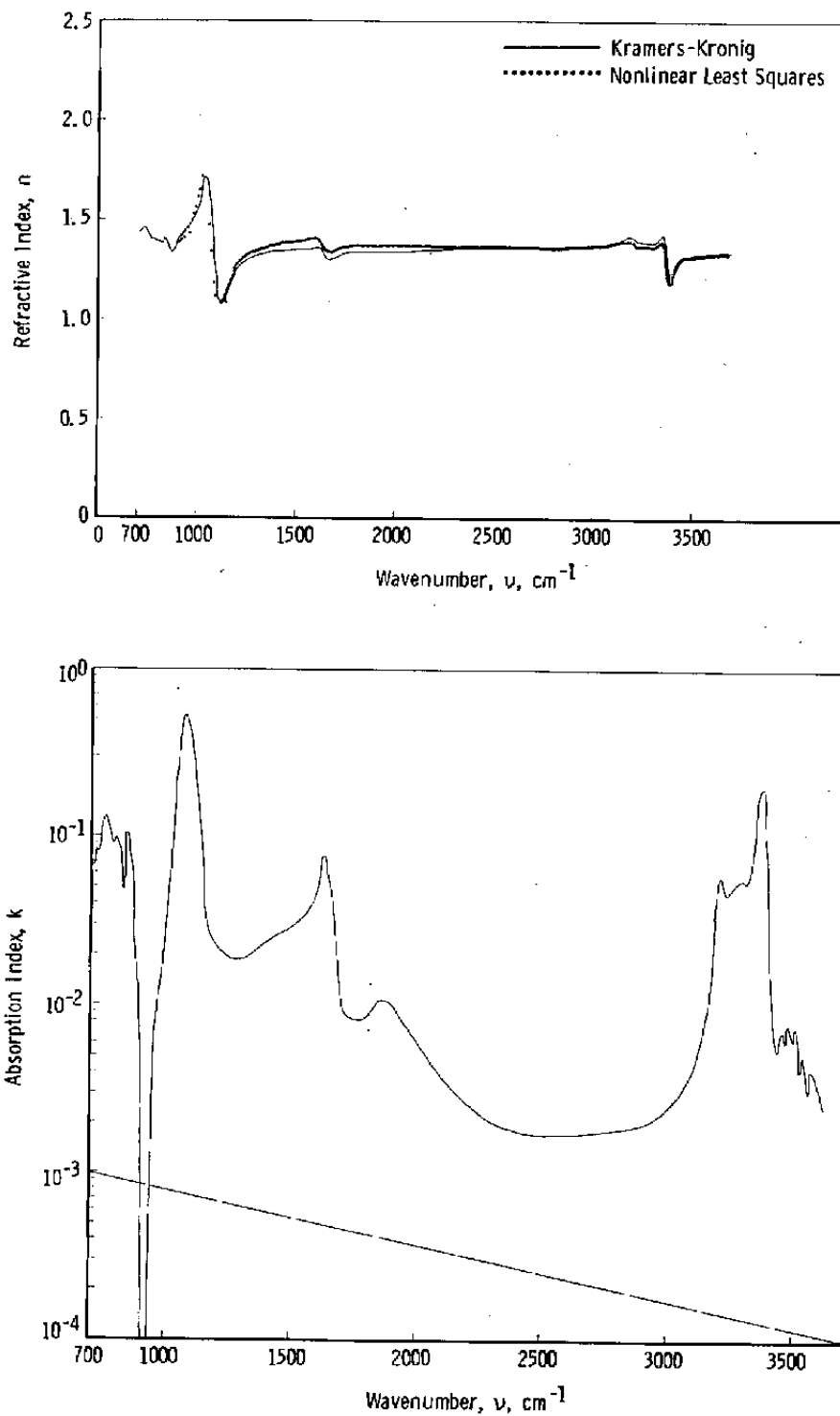


Figure 37. Optical properties for NH_3 condensed on 20°K germanium.

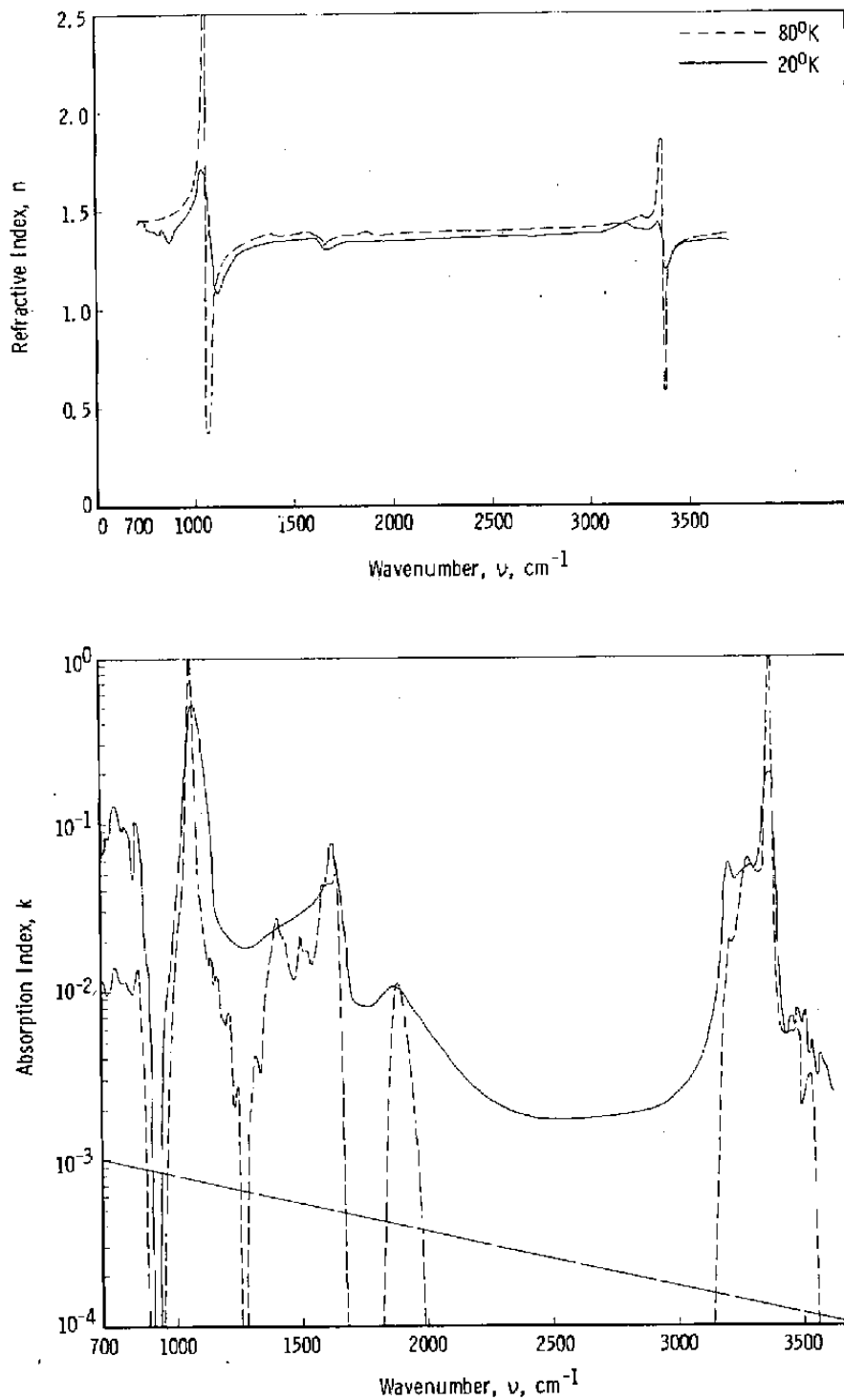


Figure 38. Effect of substrate temperature on NH_3 optical properties (20 and 80°K).

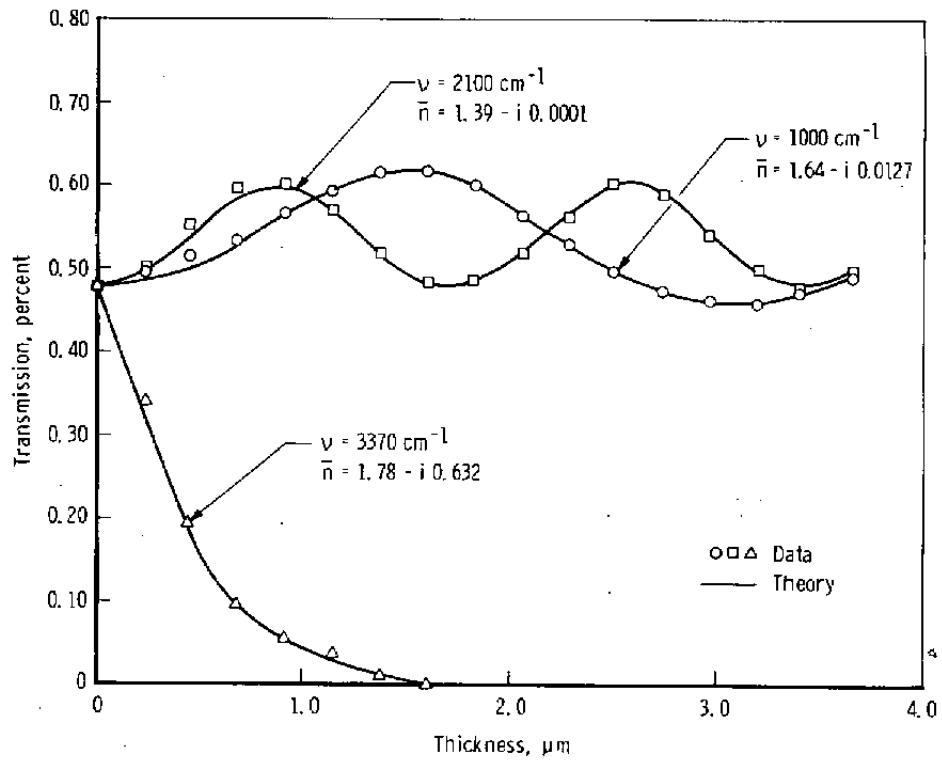


Figure 39. Comparison of theory and data for 80°K solid NH_3 for three different wavenumbers.

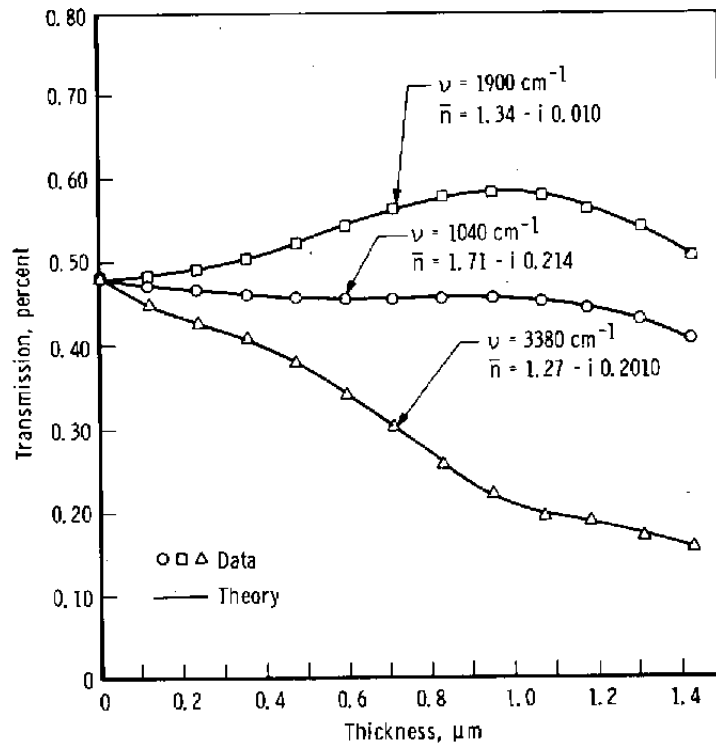


Figure 40. Comparison of theory and data for 20°K solid NH₃ for three different wavenumbers.

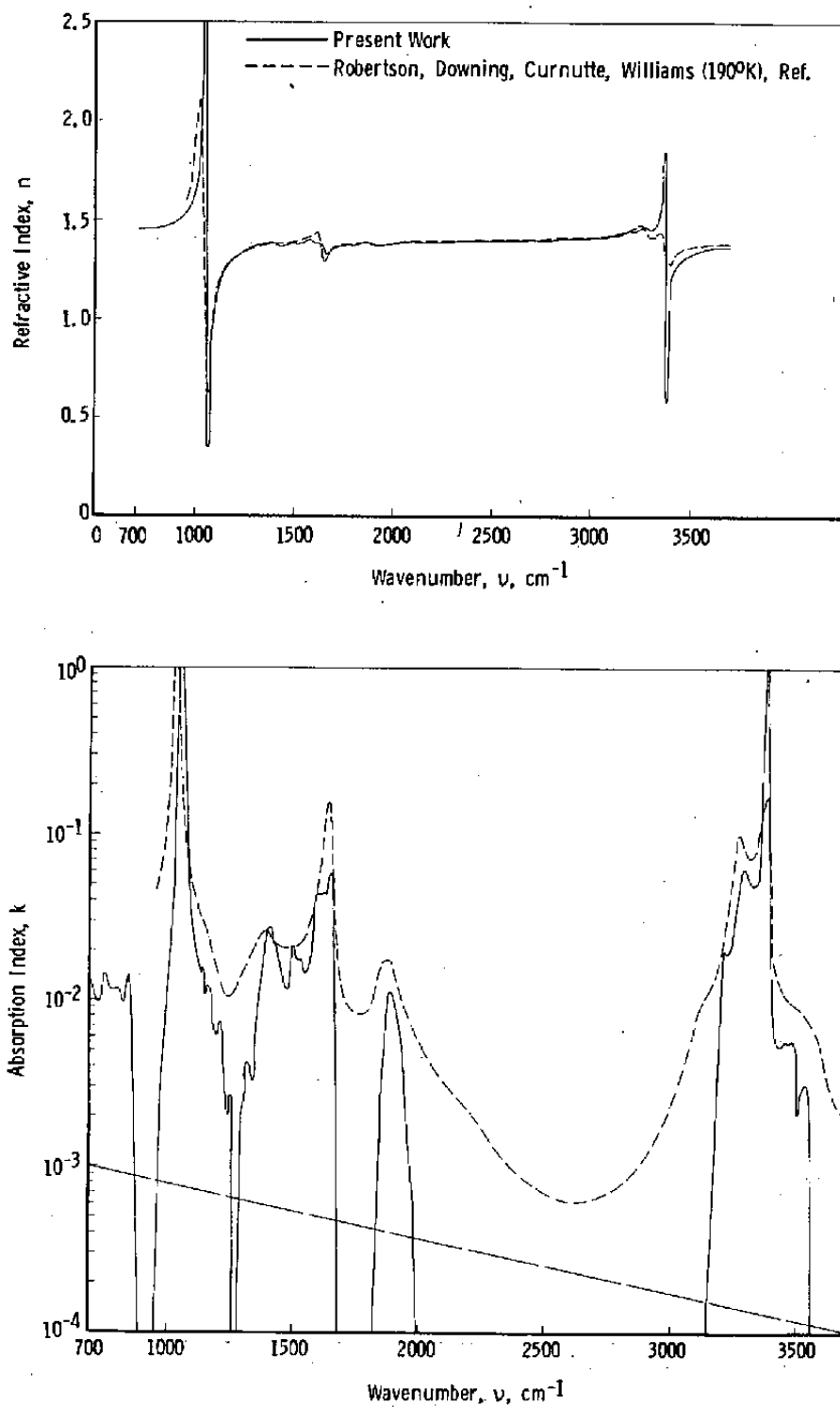


Figure 41. Comparison of results at 80°K with those of Ref. 14 at 190°K.

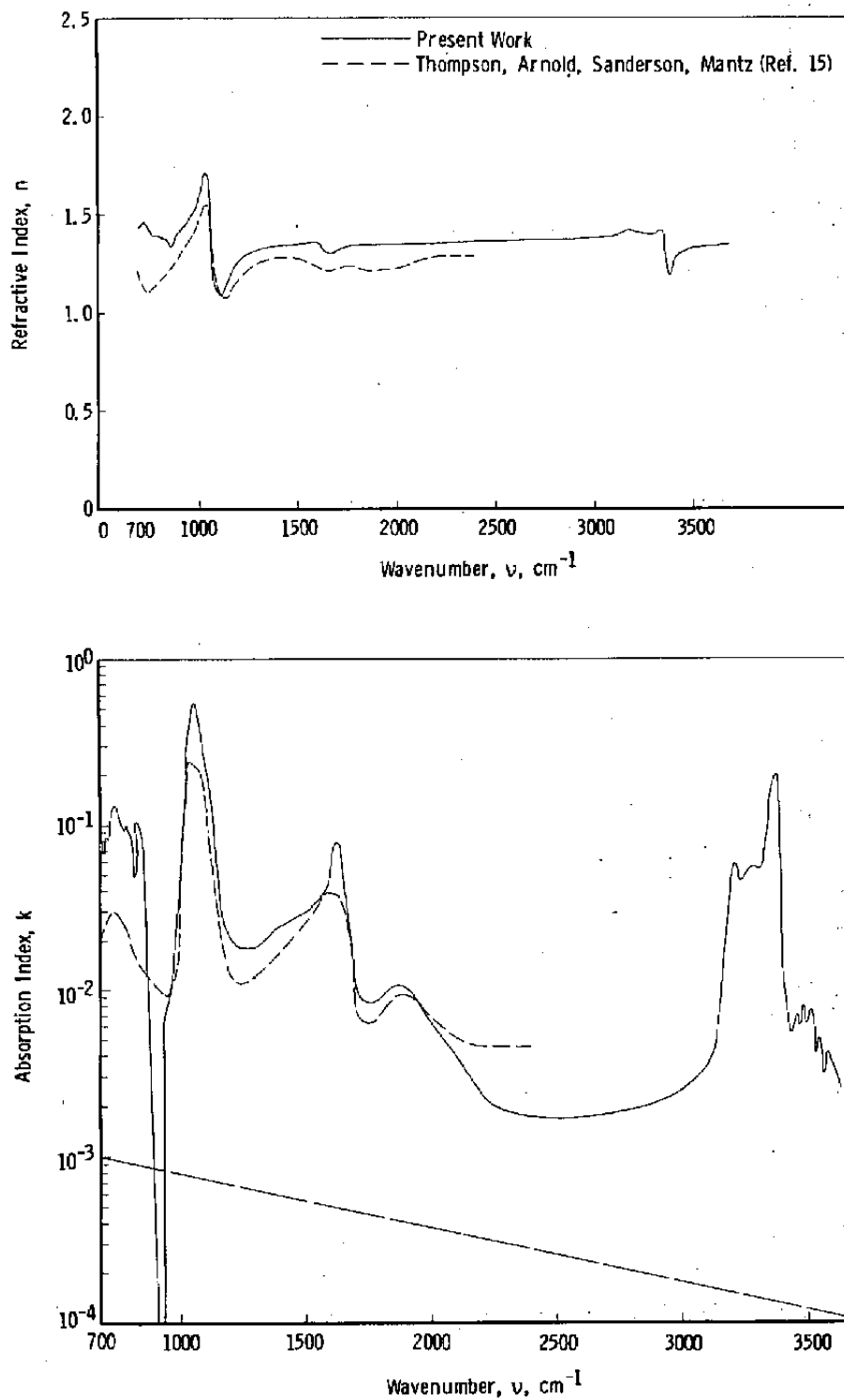


Figure 42. Comparison of results at 20°K with those of Ref. 15 at 30°K.

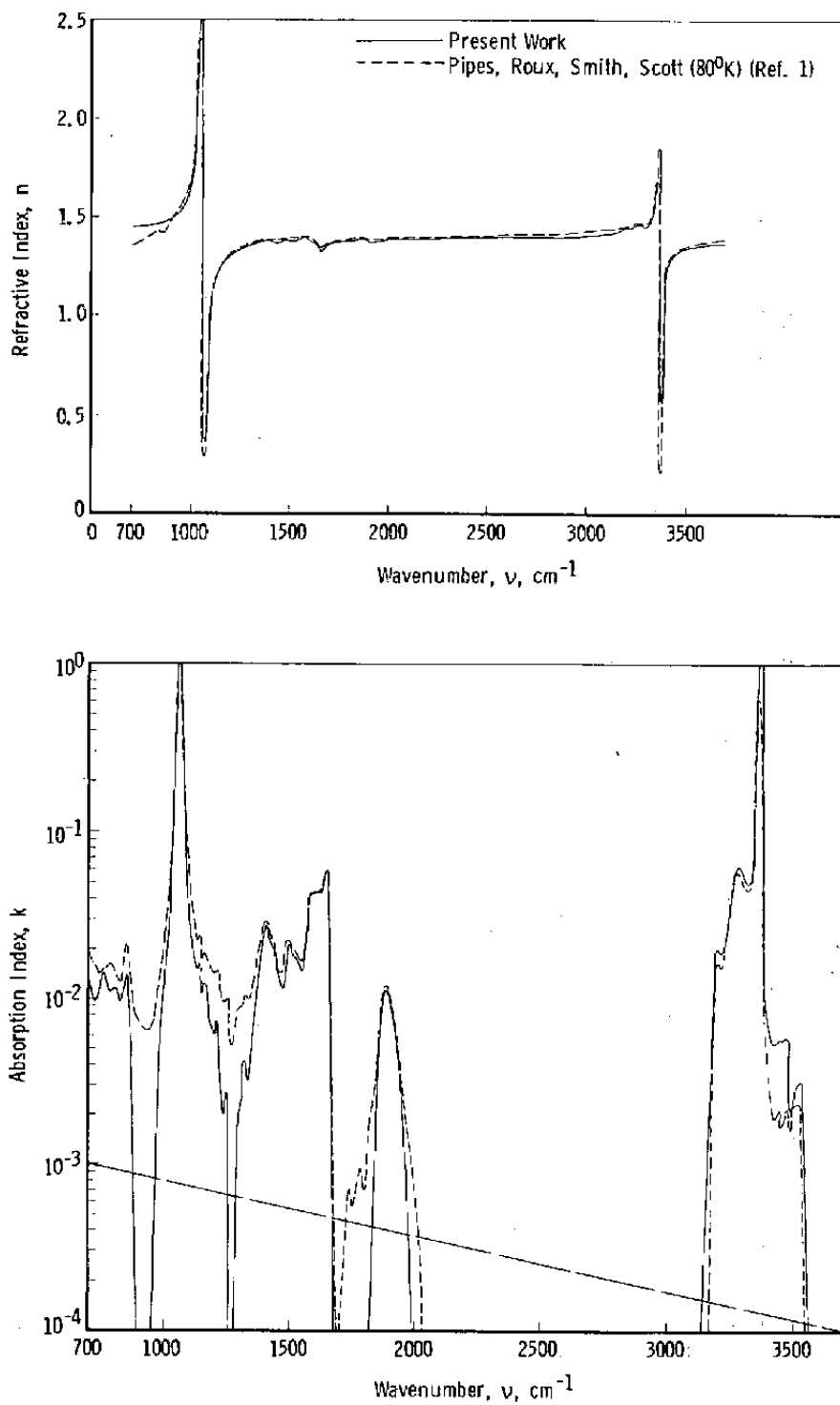


Figure 43. Comparison of results at 80°K with those of Ref. 1 at 80°K.

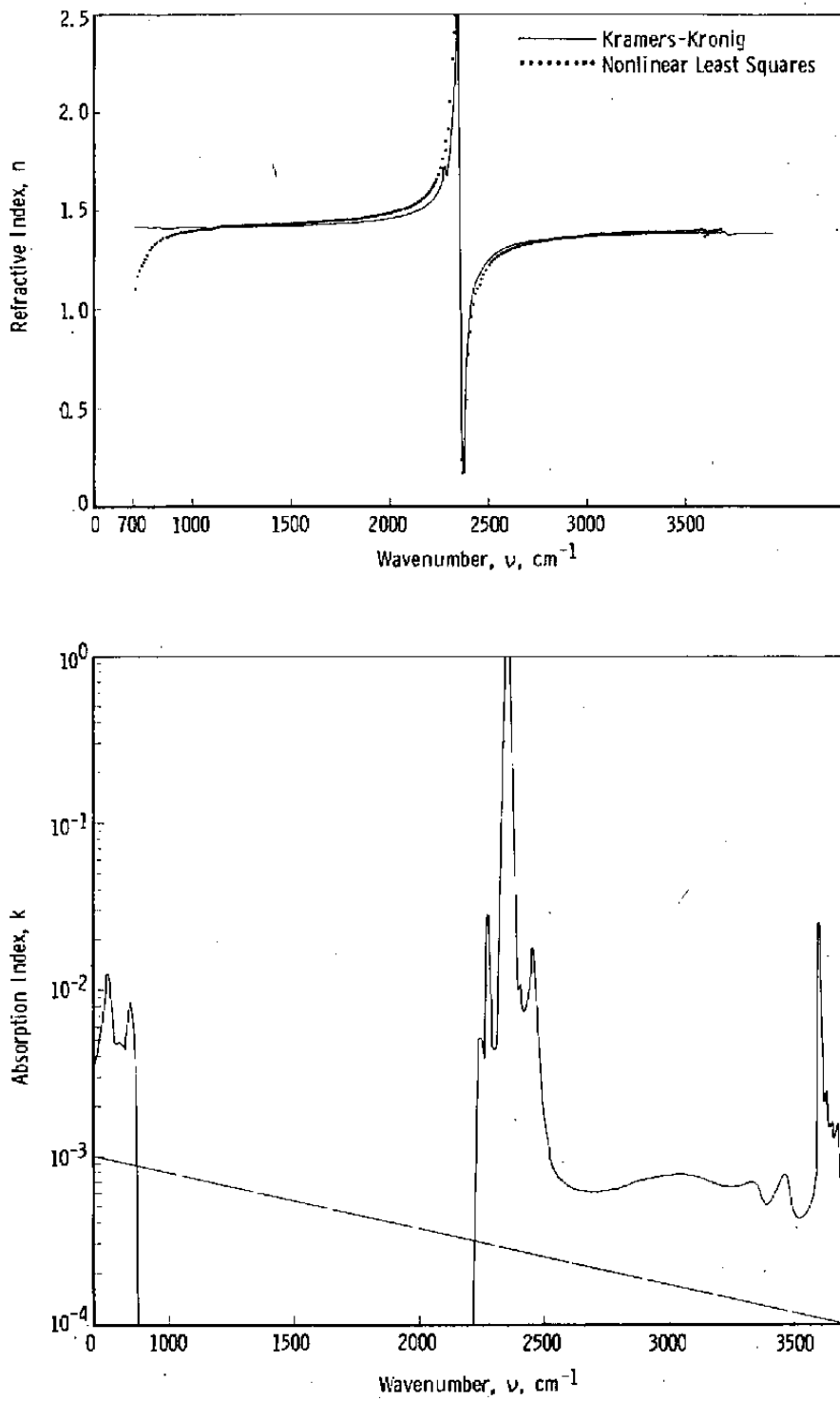


Figure 44. Optical properties of CO_2 condensed on 80°K germanium.

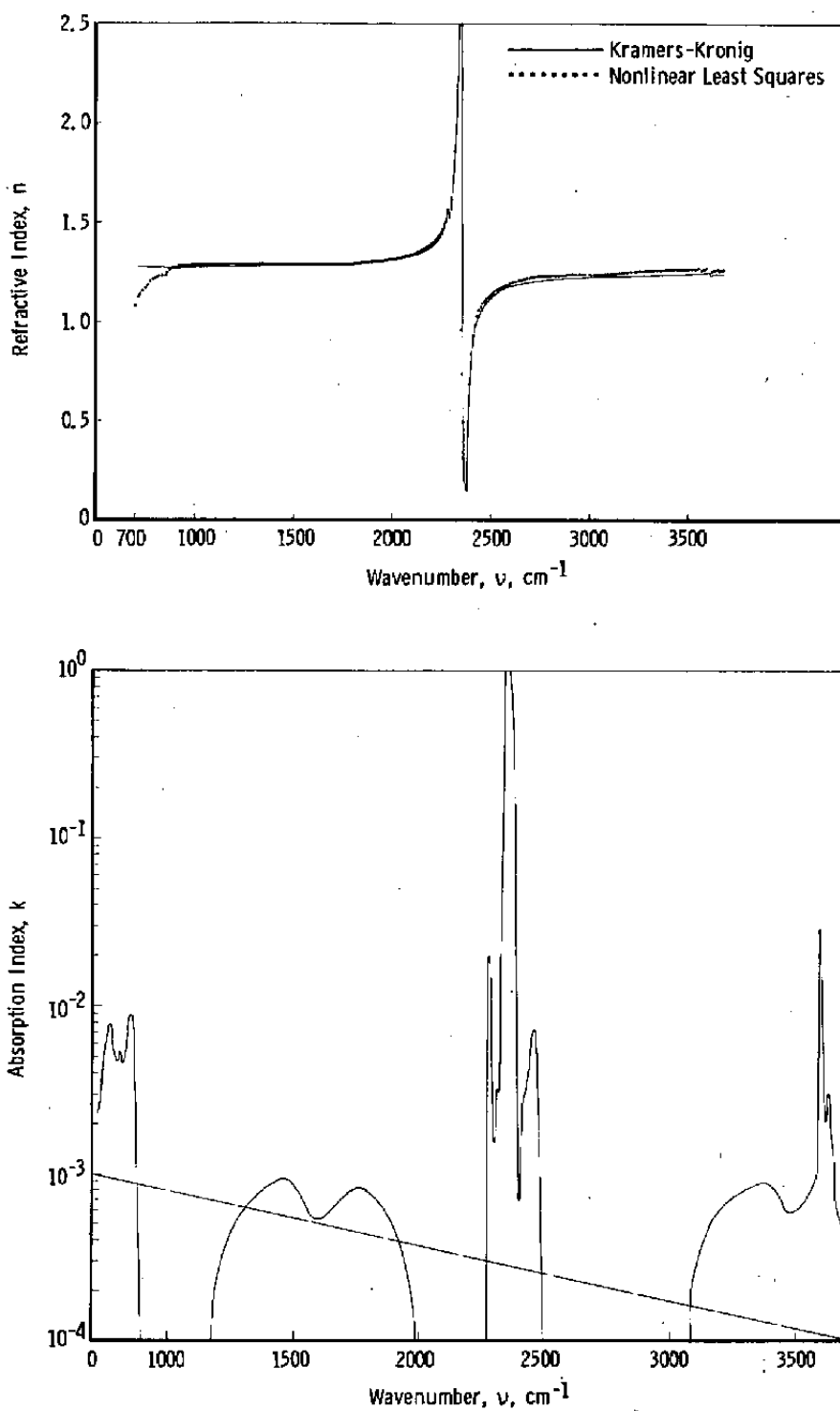


Figure 45. Optical properties of CO_2 condensed on 20°K germanium.

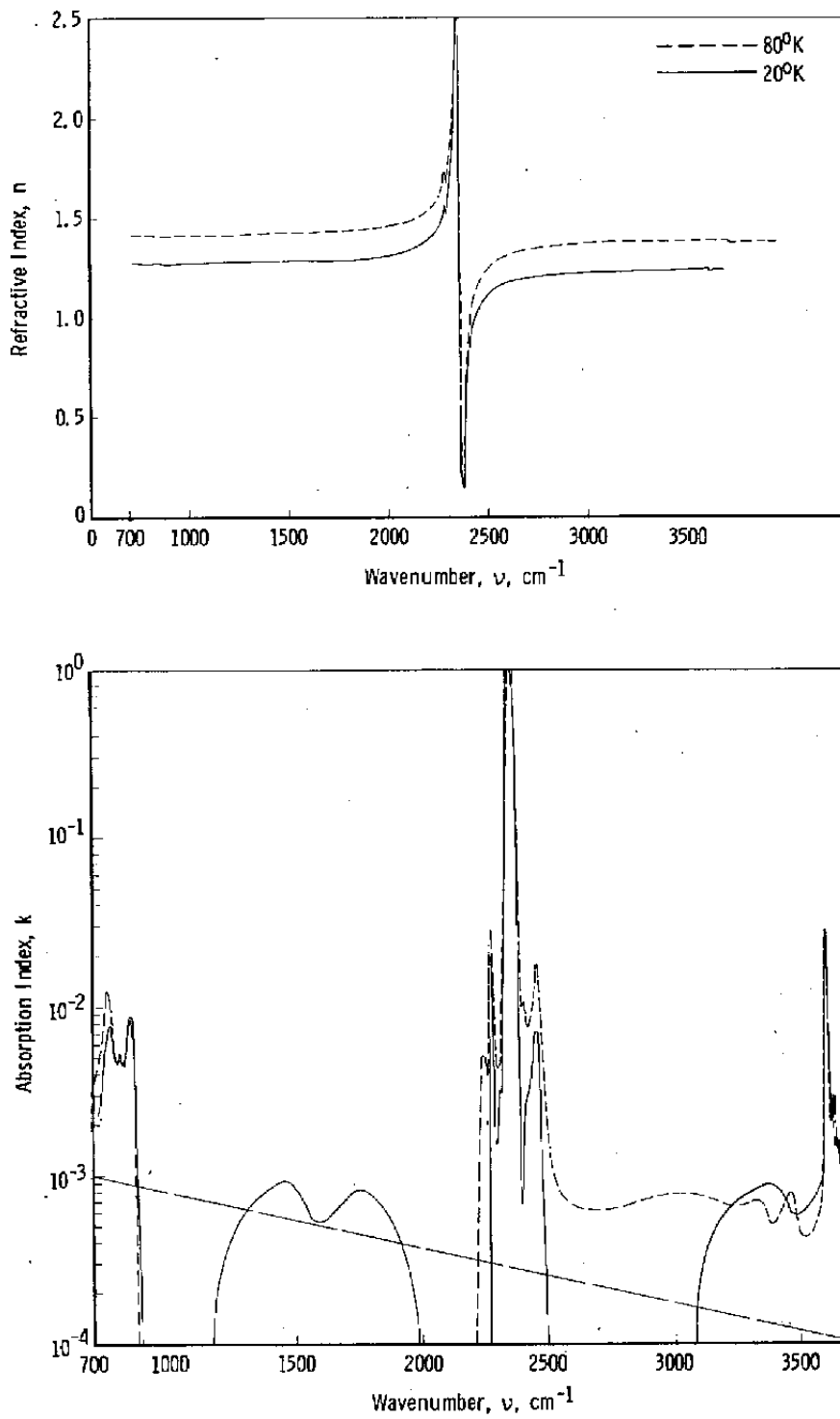


Figure 46. Effect of substrate temperature on CO_2 optical properties (20 and 80°K).

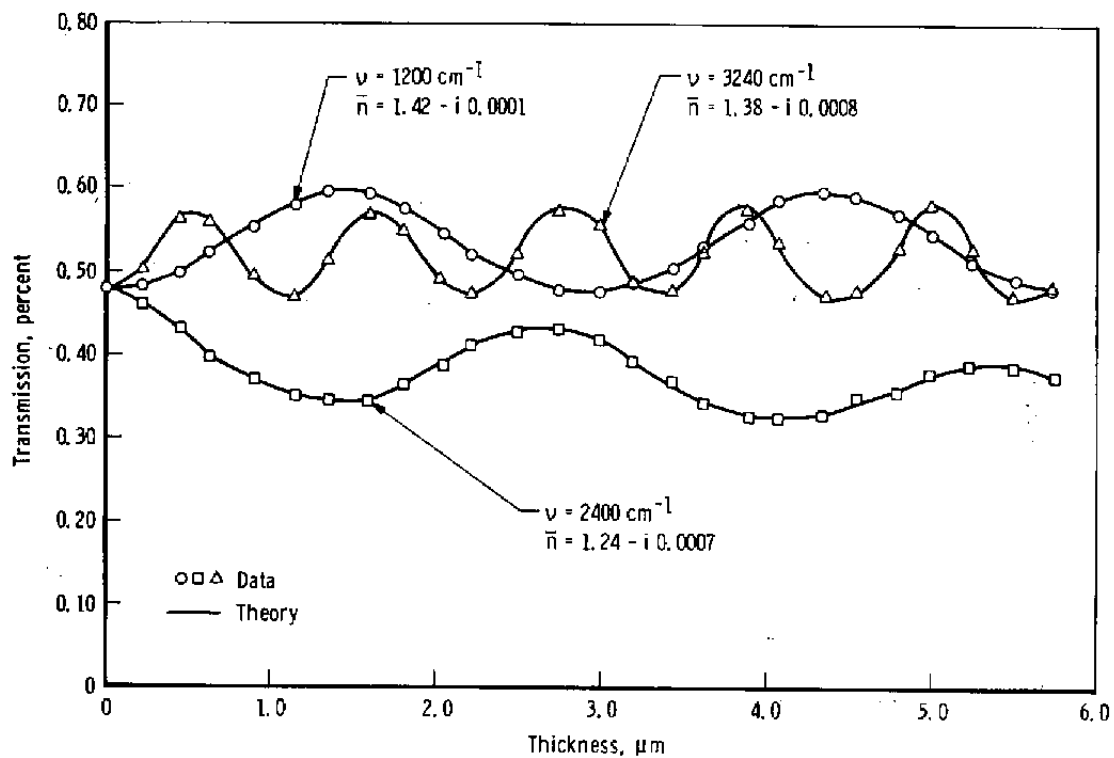


Figure 47. Comparison of theory and data for 80°K solid CO_2 for three different wavenumbers.

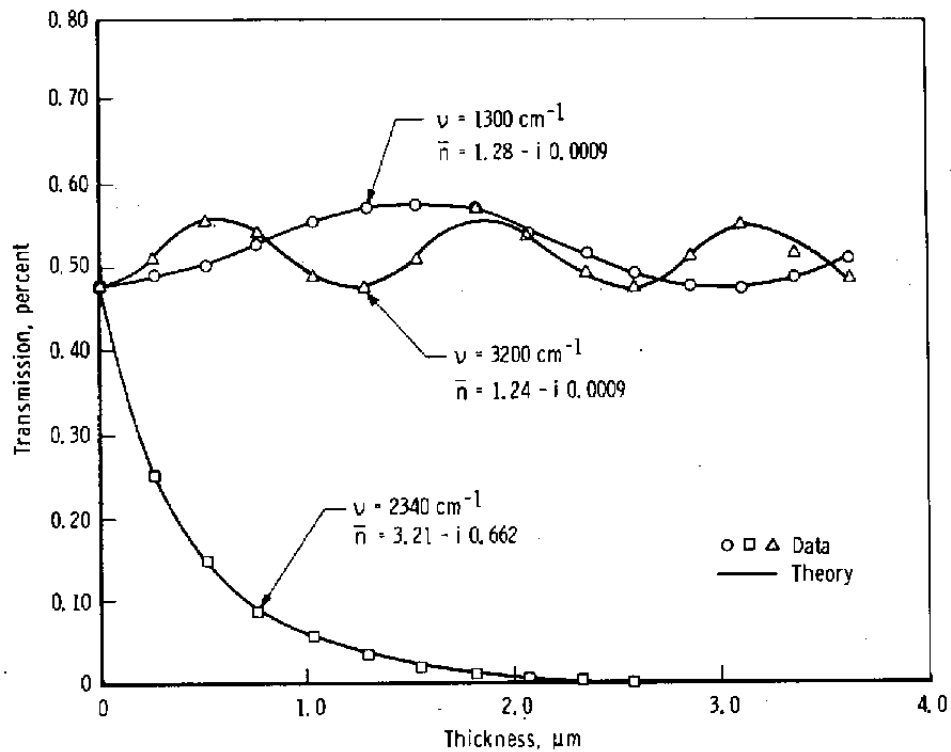


Figure 48. Comparison of theory and data for 20°K solid CO₂ for three different wavenumbers.

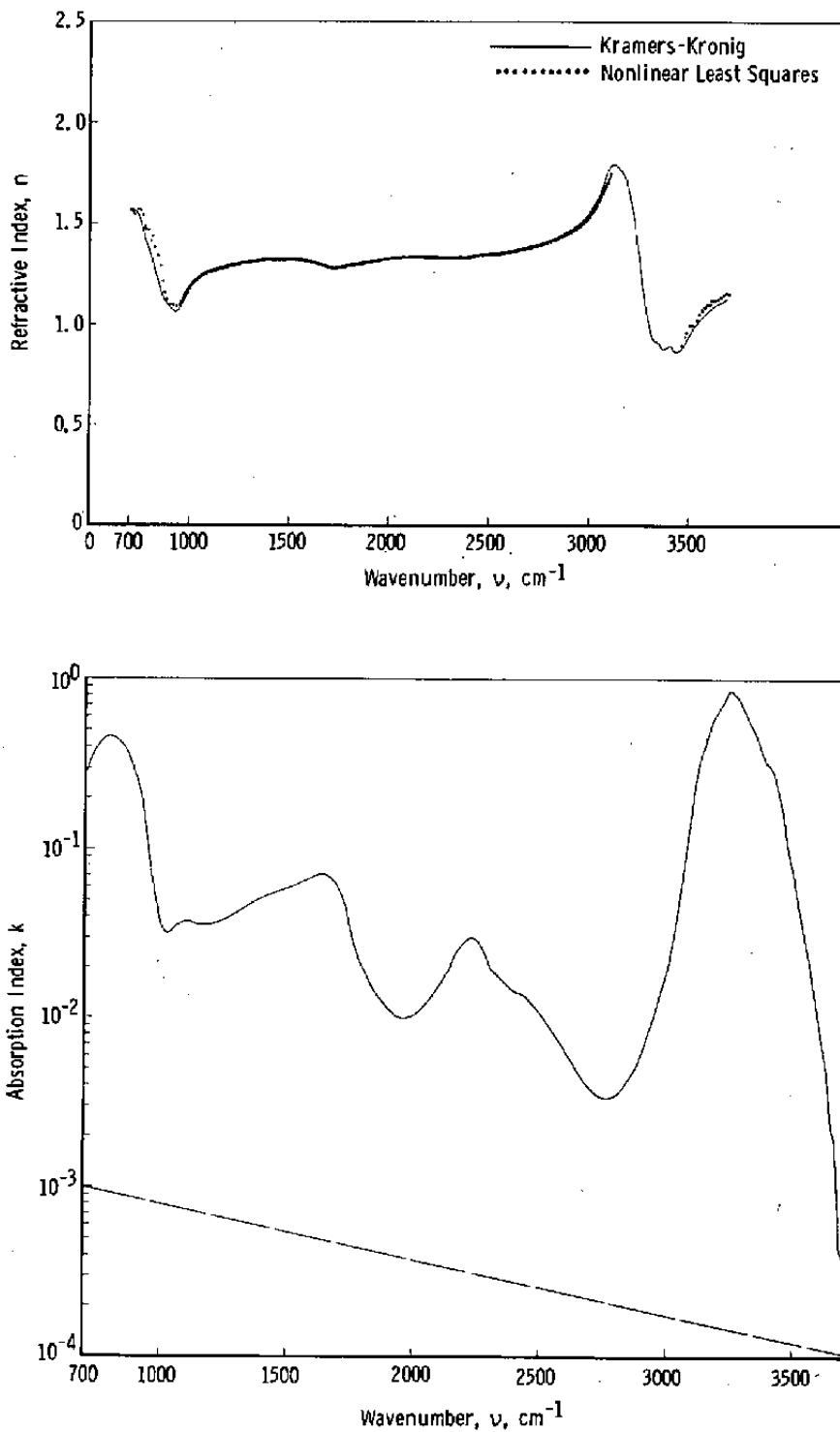


Figure 49. Optical properties for H_2O condensed on 80°K germanium.

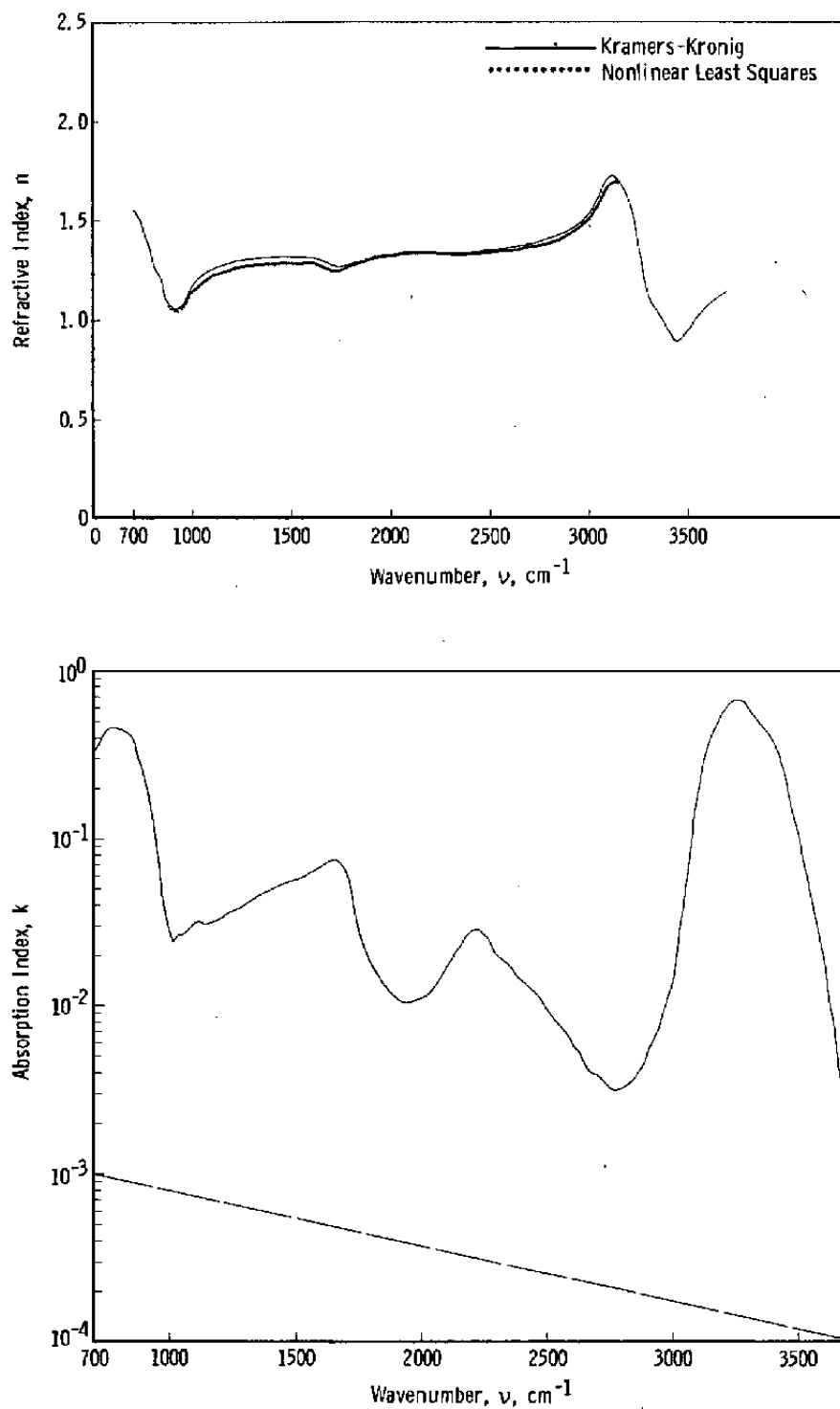


Figure 50. Optical properties for H_2O condensed on 50°K germanium.

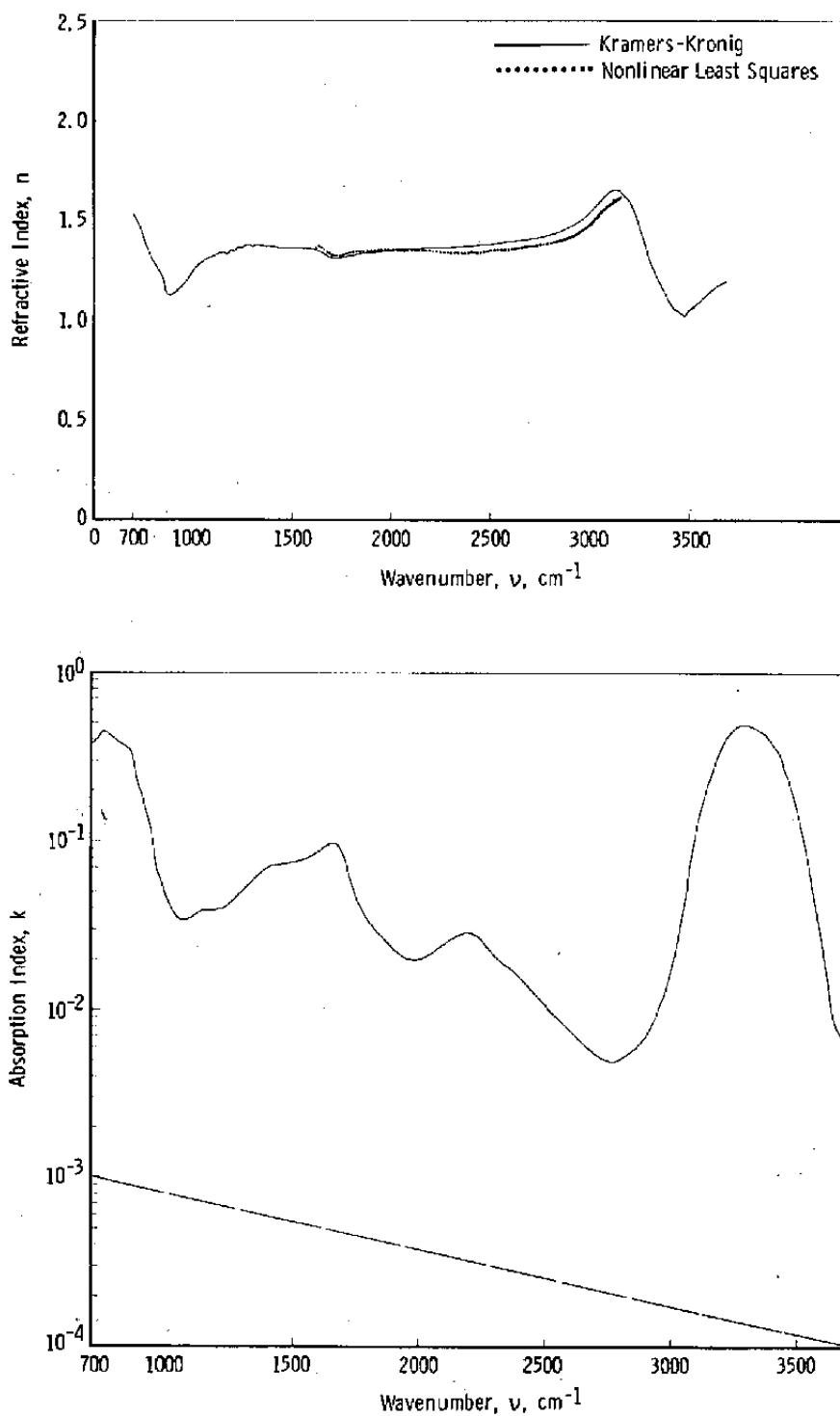


Figure 51. Optical properties for H_2O condensed on 20°K germanium.

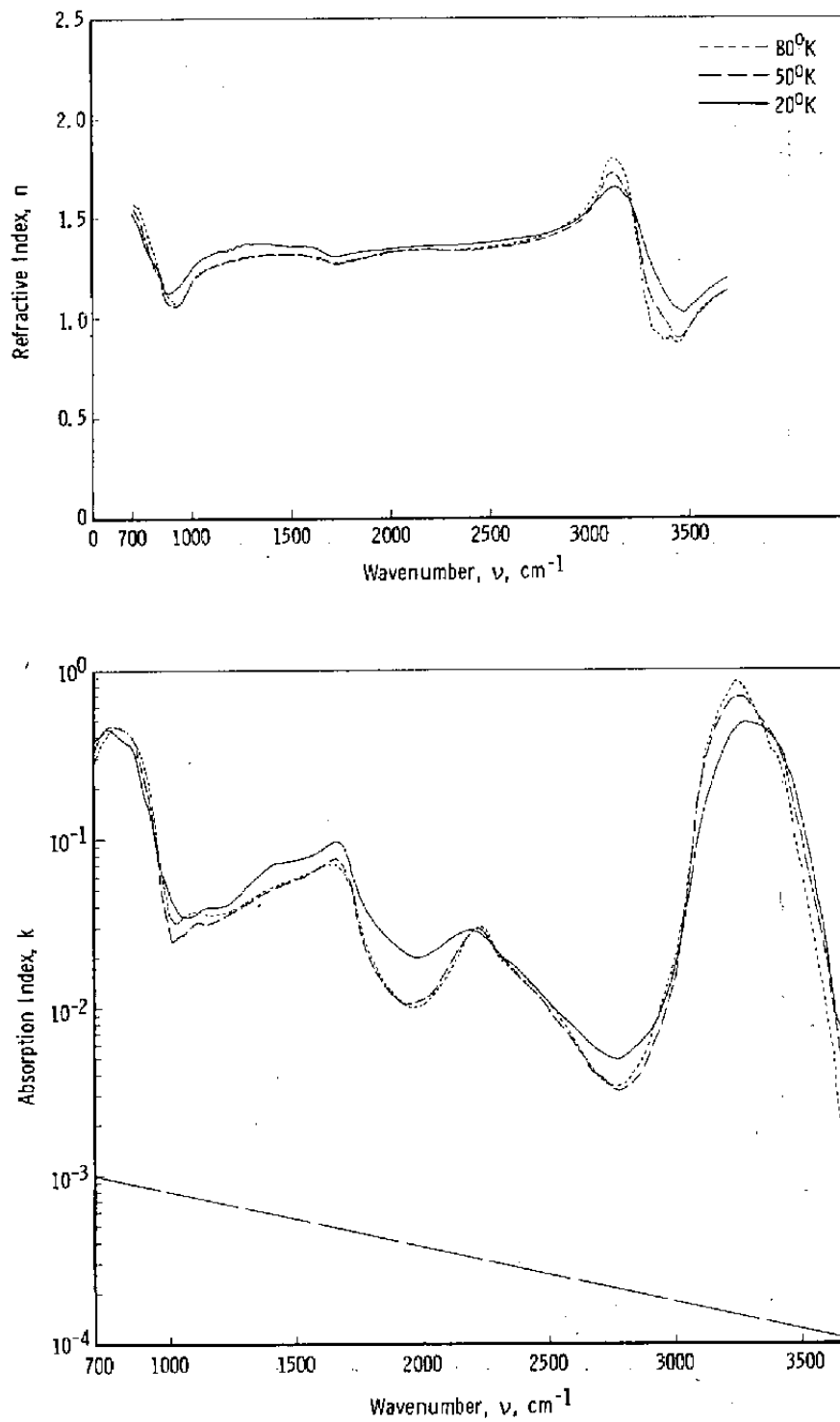


Figure 52. Effect of substrate temperature on H_2O optical properties (20, 50, and 80°K).

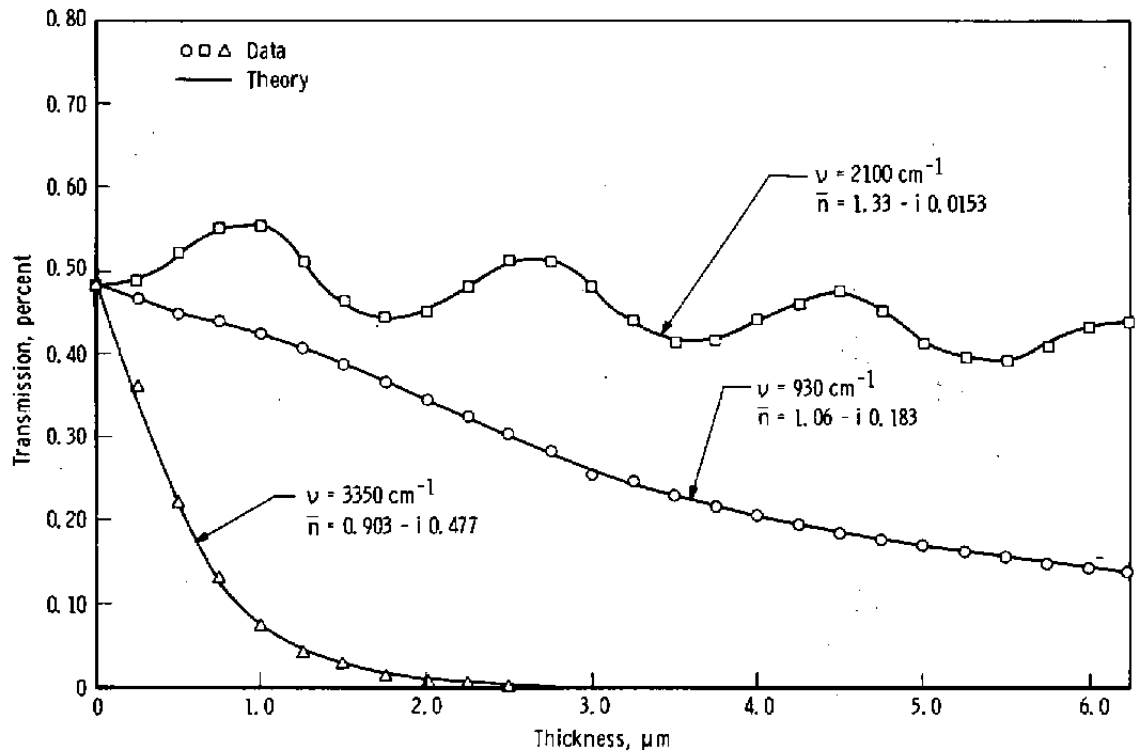


Figure 53. Comparison of theory and data for 80°K solid H₂O for three different wavenumbers.

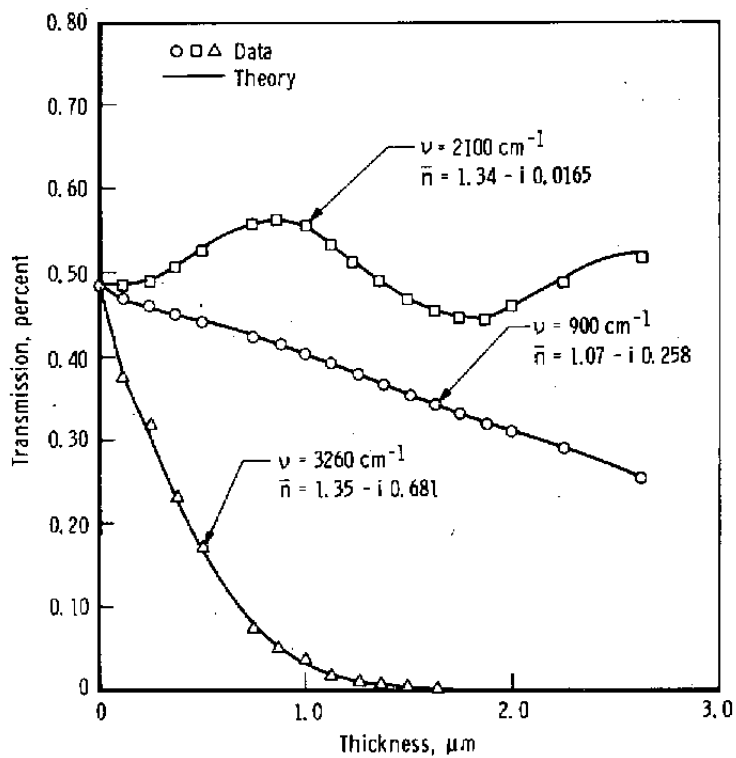


Figure 54. Comparison of theory and data for 50°K solid H₂O for three different wavenumbers.

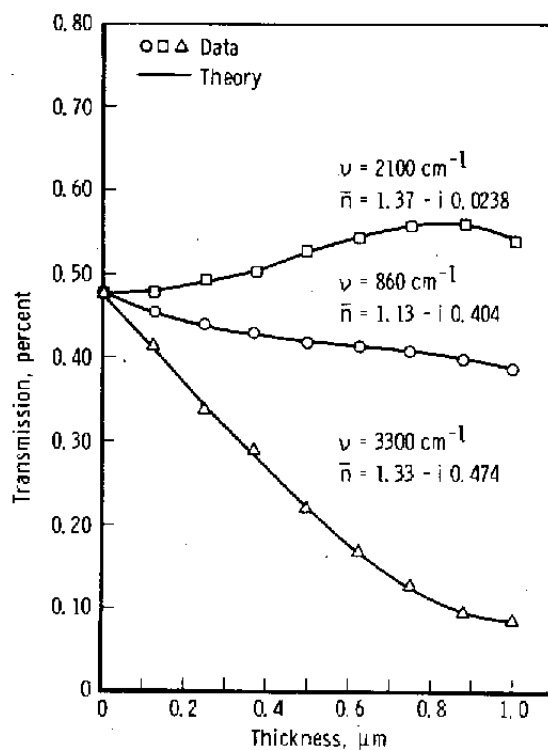


Figure 55. Comparison of theory and data for 20°K solid H₂O for three different wavenumbers.

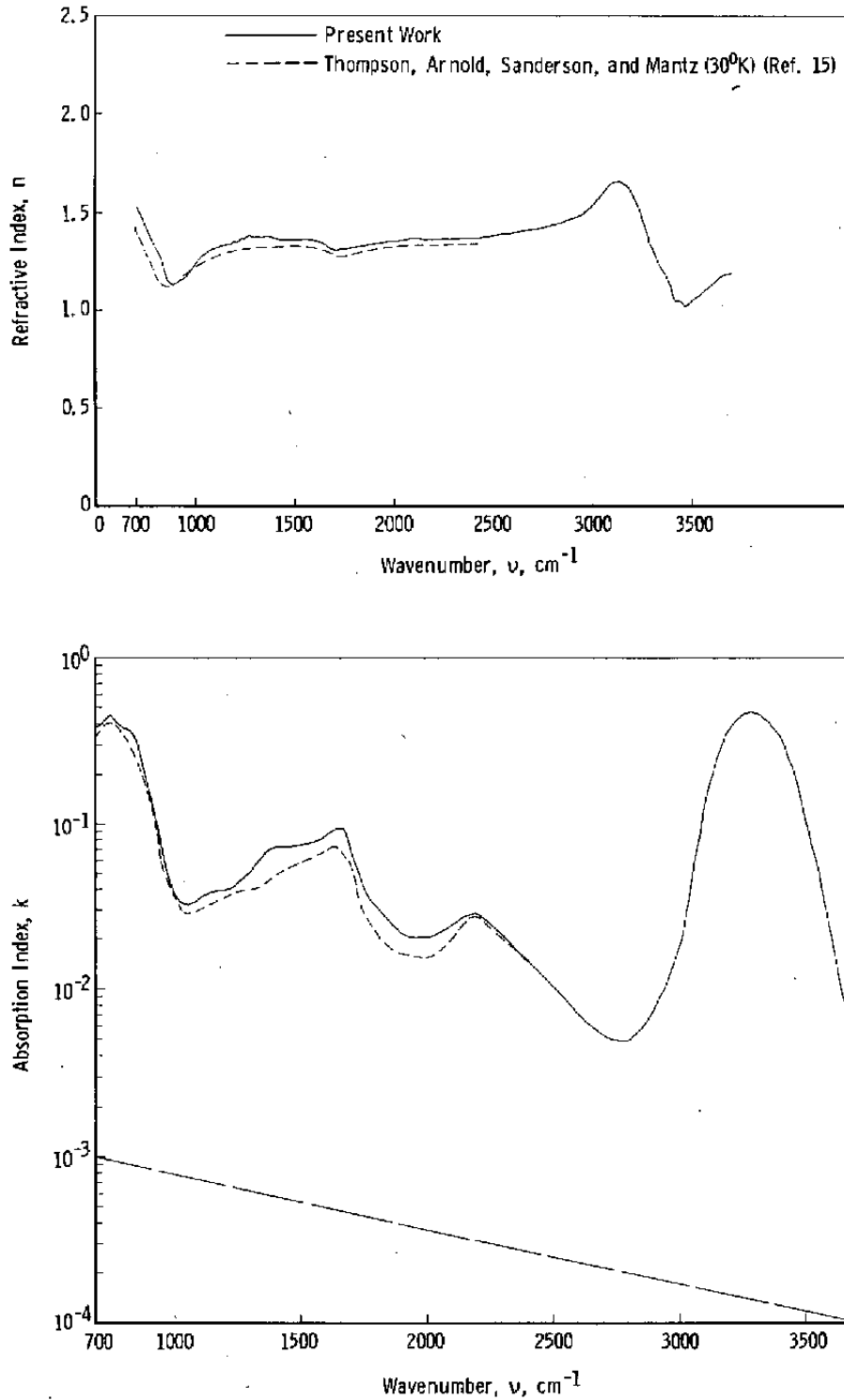


Figure 56. Comparison of results at 20°K with those of Ref. 4 at 30°K.

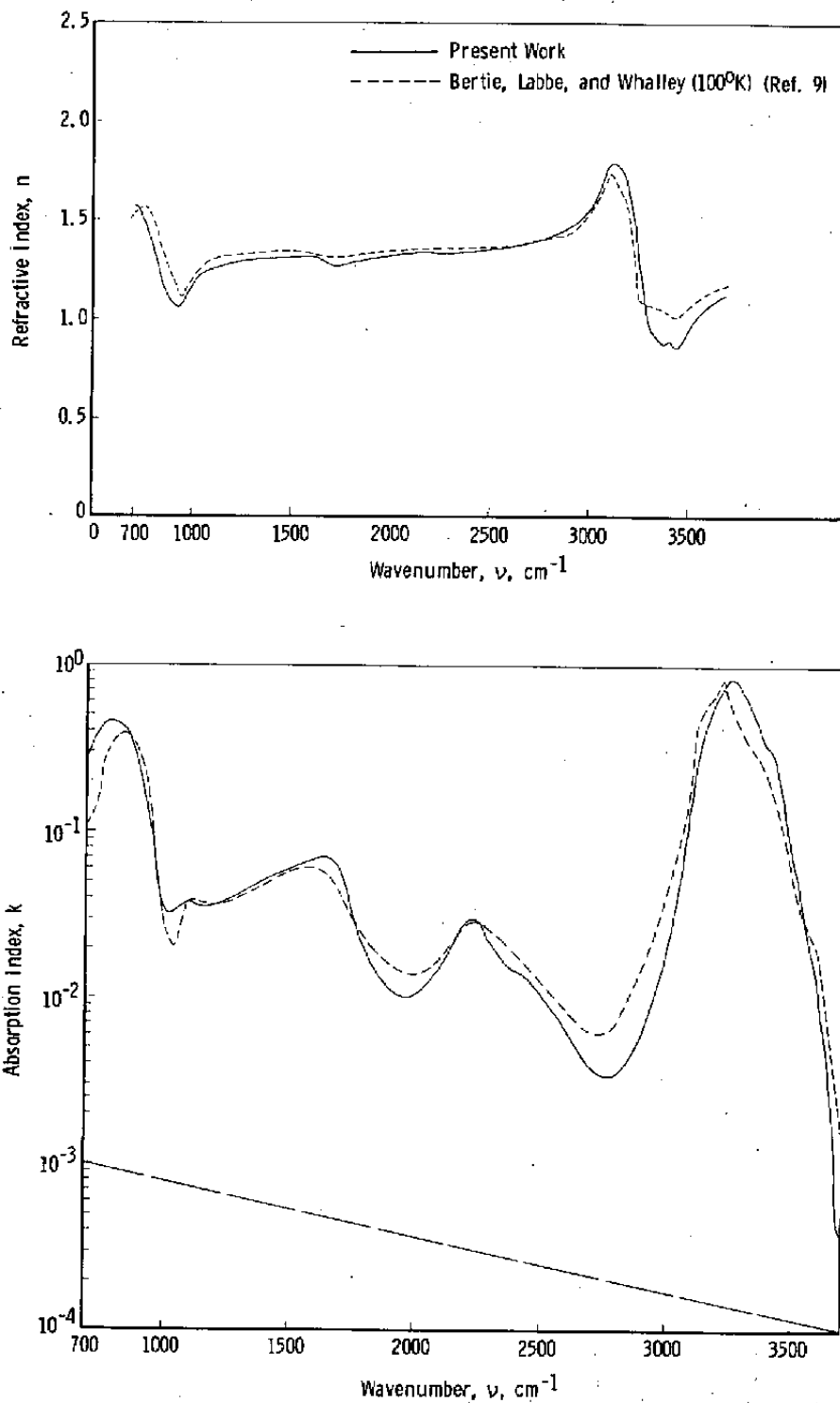


Figure 57. Comparison of results at 80°K with those of Ref. 9 at 100°K.

Table 1. Molecular Bands in NH_3 (cm^{-1})

Solid ⁴	Solid ¹	Vapor ⁷	Identification	Present	Work
				20°K	80°K
530	530	---	Lattice	525	535
1,050	1,060	950	ν_2	1,075	1,065
1,625	1,646	1,682	ν_4	1,625	1,650
3,200	3,291	3,336	ν_1	3,215	3,220
3,350	3,375	3,414	ν_3	3,380	3,385

Table 2. Molecular Bands in CO_2 (cm^{-1})

Vapor ⁷	Solid ⁴	Solid ⁸	Solid ¹	Present Work (20 and 77°K)	Identification
648	638	637	638	630	$\nu_2 - \text{C}^{13}\text{O}_2$
	654	653	654	650	$\nu_2 - \text{C}^{12}\text{O}_2$
667	660	660	660	665	$\nu_2 - \text{C}^{12}\text{O}_2$
				755	
2,283	2,282	2,280	2,282	2,270	
				2,285	$\nu_3 - \text{C}^{13}\text{O}_2$
2,349	2,343	2,344	2,345	2,320	
				2,345	$\nu_3 - \text{C}^{12}\text{O}_2$
3,609	2,370/2,460	2,379/2,454	2,455	2,460	$\nu_3 + \text{Lattice}$
	3,600	3,610	3,600	3,600	$2\nu_2 + \nu_3$
3,716				3,635	
	3,710	3,712		3,710	$\nu_1 + \nu_3$

Table 3. Molecular Bands in H_2O (cm^{-1})

Solid ⁴	Vapor ⁷	Present Work			Identification
		80°K	50°K	20°K	
750		825	820	800	Libration- ν_L
1,650	1,595	1,665	1,665	1,665	ν_2
		2,245	2,220	2,220	$\nu_2 + \nu_L$
3,300	3,652	3,255	3,260	3,300	ν_1
	3,756				ν_3

Table 4. Solid NH₃ Optical Properties at 80°K

ν , cm ⁻¹	n	k	ν , cm ⁻¹	n	k
3690	1.369652	0.000100	3452	1.314741	0.005868
3680	1.369030	0.000100	3450	1.312998	0.005745
3670	1.368171	0.000100	3448	1.311069	0.005732
3660	1.367454	0.000100	3446	1.309055	0.005787
3650	1.366476	0.000100	3444	1.307181	0.006029
3640	1.365643	0.000100	3442	1.305237	0.005843
3630	1.364513	0.000100	3440	1.302949	0.005473
3620	1.363531	0.000100	3438	1.300343	0.005455
3610	1.362203	0.000100	3436	1.297675	0.005262
3600	1.361022	0.000100	3434	1.294639	0.005161
3590	1.359419	0.000100	3432	1.291512	0.005224
3580	1.357947	0.000100	3430	1.288159	0.005286
3570	1.355891	0.000100	3428	1.284704	0.005290
3560	1.353596	0.000100	3426	1.280824	0.005297
3550	1.350690	0.001100	3424	1.276667	0.005246
3540	1.349263	0.003000	3422	1.272056	0.005480
3530	1.347668	0.003200	3420	1.267297	0.005638
3520	1.346169	0.003000	3418	1.262006	0.005797
3510	1.342537	0.002800	3416	1.256327	0.005932
3500	1.334663	0.002100	3414	1.249821	0.005981
3498	1.335836	0.005243	3412	1.242789	0.006377
3496	1.335575	0.005176	3410	1.234765	0.006516
3494	1.336061	0.005235	3408	1.225845	0.007095
3492	1.334957	0.005365	3406	1.215856	0.007861
3490	1.334805	0.005423	3404	1.204617	0.008662
3488	1.333764	0.005720	3402	1.191882	0.009751
3486	1.333629	0.006012	3400	1.177144	0.011273
3484	1.332830	0.005888	3396	1.136586	0.012352
3482	1.332334	0.005885	3394	1.109916	0.017065
3480	1.331269	0.005872	3392	1.075804	0.022933
3478	1.330694	0.006097	3390	1.033684	0.033977
3476	1.329899	0.006090	3388	0.978942	0.052102
3474	1.329165	0.005733	3386	0.905191	0.083600
3472	1.327860	0.005604	3384	0.805877	0.146280
3470	1.326794	0.005738	3382	0.689814	0.280650
3468	1.325594	0.005738	3380	0.579397	0.510160
3466	1.324516	0.005815	3378	0.697236	0.971980
3464	1.323250	0.005779	3376	1.154419	1.279300
3462	1.322052	0.005836	3374	1.606706	1.056700
3460	1.320583	0.005690	3372	1.762773	0.774990
3458	1.319165	0.005920	3370	1.782904	0.632150
3456	1.317752	0.005983	3368	1.828267	0.546490
3454	1.316349	0.005954	3366	1.858737	0.395460
			3364	1.835265	0.277470

Table 4. Continued

ν , cm^{-1}	n	k	ν , cm^{-1}	n	k
3362	1.784056	0.195470	3274	1.466587	0.053488
3360	1.735695	0.145960	3272	1.467364	0.051349
3358	1.691406	0.115260	3270	1.467538	0.049568
3356	1.657908	0.094924	3268	1.468267	0.047407
3354	1.627877	0.080823	3266	1.468154	0.045195
3352	1.604536	0.070959	3264	1.468494	0.043063
3350	1.583241	0.064396	3262	1.468120	0.040780
3348	1.566785	0.059380	3260	1.467335	0.037827
3346	1.551041	0.055868	3258	1.466060	0.037122
3344	1.538840	0.053852	3256	1.465909	0.035469
3342	1.527492	0.052550	3254	1.465244	0.033851
3340	1.518858	0.051291	3252	1.464729	0.032182
3338	1.509908	0.050241	3250	1.463780	0.030719
3336	1.503005	0.050061	3248	1.463237	0.029323
3334	1.496249	0.050021	3246	1.462207	0.027818
3332	1.491165	0.049776	3244	1.461507	0.026543
3330	1.485592	0.049852	3242	1.460383	0.025271
3328	1.481529	0.050207	3240	1.459549	0.023965
3326	1.477302	0.050657	3238	1.458163	0.022947
3324	1.474609	0.051102	3236	1.457331	0.022121
3322	1.471384	0.050968	3234	1.456039	0.021192
3320	1.468914	0.050878	3232	1.455145	0.020452
3318	1.465879	0.051112	3230	1.453802	0.019865
3316	1.463663	0.051024	3228	1.452904	0.019261
3314	1.460715	0.051479	3226	1.451465	0.018969
3312	1.458809	0.052229	3224	1.450657	0.018913
3310	1.456717	0.053136	3222	1.449479	0.018968
3308	1.455354	0.053714	3220	1.449049	0.019287
3306	1.453504	0.054877	3218	1.448413	0.019651
3304	1.452811	0.056273	3216	1.448612	0.019938
3302	1.451894	0.057360	3214	1.448472	0.020166
3300	1.451857	0.058732	3212	1.449338	0.020394
3298	1.451864	0.060133	3210	1.449944	0.020069
3296	1.452899	0.060974	3208	1.451215	0.019170
3294	1.453501	0.061549	3206	1.451433	0.017701
3292	1.454720	0.061864	3204	1.451993	0.016254
3290	1.455574	0.062148	3202	1.451508	0.014676
3288	1.457224	0.062175	3200	1.451486	0.013089
3286	1.458426	0.061756	3198	1.450356	0.011774
3284	1.460202	0.061213	3196	1.450063	0.010620
3282	1.461534	0.060304	3194	1.448728	0.009612
3280	1.463341	0.059006	3192	1.448529	0.008814
3278	1.464441	0.057422	3190	1.447171	0.007987
3276	1.465945	0.055647	3188	1.447106	0.007221

Table 4. Continued

ν , cm^{-1}	n	k	ν , cm^{-1}	n	k
3186	1.445558	0.006763	2770	1.401098	0.000100
3184	1.446288	0.006378	2760	1.400826	0.000100
3182	1.445833	0.005961	2750	1.400556	0.000100
3180	1.447212	0.002200	2740	1.400296	0.000100
3170	1.438022	0.001300	2730	1.400038	0.000100
3160	1.433626	0.000700	2720	1.399789	0.000100
3150	1.430910	0.000300	2710	1.399541	0.000100
3140	1.427995	0.000100	2700	1.399302	0.000100
3130	1.425840	0.000100	2690	1.399063	0.000100
3120	1.423788	0.000100	2680	1.398832	0.000100
3110	1.422163	0.000100	2670	1.398602	0.000100
3100	1.420575	0.000100	2660	1.398379	0.000100
3090	1.419250	0.000100	2650	1.398155	0.000100
3080	1.417958	0.000100	2640	1.397939	0.000100
3070	1.416846	0.000100	2630	1.397722	0.000100
3060	1.415763	0.000100	2620	1.397511	0.000100
3050	1.414810	0.000100	2610	1.397299	0.000100
3040	1.413883	0.000100	2600	1.397093	0.000100
3030	1.413053	0.000100	2590	1.396886	0.000100
3020	1.412249	0.000100	2580	1.396684	0.000100
3010	1.411517	0.000100	2570	1.396481	0.000100
3000	1.410808	0.000100	2560	1.396282	0.000100
2990	1.410156	0.000100	2550	1.396082	0.000100
2980	1.409526	0.000100	2540	1.395887	0.000100
2970	1.408939	0.000100	2530	1.395690	0.000100
2960	1.408373	0.000100	2520	1.395496	0.000100
2950	1.407841	0.000100	2510	1.395301	0.000100
2940	1.407329	0.000100	2500	1.395110	0.000100
2930	1.406844	0.000100	2490	1.394916	0.000100
2920	1.406376	0.000100	2480	1.394725	0.000100
2910	1.405930	0.000100	2470	1.394533	0.000100
2900	1.405501	0.000100	2460	1.394343	0.000100
2890	1.405090	0.000100	2450	1.394151	0.000100
2880	1.404693	0.000100	2440	1.393961	0.000100
2870	1.404311	0.000100	2430	1.393769	0.000100
2860	1.403943	0.000100	2420	1.393578	0.000100
2850	1.403586	0.000100	2410	1.393386	0.000100
2840	1.403242	0.000100	2400	1.393194	0.000100
2830	1.402908	0.000100	2390	1.393001	0.000100
2820	1.402586	0.000100	2380	1.392808	0.000100
2810	1.402270	0.000100	2370	1.392612	0.000100
2800	1.401967	0.000100	2360	1.392417	0.000100
2790	1.401669	0.000100	2350	1.392219	0.000100
2780	1.401382	0.000100	2340	1.392022	0.000100

Table 4. Continued

ν , cm^{-1}	\underline{n}	\underline{k}	ν , cm^{-1}	\underline{n}	\underline{k}
2330	1.391821	0.000100	1870	1.386197	0.007500
2320	1.391620	0.000100	1860	1.386017	0.004400
2310	1.391416	0.000100	1850	1.384753	0.002500
2300	1.391211	0.000100	1840	1.383249	0.001200
2290	1.391003	0.000100	1830	1.381593	0.000300
2280	1.390793	0.000100	1820	1.379957	0.000100
2270	1.390580	0.000100	1810	1.378630	0.000100
2260	1.390365	0.000100	1800	1.377458	0.000100
2250	1.390146	0.000100	1790	1.376330	0.000100
2240	1.389925	0.000100	1780	1.375175	0.000100
2230	1.389699	0.000100	1770	1.373990	0.000100
2220	1.389470	0.000100	1760	1.372709	0.000100
2200	1.389000	0.000100	1750	1.371339	0.000100
2180	1.388511	0.000100	1740	1.369798	0.000100
2170	1.388258	0.000100	1730	1.368072	0.000100
2160	1.387999	0.000100	1720	1.366044	0.000100
2150	1.387734	0.000100	1710	1.363622	0.000100
2140	1.387462	0.000100	1700	1.360557	0.000100
2130	1.387182	0.000100	1698	1.359847	0.000100
2120	1.386894	0.000100	1696	1.359071	0.000100
2110	1.386595	0.000100	1694	1.358260	0.000100
2100	1.386288	0.000100	1692	1.357371	0.000100
2090	1.385967	0.000100	1690	1.356425	0.000100
2080	1.385635	0.000100	1688	1.355384	0.000100
2070	1.385286	0.000100	1686	1.354250	0.000100
2060	1.384921	0.000100	1684	1.352986	0.000100
2050	1.384535	0.000100	1682	1.351554	0.000100
2040	1.384126	0.000100	1680	1.349861	0.000129
2030	1.383684	0.000100	1678	1.347922	0.000349
2020	1.383207	0.000100	1676	1.345796	0.000797
2010	1.382677	0.000100	1674	1.343433	0.001346
2000	1.382066	0.000100	1672	1.340745	0.002204
1990	1.381241	0.000100	1670	1.337785	0.003521
1980	1.380432	0.000500	1668	1.334529	0.005266
1970	1.379741	0.000900	1666	1.330814	0.007665
1960	1.378765	0.001000	1664	1.326742	0.011310
1950	1.377457	0.001900	1662	1.323127	0.016899
1940	1.376597	0.003500	1660	1.320640	0.023701
1930	1.376525	0.005300	1658	1.319966	0.031957
1920	1.376614	0.006400	1656	1.321493	0.040541
1910	1.376974	0.008300	1654	1.325963	0.049182
1900	1.378425	0.010300	1652	1.333519	0.056113
1890	1.381176	0.011300	1650	1.342196	0.058494
1880	1.384282	0.010500	1648	1.349766	0.058526

Table 4. Continued

ν , cm^{-1}	n	k	ν , cm^{-1}	n	k
1646	1.355817	0.056823	1558	1.388994	0.016037
1644	1.360241	0.054269	1556	1.387915	0.015366
1642	1.363197	0.051716	1554	1.386767	0.014991
1640	1.365099	0.049347	1552	1.385641	0.014760
1638	1.366417	0.047619	1550	1.384573	0.014724
1636	1.367405	0.046022	1548	1.383580	0.014838
1634	1.367911	0.044578	1546	1.382717	0.015080
1632	1.368012	0.043736	1544	1.381972	0.015415
1630	1.368180	0.043509	1542	1.381471	0.015859
1628	1.368523	0.043467	1540	1.381061	0.016097
1626	1.368982	0.043589	1538	1.380668	0.016346
1624	1.369651	0.043977	1536	1.380318	0.016693
1622	1.370611	0.044297	1534	1.380088	0.016943
1620	1.371647	0.044426	1532	1.379930	0.017248
1618	1.372871	0.044679	1530	1.379878	0.017394
1616	1.374139	0.044472	1528	1.379732	0.017396
1614	1.375227	0.044125	1526	1.379548	0.017491
1612	1.376150	0.043926	1524	1.379389	0.017580
1610	1.377074	0.043635	1522	1.379323	0.017625
1608	1.377911	0.043441	1520	1.379061	0.017419
1606	1.378676	0.043205	1518	1.378618	0.017402
1604	1.379364	0.043202	1516	1.378197	0.017703
1602	1.380194	0.043411	1514	1.377833	0.017832
1600	1.381150	0.043633	1512	1.377419	0.018283
1598	1.382437	0.044147	1510	1.377243	0.018885
1596	1.384138	0.044504	1508	1.377271	0.019419
1594	1.386230	0.044561	1506	1.377411	0.019853
1592	1.388603	0.044343	1504	1.377522	0.020238
1590	1.391281	0.043464	1502	1.377732	0.020749
1588	1.393912	0.041894	1500	1.378233	0.021394
1586	1.396091	0.039389	1498	1.379035	0.021647
1584	1.397608	0.036760	1496	1.379844	0.021644
1582	1.398516	0.033802	1494	1.380638	0.021431
1580	1.398708	0.030909	1492	1.381416	0.021070
1578	1.398513	0.028477	1490	1.382164	0.020409
1576	1.398064	0.026079	1488	1.382707	0.019502
1574	1.397150	0.023757	1486	1.382973	0.018432
1572	1.395969	0.022160	1484	1.383011	0.017431
1570	1.394900	0.020825	1482	1.382844	0.016321
1568	1.393804	0.019563	1480	1.382357	0.015244
1566	1.392632	0.018578	1478	1.381711	0.014492
1564	1.391482	0.017854	1476	1.381024	0.013789
1562	1.390536	0.017361	1474	1.380367	0.013253
1560	1.389796	0.016849	1472	1.379603	0.012562

Table 4. Continued

ν , cm^{-1}	n	k	ν , cm^{-1}	n	k
1470	1.378526	0.011904	1382	1.382257	0.016071
1468	1.377259	0.011722	1380	1.382241	0.015526
1466	1.376224	0.011912	1378	1.382131	0.015064
1464	1.375225	0.011868	1370	1.381371	0.011000
1462	1.374192	0.012173	1360	1.378330	0.007600
1460	1.373218	0.012586	1350	1.374738	0.005600
1458	1.372494	0.013195	1340	1.370607	0.003300
1456	1.371791	0.013613	1330	1.366658	0.004000
1454	1.371041	0.014112	1320	1.364407	0.004200
1452	1.370218	0.014880	1310	1.361500	0.002400
1450	1.369695	0.015914	1300	1.358121	0.002100
1448	1.369473	0.016989	1290	1.354594	0.001500
1446	1.369434	0.017759	1280	1.350542	0.000100
1444	1.369361	0.018623	1270	1.345267	0.000100
1442	1.369532	0.019560	1260	1.339770	0.000100
1440	1.369851	0.020293	1250	1.335093	0.002700
1438	1.370347	0.020936	1240	1.330449	0.002000
1436	1.370886	0.021338	1230	1.323926	0.002800
1434	1.371334	0.021393	1220	1.318036	0.005700
1432	1.371618	0.021554	1210	1.313349	0.007400
1430	1.371877	0.021543	1200	1.307142	0.006200
1428	1.371863	0.021398	1190	1.298144	0.006800
1426	1.371660	0.021505	1180	1.285815	0.007200
1424	1.371245	0.021688	1176	1.282368	0.010506
1422	1.370856	0.022378	1174	1.280259	0.010981
1420	1.370720	0.023399	1172	1.279009	0.011573
1418	1.370993	0.024427	1170	1.276768	0.011921
1416	1.371488	0.025469	1168	1.275158	0.012262
1414	1.372299	0.026441	1166	1.272796	0.012597
1412	1.373431	0.027386	1164	1.271159	0.012941
1410	1.374921	0.027943	1162	1.269024	0.012888
1408	1.376475	0.028084	1160	1.267099	0.012304
1406	1.378131	0.027982	1158	1.264057	0.011489
1404	1.379786	0.027399	1156	1.260810	0.010803
1402	1.381127	0.026242	1154	1.256677	0.010488
1400	1.382025	0.025091	1152	1.252617	0.010514
1398	1.382841	0.024059	1150	1.248080	0.011058
1396	1.383472	0.022613	1148	1.243866	0.011859
1394	1.383747	0.021211	1146	1.239397	0.013038
1392	1.383601	0.019797	1144	1.235715	0.014650
1390	1.383307	0.018856	1142	1.232372	0.015814
1388	1.383080	0.018058	1140	1.229255	0.015932
1386	1.382799	0.017172	1138	1.225113	0.015437
1384	1.382500	0.016585	1136	1.220091	0.014748

Table 4. Continued

ν , cm^{-1}	n	k	ν , cm^{-1}	n	k
1134	1.214132	0.014844	1046	2.313930	0.202740
1132	1.208176	0.015337	1044	2.213688	0.155590
1130	1.201988	0.015961	1042	2.132301	0.125140
1128	1.195509	0.016384	1040	2.067610	0.103260
1126	1.188435	0.017118	1038	2.014596	0.085295
1124	1.181139	0.018068	1036	1.968643	0.069575
1122	1.173492	0.018950	1034	1.927697	0.057295
1120	1.165212	0.019666	1032	1.891313	0.048501
1118	1.156167	0.020553	1030	1.859811	0.042121
1116	1.146361	0.021686	1028	1.832071	0.037128
1114	1.135839	0.022828	1026	1.807817	0.033395
1112	1.123929	0.024091	1024	1.786266	0.030483
1110	1.110687	0.025999	1022	1.767480	0.028121
1108	1.096089	0.029455	1020	1.750618	0.025909
1106	1.081979	0.034503	1018	1.735504	0.023668
1104	1.067673	0.039306	1016	1.721503	0.021753
1102	1.053266	0.043302	1014	1.709036	0.019999
1100	1.036758	0.046971	1012	1.697258	0.017879
1098	1.019013	0.049207	1010	1.686066	0.015892
1096	0.995408	0.050557	1008	1.675148	0.014563
1094	0.969345	0.054343	1006	1.665371	0.013787
1092	0.936215	0.059963	1004	1.656106	0.013150
1090	0.905867	0.068609	1002	1.648080	0.012918
1088	0.878099	0.079450	1000	1.640472	0.012777
1086	0.807715	0.035025	990	1.610502	0.008100
1084	0.704925	0.080081	980	1.585734	0.004100
1082	0.605809	0.135780	970	1.565522	0.002600
1080	0.509672	0.221240	960	1.549005	0.000400
1078	0.417647	0.353090	950	1.534837	0.000100
1076	0.368738	0.519430	940	1.523272	0.000100
1074	0.349507	0.688130	930	1.513635	0.000100
1072	0.356943	0.858800	920	1.505240	0.000100
1070	0.377601	1.046800	910	1.497781	0.000100
1068	0.420007	1.241000	900	1.490985	0.000100
1066	0.480795	1.482800	890	1.484353	0.000100
1064	0.611544	1.777600	880	1.476878	0.000300
1062	0.844812	2.125600	870	1.469653	0.003900
1060	1.366017	2.530900	860	1.466610	0.010600
1058	2.319151	2.722900	850	1.468205	0.014200
1056	3.124440	1.910200	840	1.469326	0.012000
1054	3.181357	0.930280	830	1.466804	0.009500
1052	2.843344	0.553220	820	1.463310	0.010100
1050	2.600180	0.378120	810	1.461596	0.011700
1048	2.439704	0.272630	800	1.460722	0.011600

Table 4. Concluded

<u>ν, cm^{-1}</u>	<u>n</u>	<u>k</u>
790	1.459206	0.011300
780	1.457333	0.011700
770	1.456177	0.012900
760	1.456797	0.014300
750	1.457655	0.012700
740	1.456386	0.010000
730	1.453809	0.009700
720	1.451608	0.010000
710	1.450015	0.011400

Table 5. Solid NH₃ Optical Properties at 20°K

ν , cm ⁻¹	n	k	ν , cm ⁻¹	n	k
3690	1.342685	0.003200	3452	1.311614	0.006917
3680	1.344423	0.003700	3450	1.310408	0.006755
3670	1.343452	0.000100	3448	1.309212	0.006788
3660	1.342696	0.003700	3446	1.308360	0.007085
3650	1.342977	0.001600	3444	1.307375	0.006274
3640	1.341386	0.000600	3442	1.305553	0.005617
3630	1.339745	0.002600	3440	1.303321	0.005590
3620	1.339592	0.002500	3438	1.301418	0.006189
3610	1.338665	0.002900	3436	1.299768	0.006443
3600	1.337920	0.003300	3434	1.298134	0.006620
3590	1.337210	0.003900	3432	1.296359	0.006589
3580	1.336796	0.004100	3430	1.294105	0.006138
3570	1.336246	0.004200	3428	1.291010	0.006048
3560	1.334643	0.003100	3426	1.288012	0.007090
3550	1.332975	0.004500	3424	1.285772	0.008288
3540	1.332156	0.005100	3422	1.283283	0.008013
3530	1.330233	0.004100	3420	1.280118	0.008508
3520	1.328241	0.006400	3418	1.276777	0.008861
3510	1.327911	0.007500	3416	1.272827	0.008790
3500	1.327012	0.006200	3414	1.267709	0.009079
3498	1.326105	0.005806	3412	1.261979	0.010354
3496	1.325130	0.006045	3410	1.255858	0.012171
3494	1.324566	0.006872	3408	1.248884	0.014208
3492	1.324329	0.006900	3406	1.240800	0.017586
3490	1.324222	0.007586	3404	1.232077	0.022641
3488	1.324546	0.007382	3402	1.222577	0.029147
3486	1.324346	0.006573	3400	1.212692	0.038672
3484	1.322951	0.005554	3398	1.203555	0.051386
3482	1.321570	0.006669	3396	1.196331	0.067017
3480	1.321796	0.007969	3394	1.191460	0.085048
3478	1.322225	0.007132	3392	1.189584	0.105350
3476	1.321712	0.006290	3390	1.192731	0.128540
3474	1.320734	0.005983	3388	1.202712	0.151040
3472	1.319312	0.005218	3386	1.217478	0.168620
3470	1.317899	0.006133	3384	1.233690	0.181760
3468	1.317186	0.006675	3382	1.250806	0.192710
3466	1.316517	0.006874	3380	1.269598	0.200750
3464	1.315974	0.007512	3378	1.288194	0.203630
3462	1.315887	0.007731	3376	1.305025	0.204050
3460	1.315432	0.007025	3374	1.320542	0.203180
3458	1.314173	0.006573	3372	1.333694	0.199370
3456	1.313050	0.007098	3370	1.344699	0.197260
3454	1.312387	0.007256	3368	1.356906	0.197060
			3366	1.370583	0.193760

Table 5. Continued

ν , cm^{-1}	n	k	ν , cm^{-1}	n	k
3364	1.384547	0.189230	3276	1.390854	0.053875
3362	1.397537	0.181140	3274	1.390933	0.053679
3360	1.408190	0.171000	3272	1.391138	0.053419
3358	1.416657	0.161170	3270	1.391532	0.053406
3356	1.423560	0.149910	3268	1.392055	0.052877
3354	1.428500	0.139000	3266	1.392244	0.052245
3352	1.431694	0.127720	3264	1.392416	0.052009
3350	1.432859	0.116880	3262	1.393072	0.051898
3348	1.432672	0.107420	3260	1.393570	0.050672
3346	1.431522	0.098533	3258	1.393332	0.049688
3344	1.429313	0.090478	3256	1.393092	0.049529
3342	1.426275	0.083923	3254	1.393158	0.049095
3340	1.423155	0.078508	3252	1.393229	0.048629
3338	1.420218	0.074152	3250	1.393119	0.048078
3336	1.416958	0.069641	3248	1.392728	0.047560
3334	1.413345	0.066787	3246	1.392735	0.047964
3332	1.410717	0.065269	3244	1.393203	0.047523
3330	1.409119	0.063210	3242	1.392974	0.046290
3328	1.406858	0.060142	3240	1.392331	0.046244
3326	1.404018	0.058527	3238	1.391886	0.046101
3324	1.402023	0.057957	3236	1.391287	0.045886
3322	1.400085	0.055963	3234	1.390586	0.046383
3320	1.397707	0.055248	3232	1.390244	0.046997
3318	1.395536	0.055058	3230	1.390241	0.047713
3316	1.394066	0.054981	3228	1.389956	0.047857
3314	1.392998	0.055380	3226	1.389083	0.048598
3312	1.392189	0.054846	3224	1.388931	0.051094
3310	1.391237	0.054895	3222	1.390168	0.053081
3308	1.390452	0.054688	3220	1.391650	0.053996
3306	1.389550	0.054631	3218	1.393020	0.055253
3304	1.388473	0.054722	3216	1.394835	0.056435
3302	1.388061	0.055921	3214	1.397055	0.057313
3300	1.388613	0.056465	3212	1.399555	0.057813
3298	1.388883	0.055762	3210	1.402467	0.058058
3296	1.388538	0.055644	3208	1.405423	0.057216
3294	1.388748	0.056258	3206	1.407976	0.055893
3292	1.389209	0.055717	3204	1.410048	0.054397
3290	1.389241	0.055067	3202	1.411674	0.052733
3288	1.388816	0.054861	3200	1.413577	0.051894
3286	1.388490	0.055079	3198	1.415973	0.050118
3284	1.388835	0.055908	3196	1.417537	0.047071
3282	1.389938	0.056055	3194	1.418200	0.044744
3280	1.390858	0.055176	3192	1.418859	0.043060
3278	1.390908	0.054157	3190	1.419622	0.041068

Table 5. Continued

ν , cm^{-1}	n	k	ν , cm^{-1}	n	k
3188	1.420311	0.039231	2790	1.370402	0.001900
3186	1.421231	0.037521	2780	1.370115	0.001600
3184	1.422202	0.035091	2770	1.369724	0.001800
3182	1.422549	0.032073	2760	1.369577	0.002000
3180	1.422177	0.029537	2750	1.369400	0.001700
3178	1.421632	0.027554	2740	1.368903	0.001600
3170	1.419331	0.019800	2730	1.368638	0.002000
3160	1.414327	0.012400	2720	1.368400	0.001800
3150	1.408032	0.008200	2710	1.368296	0.002000
3140	1.403813	0.006200	2700	1.368111	0.001800
3130	1.399776	0.004700	2690	1.367921	0.001800
3120	1.396448	0.004300	2680	1.367590	0.001600
3110	1.393967	0.004200	2670	1.367377	0.001700
3100	1.392098	0.003800	2660	1.367031	0.001500
3090	1.390385	0.003500	2650	1.366669	0.001500
3080	1.388059	0.002900	2640	1.366541	0.001900
3070	1.386929	0.002900	2630	1.366322	0.001300
3060	1.385839	0.003200	2620	1.365862	0.001600
3050	1.384861	0.002700	2610	1.365814	0.001800
3040	1.383598	0.002400	2600	1.365551	0.001300
3030	1.382536	0.002700	2590	1.365061	0.001500
3020	1.381980	0.002600	2580	1.364913	0.001600
3010	1.380901	0.001900	2570	1.364759	0.001500
3000	1.379778	0.002200	2560	1.364399	0.001600
2990	1.379207	0.002700	2550	1.364144	0.001700
2980	1.378673	0.002100	2540	1.363950	0.001700
2970	1.378033	0.002500	2530	1.363755	0.001800
2960	1.377496	0.002100	2520	1.363467	0.001600
2950	1.376700	0.002100	2500	1.363000	0.001700
2940	1.376288	0.002400	2480	1.362539	0.001800
2930	1.375850	0.002100	2470	1.362393	0.002000
2920	1.375352	0.002200	2460	1.362282	0.002000
2910	1.374962	0.002200	2450	1.361961	0.001700
2900	1.374519	0.001900	2440	1.361816	0.002200
2890	1.373839	0.002000	2430	1.361594	0.001700
2880	1.373405	0.002200	2420	1.361332	0.002000
2870	1.373250	0.002400	2410	1.361134	0.002000
2860	1.373228	0.002200	2400	1.361033	0.001900
2850	1.372850	0.001900	2390	1.360680	0.001900
2840	1.372245	0.001500	2380	1.360585	0.002000
2830	1.371808	0.002100	2370	1.360544	0.002000
2820	1.371576	0.001600	2360	1.360249	0.001400
2810	1.371149	0.001800	2350	1.359722	0.001600
2800	1.370739	0.001600	2340	1.359432	0.001600

Table 5. Continued

ν , cm^{-1}	n	k	ν , cm^{-1}	n	k
2330	1.359170	0.001600	1890	1.344010	0.010300
2320	1.358820	0.001500	1880	1.343986	0.010500
2310	1.358329	0.001500	1870	1.343812	0.010500
2300	1.358046	0.001800	1860	1.343837	0.010700
2290	1.357955	0.001900	1850	1.343578	0.010300
2280	1.357572	0.001400	1840	1.343351	0.010300
2270	1.357164	0.001900	1830	1.343108	0.010100
2260	1.356882	0.001600	1820	1.342605	0.009200
2250	1.356435	0.001700	1810	1.341455	0.008900
2240	1.355968	0.001800	1800	1.340575	0.008900
2230	1.355676	0.002000	1790	1.339411	0.008400
2220	1.355328	0.002000	1780	1.338141	0.008400
2210	1.354976	0.002100	1770	1.336631	0.008300
2200	1.354628	0.002200	1760	1.335114	0.008300
2190	1.354143	0.002100	1750	1.333170	0.008400
2180	1.353572	0.002400	1740	1.331456	0.008800
2170	1.353220	0.002800	1730	1.329075	0.008600
2160	1.353194	0.003100	1720	1.326190	0.008800
2150	1.352856	0.002800	1710	1.322204	0.009400
2140	1.352261	0.002900	1700	1.316832	0.010300
2130	1.352014	0.003600	1696	1.314024	0.011560
2120	1.351761	0.003100	1694	1.312720	0.012464
2110	1.351076	0.003400	1692	1.311139	0.013242
2100	1.350573	0.003600	1690	1.309778	0.014629
2090	1.350346	0.004200	1688	1.308334	0.015924
2080	1.350166	0.004400	1686	1.306869	0.017215
2070	1.349795	0.004300	1684	1.305704	0.019760
2060	1.349290	0.004600	1682	1.305127	0.021197
2050	1.348984	0.005000	1680	1.303916	0.022758
2040	1.348583	0.004900	1678	1.303058	0.025320
2030	1.348113	0.005400	1676	1.302740	0.027625
2020	1.347761	0.005600	1674	1.302565	0.029385
2010	1.347309	0.005800	1672	1.302057	0.031506
2000	1.347029	0.006400	1670	1.302073	0.033939
1990	1.346675	0.006300	1668	1.302163	0.035931
1980	1.346122	0.006700	1666	1.302418	0.037965
1970	1.345805	0.007300	1664	1.302390	0.039870
1960	1.345565	0.007400	1662	1.302644	0.042108
1950	1.344967	0.007600	1660	1.302841	0.044274
1940	1.344583	0.008400	1658	1.303216	0.046399
1930	1.344189	0.008600	1656	1.303444	0.048922
1920	1.343996	0.009500	1654	1.304233	0.051636
1910	1.344064	0.010000	1652	1.305359	0.054351
1900	1.344166	0.010100	1650	1.306778	0.056578

Table 5. Continued

ν , cm^{-1}	n	k	ν , cm^{-1}	n	k
1648	1.307709	0.058648	1560	1.355526	0.035187
1646	1.309366	0.062016	1558	1.355711	0.034423
1644	1.311471	0.064175	1556	1.355204	0.033986
1642	1.313963	0.066558	1554	1.355040	0.033613
1640	1.316135	0.068282	1552	1.354564	0.033342
1638	1.318801	0.070531	1550	1.354226	0.032898
1636	1.321575	0.072446	1548	1.353472	0.033038
1634	1.325034	0.074101	1546	1.353465	0.033454
1632	1.328320	0.075384	1544	1.353508	0.033637
1630	1.332247	0.076480	1542	1.354055	0.033527
1628	1.336107	0.077083	1540	1.354230	0.033150
1626	1.340352	0.077039	1538	1.354433	0.032325
1624	1.344622	0.076982	1536	1.353882	0.031807
1622	1.349439	0.075607	1534	1.353551	0.031490
1620	1.353381	0.073125	1532	1.353093	0.031657
1618	1.357051	0.070510	1530	1.353397	0.031646
1616	1.359720	0.066927	1528	1.353310	0.031110
1614	1.361774	0.063312	1526	1.352996	0.030397
1612	1.362720	0.059825	1524	1.352182	0.030487
1610	1.363143	0.056233	1522	1.352127	0.030814
1608	1.362706	0.053720	1520	1.351842	0.030691
1606	1.362424	0.051357	1518	1.352244	0.031138
1604	1.361646	0.049528	1516	1.352443	0.030621
1602	1.361348	0.048325	1514	1.352328	0.029666
1600	1.361065	0.047046	1512	1.351442	0.029729
1598	1.360932	0.045543	1510	1.351362	0.029972
1596	1.360404	0.044438	1508	1.351227	0.030107
1594	1.360254	0.043352	1506	1.351539	0.029980
1592	1.359613	0.042049	1504	1.351276	0.029625
1590	1.359059	0.041264	1502	1.351360	0.029570
1588	1.358406	0.040722	1500	1.350992	0.029265
1586	1.358242	0.040170	1498	1.350938	0.029168
1584	1.357481	0.039322	1496	1.350722	0.029346
1582	1.357116	0.039401	1494	1.350814	0.028896
1580	1.357002	0.039421	1492	1.350333	0.028903
1578	1.357541	0.038923	1490	1.350700	0.029324
1576	1.357447	0.038021	1488	1.350662	0.028556
1574	1.357157	0.037015	1486	1.350682	0.028461
1572	1.356399	0.036801	1484	1.350292	0.028117
1570	1.356415	0.036728	1482	1.350545	0.028100
1568	1.356179	0.036189	1480	1.350096	0.027300
1566	1.356139	0.035802	1478	1.349657	0.027003
1564	1.355633	0.035400	1476	1.348708	0.027160
1562	1.355616	0.035297	1474	1.349042	0.027903

Table 5. Continued

ν , cm^{-1}	n	k	ν , cm^{-1}	n	k
1472	1.348951	0.027321	1384	1.340284	0.022886
1470	1.348738	0.026899	1382	1.340660	0.022979
1468	1.347764	0.027186	1380	1.340160	0.023168
1466	1.348347	0.028090	1378	1.341012	0.021911
1464	1.348512	0.027500	1370	1.338008	0.022200
1462	1.348235	0.026536	1360	1.337119	0.021700
1460	1.347330	0.027473	1350	1.335324	0.020900
1458	1.347823	0.027716	1340	1.333342	0.019100
1456	1.348060	0.027862	1330	1.329921	0.019200
1454	1.348946	0.027461	1320	1.327033	0.018100
1452	1.348372	0.025988	1310	1.323934	0.020100
1450	1.347978	0.026069	1300	1.322165	0.018700
1448	1.347415	0.026084	1290	1.318653	0.018800
1446	1.347360	0.025455	1280	1.314703	0.017000
1444	1.346625	0.025879	1270	1.309464	0.018800
1442	1.346672	0.025496	1260	1.305929	0.018900
1440	1.345925	0.025629	1250	1.301954	0.020400
1438	1.345961	0.025831	1240	1.296192	0.016500
1436	1.345704	0.026044	1230	1.288879	0.020500
1434	1.345754	0.025624	1220	1.282164	0.018500
1432	1.345188	0.025989	1210	1.272910	0.020700
1430	1.345622	0.026286	1200	1.262458	0.020600
1428	1.345299	0.025725	1190	1.251235	0.025200
1426	1.345571	0.026178	1180	1.231686	0.021400
1424	1.345199	0.025679	1176	1.223066	0.026569
1422	1.345849	0.026077	1174	1.218407	0.030010
1420	1.345875	0.025383	1172	1.217158	0.032526
1418	1.345711	0.023897	1170	1.212358	0.031691
1416	1.344608	0.024493	1168	1.209989	0.035763
1414	1.344483	0.023787	1166	1.205161	0.033319
1412	1.343590	0.024213	1164	1.197488	0.032671
1410	1.343623	0.024381	1162	1.187580	0.038546
1408	1.343089	0.024450	1160	1.183094	0.045230
1406	1.343890	0.025260	1158	1.179937	0.050866
1404	1.344019	0.024122	1156	1.175932	0.051255
1402	1.343862	0.023215	1154	1.168807	0.056040
1400	1.342743	0.023249	1152	1.165810	0.062787
1398	1.342981	0.023290	1150	1.159244	0.061231
1396	1.341958	0.022507	1148	1.148168	0.065611
1394	1.341724	0.022932	1146	1.140458	0.079513
1392	1.341019	0.023200	1144	1.134750	0.083495
1390	1.341287	0.022928	1142	1.126520	0.095169
1388	1.340428	0.023228	1140	1.126298	0.111900
1386	1.341054	0.023365	1138	1.127135	0.114030

Table 5. Continued

ν , cm^{-1}	n	k	ν , cm^{-1}	n	k
1136	1.120574	0.117750	1048	1.711452	0.314970
1134	1.113905	0.130630	1046	1.716230	0.288240
1132	1.111493	0.139600	1044	1.717934	0.262250
1130	1.105796	0.145880	1042	1.716886	0.237000
1128	1.098035	0.157390	1040	1.712929	0.213700
1126	1.090739	0.171440	1038	1.707985	0.193240
1124	1.086678	0.188630	1036	1.702260	0.173840
1122	1.086213	0.206630	1034	1.695495	0.155070
1120	1.086801	0.219860	1032	1.687427	0.138690
1118	1.086529	0.235980	1030	1.679208	0.123170
1116	1.088465	0.252500	1028	1.669804	0.108840
1114	1.089955	0.266170	1026	1.659632	0.096008
1112	1.091035	0.283130	1024	1.649255	0.085935
1110	1.093979	0.301780	1022	1.639502	0.076465
1108	1.098403	0.318910	1020	1.629678	0.068380
1106	1.104194	0.338970	1018	1.620302	0.061486
1104	1.112741	0.357850	1016	1.611436	0.055788
1102	1.122279	0.375540	1014	1.603464	0.050283
1100	1.132954	0.394140	1012	1.595414	0.045042
1098	1.144852	0.411840	1010	1.586939	0.039953
1096	1.158150	0.430230	1008	1.578664	0.037250
1094	1.174573	0.449660	1006	1.572806	0.035400
1092	1.193510	0.465690	1004	1.565961	0.029809
1090	1.213258	0.480630	1002	1.557969	0.027537
1088	1.234655	0.495290	1000	1.550487	0.027487
1086	1.257087	0.506960	990	1.527928	0.020700
1084	1.280855	0.519190	980	1.508720	0.014100
1082	1.307365	0.529730	970	1.493316	0.011200
1080	1.334504	0.535350	960	1.474359	0.000100
1078	1.361166	0.540980	950	1.458968	0.007200
1076	1.389707	0.545760	940	1.449544	0.006400
1074	1.420649	0.547550	930	1.439874	0.000100
1072	1.451357	0.544340	920	1.423985	0.000100
1070	1.482051	0.540210	910	1.410470	0.000100
1068	1.512853	0.532260	900	1.399045	0.007400
1066	1.543140	0.520630	890	1.383463	0.001000
1064	1.572152	0.506830	880	1.348449	0.006400
1062	1.599860	0.488530	870	1.336603	0.060200
1060	1.624847	0.468200	860	1.350938	0.088300
1058	1.647701	0.445130	850	1.379491	0.099000
1056	1.666823	0.419170	840	1.406827	0.106100
1054	1.681467	0.392230	830	1.403059	0.048900
1052	1.693236	0.367530	820	1.380919	0.083100
1050	1.703736	0.341570	810	1.383820	0.088300

Table 5. Concluded

<u>ν, cm⁻¹</u>	<u>n</u>	<u>k</u>
800	1.394509	0.099400
790	1.396013	0.093900
780	1.393550	0.100200
770	1.397325	0.119700
760	1.417858	0.131200
750	1.442421	0.128100
740	1.460778	0.112000
730	1.459478	0.083000
720	1.453353	0.084900
710	1.438524	0.068100

Table 6. Solid CO₂ Optical Properties at 80°K

ν , cm ⁻¹	n	k	ν , cm ⁻¹	n	k
3950		0.000100	3604	1.374055	0.005729
3940	1.385230	0.000100	3602	1.374382	0.017194
3930	1.384828	0.000100	3600	1.387211	0.025532
3920	1.385010	0.000100	3598	1.397022	0.012927
3910	1.384580	0.000100	3596	1.396056	0.004510
3900	1.384775	0.000100	3594	1.392137	0.002857
3890	1.384311	0.000100	3592	1.390628	0.001097
3880	1.384521	0.000100	3590	1.388625	0.000869
3870	1.384013	0.000100	3588	1.388051	0.000977
3860	1.384242	0.000100	3586	1.387105	0.000533
3850	1.383670	0.000100	3584	1.386547	0.000653
3840	1.383931	0.000100	3582	1.386156	0.001180
3830	1.383282	0.000100	3580	1.386580	0.001062
3820	1.383573	0.000100	3578	1.386417	0.000100
3810	1.382819	0.000100	3570	1.384682	0.000600
3800	1.383142	0.000100	3560	1.383913	0.001000
3790	1.382226	0.000100	3550	1.384001	0.000600
3780	1.382590	0.000100	3540	1.383396	0.000700
3770	1.381376	0.000100	3530	1.383279	0.000400
3760	1.381782	0.000100	3520	1.382665	0.000400
3750	1.379925	0.000100	3510	1.382521	0.000500
3740	1.380229	0.000100	3500	1.382070	0.000400
3730	1.374978	0.000100	3490	1.381966	0.000600
3720	1.370800	0.003800	3480	1.381577	0.000500
3710	1.382582	0.027500	3470	1.381509	0.000700
3700	1.394074	0.003000	3460	1.381393	0.000800
3690	1.388981	0.000700	3450	1.381333	0.000400
3680	1.384268	0.001000	3440	1.380786	0.000400
3670	1.384699	0.001600	3430	1.380671	0.000700
3660	1.383301	0.001300	3420	1.380534	0.000600
3650	1.383394	0.001600	3410	1.380424	0.000500
3640	1.382128	0.001500	3400	1.380033	0.000400
3630	1.382608	0.002500	3390	1.379824	0.000500
3626	1.382012	0.002058	3380	1.379510	0.000500
3624	1.382104	0.001627	3370	1.379391	0.000600
3622	1.380984	0.001863	3360	1.379051	0.000500
3620	1.381051	0.002181	3350	1.378908	0.000700
3618	1.380184	0.002437	3340	1.378703	0.000700
3616	1.380286	0.003066	3330	1.378568	0.000600
3614	1.379869	0.003655	3320	1.378268	0.000700
3612	1.380021	0.003729	3310	1.378107	0.000600
3610	1.379190	0.004321	3300	1.377837	0.000700
3608	1.379624	0.005388	3290	1.377685	0.000600
3606	1.378276	0.004719	3280	1.377271	0.000500

Table 6. Continued

ν , cm^{-1}	n	k	ν , cm^{-1}	n	k
3270	1.377003	0.000700	2810	1.354113	0.000700
3260	1.376818	0.000800	2800	1.353377	0.000500
3250	1.376597	0.000600	2790	1.351939	0.000700
3240	1.376253	0.000800	2780	1.351237	0.000600
3230	1.376093	0.000800	2770	1.349580	0.000500
3220	1.375875	0.000800	2760	1.348707	0.000600
3210	1.375594	0.000700	2750	1.346944	0.000600
3200	1.375334	0.000800	2740	1.346003	0.000500
3190	1.375093	0.000700	2730	1.344010	0.000700
3180	1.374744	0.000600	2720	1.343022	0.000500
3170	1.374398	0.000700	2710	1.340794	0.000700
3160	1.374065	0.000600	2700	1.339651	0.000500
3150	1.373695	0.000700	2690	1.337140	0.000700
3140	1.373367	0.000700	2680	1.335883	0.000600
3130	1.373082	0.000800	2670	1.333096	0.000700
3120	1.372779	0.000700	2660	1.331637	0.000600
3100	1.372000	0.000700	2650	1.328469	0.000700
3080	1.371253	0.000600	2640	1.326689	0.000500
3070	1.370774	0.000800	2630	1.323027	0.000800
3060	1.370469	0.000800	2620	1.321133	0.000700
3050	1.370081	0.000800	2610	1.316975	0.000700
3040	1.369633	0.000600	2600	1.314467	0.000500
3030	1.369066	0.000800	2590	1.309551	0.000800
3020	1.368659	0.000700	2580	1.306666	0.000600
3010	1.368146	0.000900	2570	1.300809	0.000700
3000	1.367810	0.000800	2560	1.297156	0.000700
2990	1.367205	0.000800	2550	1.290156	0.000800
2980	1.366780	0.000800	2540	1.285545	0.000800
2970	1.366193	0.000900	2530	1.276977	0.001000
2960	1.365803	0.000700	2520	1.270835	0.000800
2950	1.365058	0.000800	2510	1.259705	0.001300
2940	1.364544	0.000600	2498	1.248905	0.001790
2930	1.363761	0.000900	2496	1.244650	0.002112
2920	1.363364	0.000700	2494	1.244424	0.001953
2910	1.362506	0.000800	2492	1.239555	0.002038
2900	1.362026	0.000700	2490	1.239149	0.002364
2890	1.361120	0.000800	2488	1.234154	0.002432
2880	1.360563	0.000600	2486	1.233530	0.002537
2870	1.359597	0.000900	2484	1.228049	0.002929
2860	1.359131	0.000600	2482	1.227314	0.003187
2850	1.358028	0.000700	2480	1.221250	0.003518
2840	1.357323	0.000400	2478	1.220026	0.004408
2830	1.356063	0.000700	2476	1.213771	0.005686
2820	1.355412	0.000500	2474	1.212943	0.007135

Table 6. Continued

ν , cm^{-1}	n	k	ν , cm^{-1}	n	k
2472	1.207015	0.008877	2384	0.357458	0.047393
2470	1.206935	0.010581	2382	0.233737	0.247280
2468	1.201288	0.011868	2380	0.183827	0.428680
2466	1.201227	0.013331	2378	0.219846	0.591090
2464	1.195465	0.014973	2376	0.239056	0.711740
2462	1.195912	0.016584	2374	0.292357	0.815330
2460	1.190668	0.018232	2372	0.296041	0.907930
2458	1.192313	0.019561	2370	0.340665	1.017900
2456	1.187898	0.019632	2368	0.356264	1.131500
2454	1.189237	0.018397	2366	0.422700	1.226400
2452	1.182705	0.016891	2364	0.425053	1.326800
2450	1.182145	0.015833	2362	0.462058	1.435100
2448	1.174506	0.015138	2360	0.416445	1.599700
2446	1.173959	0.014211	2358	0.482781	1.856100
2444	1.165679	0.012629	2356	0.540316	2.163500
2442	1.163796	0.010797	2354	0.793141	2.492500
2440	1.153246	0.009329	2352	0.973898	2.895200
2438	1.149894	0.008676	2350	1.662039	3.469800
2436	1.138515	0.008601	2348	3.414236	4.274300
2434	1.135299	0.008549	2346	4.580745	1.816800
2432	1.123391	0.008368	2344	4.130002	0.709750
2430	1.119598	0.008251	2342	3.410472	0.279850
2428	1.106504	0.008219	2340	3.059099	0.135790
2426	1.102064	0.008339	2338	2.734098	0.084131
2424	1.088067	0.008478	2336	2.592491	0.059014
2422	1.082912	0.007995	2334	2.419125	0.044269
2420	1.066727	0.007437	2332	2.342339	0.035971
2418	1.059522	0.007421	2330	2.232836	0.037482
2416	1.041151	0.007714	2328	2.196044	0.032992
2414	1.032407	0.008178	2326	2.120150	0.020452
2412	1.011826	0.009338	2324	2.086825	0.010094
2410	1.002071	0.010870	2322	2.019814	0.007323
2408	0.980176	0.011869	2320	1.996059	0.006551
2406	0.968701	0.011783	2318	1.945284	0.006031
2404	0.942349	0.010922	2316	1.929412	0.005648
2402	0.925543	0.010260	2314	1.888009	0.005209
2400	0.892806	0.010069	2312	1.876517	0.005032
2398	0.870007	0.009947	2310	1.841721	0.004730
2396	0.829226	0.009738	2308	1.833033	0.004359
2394	0.796224	0.009806	2306	1.802751	0.004233
2392	0.741971	0.010936	2304	1.795944	0.004253
2390	0.691007	0.013718	2302	1.769309	0.004284
2388	0.613746	0.019438	2300	1.763653	0.004391
2386	0.526390	0.033280	2298	1.739557	0.004836

Table 6. Continued

ν , cm^{-1}	<u>n</u>	<u>k</u>	ν , cm^{-1}	<u>n</u>	<u>k</u>
2296	1.734542	0.005352	2000	1.461164	0.000100
2294	1.712145	0.006040	1990	1.457687	0.000200
2292	1.706129	0.006905	1980	1.457995	0.000100
2290	1.681990	0.008815	1970	1.454732	0.000100
2288	1.667899	0.015063	1960	1.455075	0.000100
2286	1.640179	0.037847	1950	1.452004	0.000100
2284	1.667634	0.091206	1940	1.452443	0.000200
2282	1.707491	0.083475	1930	1.449725	0.000300
2280	1.726850	0.028812	1920	1.450290	0.000100
2278	1.696741	0.010321	1910	1.447549	0.000100
2276	1.684058	0.007080	1900	1.448076	0.000100
2274	1.665306	0.006293	1890	1.445527	0.000100
2272	1.662250	0.007133	1880	1.446115	0.000100
2270	1.648965	0.007749	1870	1.443687	0.000100
2268	1.649332	0.007843	1860	1.444316	0.000100
2266	1.638163	0.007126	1850	1.441995	0.000100
2264	1.638737	0.005788	1840	1.442658	0.000100
2262	1.627142	0.004585	1830	1.440430	0.000100
2260	1.627180	0.003980	1820	1.441121	0.000100
2250	1.599171	0.005200	1810	1.438967	0.000100
2240	1.588410	0.005100	1800	1.439657	0.000100
2230	1.569379	0.000200	1790	1.437627	0.000200
2220	1.559362	0.000900	1780	1.438370	0.000100
2210	1.544358	0.000500	1770	1.436402	0.000200
2200	1.538476	0.000200	1760	1.437145	0.000100
2190	1.526423	0.000300	1750	1.435130	0.000100
2180	1.522451	0.000300	1740	1.435875	0.000300
2170	1.512819	0.000300	1730	1.434193	0.000400
2160	1.509951	0.000100	1720	1.435045	0.000200
2150	1.501742	0.000200	1710	1.433194	0.000200
2140	1.499777	0.000200	1700	1.433990	0.000200
2130	1.492787	0.000100	1690	1.432238	0.000300
2120	1.491319	0.000100	1680	1.433121	0.000200
2110	1.485147	0.000100	1670	1.431337	0.000200
2100	1.484192	0.000200	1660	1.432132	0.000200
2090	1.478827	0.000200	1650	1.430436	0.000300
2080	1.478174	0.000100	1640	1.431317	0.000300
2070	1.473283	0.000200	1630	1.429737	0.000400
2060	1.472731	0.000100	1620	1.430667	0.000300
2050	1.468231	0.000500	1610	1.429000	0.000200
2040	1.468684	0.001200	1600	1.429809	0.000300
2030	1.465056	0.000200	1590	1.428222	0.000300
2020	1.464837	0.000100	1580	1.429138	0.000400
2010	1.460975	0.000200	1570	1.427671	0.000400

Table 6. Concluded

ν , cm^{-1}	n	k	ν , cm^{-1}	n	k
1560	1.428580	0.000300	1120	1.418164	0.000200
1550	1.427028	0.000300	1110	1.418001	0.000100
1540	1.427894	0.000300	1100	1.417856	0.000200
1530	1.426408	0.000300	1090	1.417678	0.000100
1520	1.427269	0.000300	1080	1.417513	0.000200
1510	1.425783	0.000300	1070	1.417386	0.000200
1500	1.426669	0.000400	1060	1.417287	0.000200
1490	1.425303	0.000400	1050	1.417092	0.000100
1480	1.426213	0.000400	1040	1.416946	0.000200
1470	1.424778	0.000300	1030	1.416786	0.000100
1460	1.425709	0.000500	1020	1.416601	0.000100
1450	1.424430	0.000400	1010	1.416389	0.000100
1440	1.425317	0.000300	1000	1.416213	0.000100
1430	1.423922	0.000300	990	1.416001	0.000100
1420	1.424826	0.000300	980	1.415804	0.000100
1410	1.423442	0.000200	970	1.415576	0.000100
1400	1.424266	0.000300	960	1.415347	0.000100
1390	1.422986	0.000300	950	1.415087	0.000100
1380	1.424035	0.000400	940	1.414808	0.000100
1370	1.422724	0.000100	930	1.414486	0.000100
1360	1.423474	0.000100	920	1.414118	0.000100
1350	1.422139	0.000100	910	1.413667	0.000100
1340	1.422128	0.000100	900	1.413113	0.000100
1330	1.421654	0.000100	890	1.412276	0.000100
1320	1.421342	0.000200	880	1.410463	0.000100
1310	1.421231	0.000100	870	1.408689	0.002500
1300	1.421114	0.000300	860	1.409212	0.006400
1290	1.420922	0.000200	850	1.412514	0.008500
1280	1.420691	0.000200	840	1.415206	0.006800
1270	1.420531	0.000300	830	1.415306	0.004400
1260	1.420447	0.000300	820	1.414248	0.004600
1250	1.420253	0.000200	810	1.414103	0.004800
1240	1.420078	0.000300	800	1.413713	0.004800
1230	1.419986	0.000300	790	1.412449	0.004700
1220	1.419855	0.000200	780	1.411759	0.007900
1210	1.419695	0.000200	770	1.413330	0.010200
1200	1.419494	0.000100	760	1.417294	0.012500
1190	1.419272	0.000100	750	1.420569	0.009300
1180	1.419103	0.000200	740	1.421203	0.006700
1170	1.418961	0.000100	730	1.420746	0.005700
1160	1.418791	0.000200	720	1.420805	0.004600
1150	1.418636	0.000100	710	1.420511	0.003700
1140	1.418476	0.000200	700		0.002700
1130	1.418318	0.000100			

Table 7. Solid CO₂ Optical Properties at 20°K

ν , cm ⁻¹	n	k	ν , cm ⁻¹	n	k
3690		0.000100	3450	1.241976	0.001100
3680	1.241888	0.000500	3440	1.241744	0.000600
3670	1.241462	0.000700	3430	1.241451	0.001000
3660	1.241255	0.001100	3420	1.241362	0.000900
3650	1.240983	0.001700	3410	1.241335	0.000900
3640	1.240649	0.001400	3400	1.241305	0.000900
3630	1.241641	0.003000	3390	1.240841	0.000100
3628	1.240923	0.002148	3380	1.240384	0.000900
3626	1.240942	0.001956	3370	1.240284	0.000700
3624	1.240103	0.001951	3360	1.240193	0.000900
3622	1.240027	0.001991	3350	1.239961	0.000800
3620	1.239286	0.002117	3340	1.239861	0.000900
3618	1.239086	0.002307	3330	1.239675	0.000900
3616	1.238425	0.002526	3320	1.239601	0.000800
3614	1.237902	0.002451	3310	1.239230	0.000700
3612	1.236309	0.002582	3300	1.238848	0.000700
3610	1.234358	0.003525	3290	1.238725	0.001300
3608	1.231940	0.006032	3280	1.238958	0.001100
3606	1.229552	0.010051	3270	1.238663	0.000700
3604	1.229068	0.018234	3260	1.238296	0.000800
3602	1.239219	0.031092	3250	1.238105	0.001000
3600	1.255572	0.028699	3240	1.237915	0.000700
3598	1.262739	0.012578	3230	1.237605	0.001000
3596	1.258846	0.004469	3220	1.237486	0.000900
3594	1.254437	0.001923	3210	1.237302	0.001000
3592	1.251457	0.000789	3200	1.237213	0.000900
3590	1.249820	0.001114	3190	1.237008	0.000800
3588	1.248807	0.000820	3180	1.236648	0.000500
3586	1.248282	0.000696	3170	1.236295	0.000800
3584	1.247200	0.000168	3160	1.236098	0.000600
3582	1.246505	0.000422	3150	1.235943	0.000800
3580	1.245713	0.000912	3140	1.235628	0.000300
3570	1.245226	0.000800	3130	1.235217	0.000500
3560	1.244549	0.000800	3120	1.234904	0.000400
3550	1.244152	0.000900	3110	1.234653	0.000400
3540	1.243717	0.000600	3100	1.234263	0.000200
3530	1.243324	0.000800	3090	1.233859	0.000200
3520	1.243066	0.000900	3080	1.233355	0.000100
3510	1.242999	0.000900	3070	1.232998	0.000300
3500	1.242840	0.000900	3060	1.232633	0.000200
3490	1.242637	0.000600	3050	1.232267	0.000200
3480	1.242328	0.000800	3040	1.231848	0.000200
3470	1.241934	0.000500	3030	1.231452	0.000100
3460	1.241776	0.001200	3020	1.230946	0.000100

Table 7. Continued

ν , cm^{-1}	n	k	ν , cm^{-1}	n	k
3010	1.230498	0.000100	2570	1.170404	0.000100
3000	1.230009	0.000100	2560	1.166148	0.000100
2990	1.229544	0.000100	2550	1.161168	0.000100
2980	1.229035	0.000100	2540	1.155919	0.000100
2970	1.228541	0.000100	2530	1.149747	0.000100
2960	1.228005	0.000100	2520	1.143099	0.000100
2950	1.227480	0.000100	2510	1.135188	0.000100
2940	1.226912	0.000100	2500	1.126458	0.000100
2930	1.226350	0.000100	2494	1.120038	0.000001
2920	1.225746	0.000100	2492	1.117947	0.000020
2910	1.225143	0.000100	2490	1.115353	0.000179
2900	1.224497	0.000100	2488	1.113160	0.000330
2890	1.223848	0.000100	2486	1.110457	0.000538
2880	1.223157	0.000100	2484	1.108070	0.000786
2870	1.222456	0.000100	2482	1.105186	0.001153
2860	1.221712	0.000100	2480	1.102690	0.001685
2850	1.220954	0.000100	2478	1.099908	0.002275
2840	1.220150	0.000100	2476	1.097445	0.002876
2830	1.219327	0.000100	2474	1.094639	0.003464
2820	1.218455	0.000100	2472	1.092188	0.004012
2810	1.217558	0.000100	2470	1.089318	0.004614
2800	1.216608	0.000100	2468	1.086733	0.005276
2790	1.215627	0.000100	2466	1.083836	0.006036
2780	1.214588	0.000100	2464	1.081602	0.006629
2770	1.213511	0.000100	2462	1.078798	0.007011
2760	1.212369	0.000100	2460	1.076459	0.007180
2750	1.211179	0.000100	2458	1.073472	0.007237
2740	1.209919	0.000100	2456	1.070694	0.007070
2730	1.208601	0.000100	2454	1.066031	0.006828
2720	1.207200	0.000100	2452	1.063929	0.006590
2710	1.205728	0.000100	2450	1.059630	0.006211
2700	1.204165	0.000100	2448	1.056175	0.005867
2690	1.202509	0.000100	2446	1.052195	0.005383
2680	1.200755	0.000100	2444	1.047205	0.005058
2670	1.198857	0.000100	2442	1.042169	0.004617
2660	1.196895	0.000100	2440	1.036905	0.004283
2650	1.194818	0.000100	2438	1.031459	0.004197
2640	1.192489	0.000100	2436	1.025552	0.004004
2630	1.190004	0.000100	2434	1.019481	0.003817
2620	1.187413	0.000100	2432	1.012929	0.003608
2610	1.184431	0.000100	2430	1.006127	0.003516
2600	1.181498	0.000100	2428	0.998814	0.003465
2590	1.178050	0.000100	2426	0.991270	0.003354
2580	1.174517	0.000100	2424	0.983102	0.003125

Table 7. Continued

ν, cm^{-1}	n	k	ν, cm^{-1}	n	k
2422	0.974351	0.002909	2334	2.456356	0.147040
2420	0.964946	0.002887	2332	2.316662	0.097573
2418	0.955077	0.002894	2330	2.203130	0.068742
2416	0.944460	0.002690	2328	2.118338	0.043298
2414	0.932981	0.002599	2326	2.038598	0.020168
2412	0.920622	0.002510	2324	1.969432	0.007990
2410	0.907229	0.002390	2322	1.908106	0.004403
2408	0.892795	0.002224	2320	1.860692	0.003400
2406	0.876858	0.001925	2318	1.818805	0.003160
2404	0.859398	0.001455	2316	1.784890	0.003201
2402	0.839648	0.001061	2314	1.753685	0.003194
2400	0.817961	0.000701	2312	1.727648	0.003079
2398	0.792962	0.000348	2310	1.702933	0.002872
2396	0.765050	0.000240	2308	1.681850	0.002787
2394	0.732251	0.000798	2306	1.661672	0.002622
2392	0.695389	0.001833	2304	1.644125	0.002317
2390	0.650445	0.003936	2302	1.626926	0.001926
2388	0.598656	0.007663	2300	1.611435	0.001554
2386	0.534686	0.014908	2298	1.596111	0.001370
2384	0.443130	0.015894	2296	1.581805	0.001153
2382	0.297192	0.052154	2294	1.567144	0.001143
2380	0.148810	0.193440	2292	1.551796	0.001474
2378	0.114696	0.450030	2290	1.533755	0.003592
2376	0.176090	0.588710	2288	1.510009	0.011824
2374	0.233651	0.681460	2286	1.496465	0.042660
2372	0.266348	0.761910	2284	1.524147	0.086877
2370	0.297362	0.842470	2282	1.563183	0.062620
2368	0.317837	0.921900	2280	1.565810	0.019874
2366	0.343182	1.015000	2278	1.544203	0.005691
2364	0.368601	1.112400	2276	1.528166	0.001713
2362	0.405560	1.219900	2274	1.515784	0.000046
2360	0.451063	1.338600	2272	1.506499	0.000100
2358	0.494920	1.445700	2270	1.498233	0.000100
2356	0.534705	1.601800	2260	1.468878	0.000100
2354	0.602853	1.803200	2250	1.446900	0.000100
2352	0.721717	2.052100	2240	1.429807	0.000100
2350	0.960278	2.391500	2230	1.415439	0.000100
2348	1.415778	2.723600	2220	1.403607	0.000100
2346	2.303266	2.995100	2210	1.393293	0.000100
2344	3.261446	2.430500	2200	1.384540	0.000100
2342	3.537995	1.232800	2190	1.376746	0.000100
2340	3.213415	0.662280	2180	1.369987	0.000100
2338	2.880177	0.376610	2170	1.363882	0.000100
2336	2.645301	0.234130	2160	1.358496	0.000100

Table 7. Continued

ν , cm^{-1}	n	k	ν , cm^{-1}	n	k
2150	1.353583	0.000100	1690	1.289210	0.000700
2140	1.349185	0.000100	1680	1.288710	0.000500
2130	1.345146	0.000100	1670	1.288240	0.000700
2120	1.341482	0.000100	1660	1.287871	0.000600
2100	1.335000	0.000100	1650	1.287540	0.000700
2080	1.329464	0.000100	1640	1.287221	0.000600
2070	1.326994	0.000100	1630	1.286883	0.000500
2060	1.324665	0.000100	1620	1.286407	0.000400
2050	1.322467	0.000100	1610	1.285948	0.000400
2040	1.320537	0.000300	1600	1.285575	0.000600
2030	1.318718	0.000100	1590	1.285296	0.000500
2020	1.316901	0.000100	1580	1.284940	0.000600
2010	1.315175	0.000100	1570	1.284558	0.000500
2000	1.313587	0.000100	1560	1.284254	0.000800
1990	1.312016	0.000100	1550	1.283983	0.000700
1980	1.310576	0.000200	1540	1.283858	0.001000
1970	1.309294	0.000300	1530	1.283741	0.000800
1960	1.308013	0.000200	1520	1.283452	0.000600
1950	1.306731	0.000300	1510	1.283048	0.000700
1940	1.305656	0.000500	1500	1.282806	0.000700
1930	1.304659	0.000400	1490	1.282551	0.000800
1920	1.303584	0.000400	1480	1.282261	0.000700
1910	1.302596	0.000500	1470	1.282028	0.001000
1900	1.301692	0.000500	1460	1.281954	0.001000
1890	1.300771	0.000500	1450	1.281863	0.001000
1880	1.299901	0.000600	1440	1.281690	0.000900
1870	1.299188	0.000700	1430	1.281507	0.000900
1860	1.298484	0.000600	1420	1.281369	0.000900
1850	1.297670	0.000500	1410	1.281260	0.000800
1840	1.296856	0.000600	1400	1.280970	0.000600
1830	1.296207	0.000700	1390	1.280681	0.000700
1820	1.295606	0.000700	1380	1.280514	0.000800
1810	1.294911	0.000600	1370	1.280514	0.000800
1800	1.294285	0.000800	1360	1.280366	0.000600
1790	1.293792	0.000800	1350	1.280085	0.000400
1780	1.293217	0.000700	1340	1.279848	0.000600
1770	1.292623	0.000800	1330	1.279643	0.000300
1760	1.292179	0.000900	1320	1.279219	0.000400
1750	1.291740	0.000800	1310	1.278972	0.000600
1740	1.291234	0.000800	1300	1.278956	0.000900
1730	1.290740	0.000800	1290	1.278800	0.000600
1720	1.290353	0.000900	1280	1.278864	0.001200
1710	1.289965	0.000800	1270	1.278946	0.000700
1700	1.289601	0.000800	1260	1.278813	0.000600

Table 7. Concluded

ν , cm^{-1}	n	k	ν , cm^{-1}	n	k
1250	1.278574	0.000600	810	1.274466	0.005300
1240	1.278473	0.000400	800	1.274624	0.004600
1230	1.278214	0.000500	790	1.274011	0.004800
1220	1.278021	0.000300	780	1.273981	0.006200
1210	1.277935	0.000700	770	1.275781	0.007900
1200	1.277908	0.000300	760	1.277852	0.006700
1190	1.277738	0.000400	750	1.279175	0.005700
1180	1.277635	0.000300	740	1.279443	0.003800
1170	1.277467	0.000100	730	1.279348	0.002800
1160	1.277171	0.000100	720	1.279436	0.002300
1150	1.276937	0.000100	710	1.278906	0.000100
1140	1.276848	0.000300	700		0.000100
1130	1.276759	0.000100			
1120	1.276566	0.000100			
1110	1.276371	0.000100			
1100	1.276232	0.000100			
1090	1.276058	0.000100			
1080	1.275920	0.000100			
1070	1.275752	0.000100			
1060	1.275613	0.000100			
1050	1.275446	0.000100			
1040	1.275304	0.000100			
1030	1.275134	0.000100			
1020	1.274986	0.000100			
1010	1.274808	0.000100			
1000	1.274650	0.000100			
990	1.274458	0.000100			
980	1.274283	0.000100			
970	1.274069	0.000100			
960	1.273867	0.000100			
950	1.273614	0.000100			
940	1.273365	0.000100			
930	1.273039	0.000100			
920	1.272698	0.000100			
910	1.272220	0.000100			
900	1.271644	0.000100			
890	1.270532	0.000100			
880	1.268688	0.000700			
870	1.267386	0.003700			
860	1.268827	0.007500			
850	1.272262	0.008800			
840	1.274861	0.007000			
830	1.275104	0.005100			
820	1.274453	0.004600			

Table 8. Solid H₂O Optical Properties at 80°K

ν , cm ⁻¹	\underline{n}	\underline{k}	ν , cm ⁻¹	\underline{n}	\underline{k}
3690	1.126278	0.000400	3260	1.247483	0.807500
3680	1.121214	0.000500	3250	1.330089	0.844200
3670	1.115688	0.001200	3240	1.435180	0.832400
3660	1.110300	0.002100	3230	1.509035	0.765200
3650	1.104173	0.002300	3220	1.558941	0.740400
3640	1.097572	0.003600	3210	1.607351	0.691000
3630	1.090860	0.005200	3200	1.644869	0.646900
3620	1.084008	0.006400	3190	1.677396	0.611600
3610	1.076252	0.008100	3180	1.714959	0.568100
3600	1.068080	0.010000	3170	1.744457	0.518100
3590	1.059523	0.012900	3160	1.761155	0.460200
3580	1.050327	0.015100	3150	1.770565	0.419700
3570	1.040077	0.018800	3140	1.783021	0.375000
3560	1.029966	0.023500	3130	1.792122	0.326500
3550	1.019428	0.027800	3120	1.793372	0.275400
3540	1.007493	0.032400	3110	1.786187	0.225600
3530	0.993840	0.038500	3100	1.771412	0.179900
3520	0.979502	0.046800	3090	1.750466	0.139000
3510	0.964825	0.056800	3080	1.724700	0.105100
3500	0.949673	0.068200	3070	1.696651	0.079000
3490	0.932759	0.081100	3060	1.668992	0.060200
3480	0.916109	0.099400	3050	1.643419	0.047100
3470	0.898580	0.118200	3040	1.620736	0.037900
3460	0.880709	0.144100	3030	1.600767	0.031200
3450	0.866071	0.177900	3020	1.583116	0.026000
3440	0.866031	0.220000	3010	1.567326	0.022100
3430	0.868253	0.246000	3000	1.553252	0.019000
3420	0.877481	0.280400	2990	1.540557	0.016500
3410	0.898973	0.311700	2980	1.529036	0.014400
3400	0.898784	0.290700	2970	1.518447	0.012700
3390	0.881076	0.329500	2960	1.508851	0.011400
3380	0.879104	0.363700	2950	1.500102	0.010200
3370	0.878858	0.389300	2940	1.491874	0.008900
3360	0.882105	0.438700	2930	1.484117	0.008100
3350	0.903258	0.477400	2920	1.477014	0.007400
3340	0.915347	0.494800	2910	1.470407	0.006700
3330	0.918243	0.534000	2900	1.464171	0.006100
3320	0.923289	0.581000	2890	1.458220	0.005500
3310	0.949446	0.648400	2880	1.452641	0.005200
3300	0.997679	0.708100	2870	1.447369	0.004800
3290	1.059351	0.745800	2860	1.442430	0.004600
3280	1.126900	0.784700	2850	1.437779	0.004400
3270	1.193188	0.791000	2840	1.433382	0.004100
			2830	1.429162	0.004000

Table 8. Continued

ν , cm^{-1}	n	k	ν , cm^{-1}	n	k
2820	1.425162	0.003700	2380	1.337088	0.016300
2810	1.421262	0.003600	2370	1.336432	0.017000
2800	1.417493	0.003400	2360	1.334476	0.017600
2790	1.413929	0.003500	2350	1.332901	0.018500
2780	1.410561	0.003400	2340	1.334124	0.024700
2770	1.407309	0.003400	2330	1.335941	0.019900
2760	1.404161	0.003400	2320	1.333808	0.020800
2750	1.401138	0.003400	2300	1.332000	0.022900
2740	1.398227	0.003500	2280	1.331463	0.025400
2730	1.395428	0.003500	2270	1.331691	0.026500
2720	1.392690	0.003600	2260	1.332078	0.027700
2710	1.390054	0.003700	2250	1.333225	0.028700
2700	1.387485	0.003800	2240	1.334869	0.029300
2690	1.385021	0.004000	2230	1.334890	0.026900
2680	1.382614	0.004100	2220	1.335156	0.029500
2670	1.380229	0.004300	2210	1.336781	0.028800
2660	1.377933	0.004600	2200	1.338218	0.027900
2650	1.375785	0.004900	2190	1.338702	0.026700
2640	1.373726	0.005200	2180	1.339383	0.025400
2630	1.371675	0.005400	2170	1.339360	0.023900
2620	1.369689	0.005800	2160	1.339317	0.022500
2610	1.367795	0.006100	2150	1.338867	0.021100
2600	1.365897	0.006400	2140	1.338334	0.019800
2590	1.364081	0.006900	2130	1.337552	0.018500
2580	1.362408	0.007300	2120	1.336659	0.017400
2570	1.360786	0.007700	2110	1.335645	0.016300
2560	1.359200	0.008100	2100	1.334507	0.015300
2550	1.357682	0.008500	2090	1.333285	0.014500
2540	1.356212	0.008900	2080	1.332030	0.013700
2530	1.354712	0.009200	2070	1.330728	0.013100
2520	1.353225	0.009700	2060	1.329433	0.012500
2510	1.351870	0.010200	2050	1.328135	0.012000
2500	1.350546	0.010600	2040	1.326708	0.011400
2490	1.349232	0.011100	2030	1.325252	0.011100
2480	1.347986	0.011600	2020	1.323820	0.010800
2470	1.346802	0.012100	2010	1.322401	0.010500
2460	1.345654	0.012600	2000	1.320894	0.010300
2450	1.344561	0.013100	1990	1.319382	0.010100
2440	1.343525	0.013600	1980	1.317836	0.010100
2430	1.342482	0.014000	1970	1.316323	0.010000
2420	1.341464	0.014500	1960	1.314788	0.010100
2410	1.340442	0.014900	1950	1.313203	0.010000
2400	1.339381	0.015300	1940	1.311536	0.010200
2390	1.338375	0.015800	1930	1.309825	0.010300

Table 8. Continued

ν , cm^{-1}	n	k	ν , cm^{-1}	n	k
1920	1.308133	0.010700	1480	1.313968	0.057600
1910	1.306454	0.011000	1470	1.314157	0.057000
1900	1.304740	0.011400	1460	1.314370	0.056300
1890	1.302997	0.011900	1450	1.314468	0.055500
1880	1.301249	0.012400	1440	1.314509	0.054800
1870	1.299429	0.013000	1430	1.314613	0.054100
1860	1.297609	0.013700	1420	1.314628	0.053100
1850	1.295724	0.014400	1410	1.314499	0.052200
1840	1.293723	0.015200	1400	1.314267	0.051200
1830	1.291648	0.016200	1390	1.313815	0.050100
1820	1.289535	0.017300	1380	1.313233	0.049300
1810	1.287276	0.018500	1370	1.312756	0.048500
1800	1.284874	0.020000	1360	1.312209	0.047500
1790	1.282393	0.021800	1350	1.311519	0.046500
1780	1.279810	0.023900	1340	1.310667	0.045500
1770	1.277127	0.026500	1330	1.309605	0.044400
1760	1.274396	0.029700	1320	1.308472	0.043700
1750	1.271842	0.033800	1310	1.307295	0.042700
1740	1.270023	0.039000	1300	1.305957	0.041900
1730	1.269382	0.044700	1290	1.304518	0.041100
1720	1.270045	0.050600	1280	1.302933	0.040300
1710	1.272194	0.056300	1270	1.301231	0.039700
1700	1.275672	0.061000	1260	1.299575	0.039200
1690	1.279567	0.064000	1250	1.297841	0.038500
1680	1.283256	0.066200	1240	1.295913	0.037900
1670	1.286764	0.067800	1230	1.293811	0.037300
1660	1.290097	0.068800	1220	1.291615	0.036900
1650	1.293254	0.069500	1210	1.289274	0.036400
1640	1.296238	0.069700	1200	1.286766	0.036100
1630	1.299024	0.069600	1190	1.284191	0.035900
1620	1.301477	0.069100	1180	1.281509	0.035700
1610	1.303584	0.068400	1170	1.278609	0.035500
1600	1.305455	0.067800	1160	1.275559	0.035600
1590	1.307150	0.066800	1150	1.272355	0.035600
1580	1.308511	0.065900	1140	1.268968	0.036000
1570	1.309586	0.064800	1130	1.265607	0.036500
1560	1.310542	0.064100	1120	1.262663	0.037400
1550	1.311339	0.063000	1110	1.259555	0.037100
1540	1.312045	0.062300	1100	1.255958	0.037100
1530	1.312620	0.061300	1090	1.252082	0.037000
1520	1.313024	0.060400	1080	1.247851	0.036400
1510	1.313293	0.059700	1070	1.242776	0.035700
1500	1.313566	0.058900	1060	1.237022	0.035000
1490	1.313757	0.058300	1050	1.230344	0.034100

Table 8. Concluded

ν , cm^{-1}	n	k
1040	1.222458	0.033100
1030	1.212575	0.032000
1020	1.200663	0.032200
1010	1.186653	0.033700
1000	1.170722	0.037400
990	1.152731	0.043900
980	1.133179	0.054200
970	1.113029	0.069900
960	1.093983	0.090900
950	1.077813	0.117900
940	1.067225	0.149900
930	1.062433	0.183200
920	1.063865	0.218100
910	1.070810	0.251700
900	1.081544	0.282300
890	1.095748	0.313900
880	1.112982	0.341400
870	1.132755	0.370300
860	1.159865	0.400000
850	1.195294	0.422700
840	1.229982	0.431800
830	1.260570	0.440300
820	1.290854	0.448400
810	1.323039	0.453100
800	1.357240	0.456400
790	1.391129	0.450700
780	1.422098	0.443600
770	1.453370	0.435400
760	1.485627	0.421000
750	1.513920	0.399300
740	1.536381	0.374600
730	1.554529	0.349600
720	1.566573	0.319300
710	1.570122	0.291300

Table 9. Solid H₂O Optical Properties at 50°K

ν , cm ⁻¹	n	k	ν , cm ⁻¹	n	k
3690	1.143263	0.003200	3260	1.348277	0.681000
3680	1.137381	0.003400	3250	1.406345	0.649100
3670	1.131382	0.003500	3240	1.454282	0.646800
3660	1.125258	0.005800	3230	1.500932	0.613900
3650	1.118988	0.005300	3220	1.535173	0.585900
3640	1.111724	0.007900	3210	1.565710	0.565800
3630	1.104828	0.009300	3200	1.603442	0.542200
3620	1.097253	0.011300	3190	1.632788	0.502800
3610	1.088966	0.013500	3180	1.657826	0.474700
3600	1.080047	0.016400	3170	1.680960	0.438900
3590	1.071092	0.020500	3160	1.700954	0.400900
3580	1.061076	0.023600	3150	1.715378	0.364000
3570	1.051059	0.029800	3140	1.728172	0.323600
3560	1.040224	0.034400	3130	1.733419	0.281200
3550	1.028460	0.041100	3120	1.733412	0.240600
3540	1.016734	0.050100	3110	1.727825	0.202100
3530	1.004903	0.057700	3100	1.718986	0.165500
3520	0.990406	0.067000	3090	1.704177	0.130600
3510	0.975336	0.080500	3080	1.685720	0.101200
3500	0.959652	0.095200	3070	1.664208	0.076900
3490	0.945812	0.116200	3060	1.642421	0.057700
3480	0.931080	0.135100	3050	1.620024	0.043400
3470	0.919053	0.163700	3040	1.599834	0.033700
3460	0.909626	0.192200	3030	1.581429	0.026800
3450	0.903225	0.222900	3020	1.565451	0.021200
3440	0.901790	0.262400	3010	1.550403	0.017300
3430	0.909008	0.296800	3000	1.537456	0.014500
3420	0.922840	0.333700	2990	1.525459	0.012300
3410	0.943271	0.361200	2980	1.514882	0.010500
3400	0.958071	0.378100	2970	1.505000	0.009500
3390	0.972714	0.405700	2960	1.496581	0.008500
3380	0.993057	0.429500	2950	1.488386	0.007400
3370	1.012413	0.442200	2940	1.480971	0.006700
3360	1.026370	0.461500	2930	1.473862	0.006300
3350	1.043202	0.481200	2920	1.467803	0.006000
3340	1.057930	0.498900	2910	1.462011	0.005600
3330	1.074644	0.523700	2900	1.456528	0.004700
3320	1.095129	0.550100	2890	1.451041	0.004700
3310	1.122161	0.575800	2880	1.446337	0.004400
3300	1.150899	0.601700	2870	1.441593	0.004000
3290	1.191788	0.630500	2860	1.437079	0.003800
3280	1.235227	0.648000	2850	1.432898	0.004000
3270	1.285859	0.662200	2840	1.429235	0.003800
			2830	1.425371	0.003400

Table 9. Continued

ν, cm^{-1}	n	k	ν, cm^{-1}	n	k
2820	1.421839	0.003600	2380	1.340424	0.015300
2810	1.418453	0.003300	2370	1.339489	0.016100
2800	1.415221	0.003200	2360	1.337183	0.017100
2790	1.411848	0.003000	2350	1.336445	0.019900
2780	1.408856	0.003200	2340	1.339537	0.025800
2770	1.405881	0.003100	2330	1.341870	0.018900
2760	1.403101	0.003100	2320	1.339042	0.019500
2750	1.400239	0.003200	2300	1.337000	0.021300
2740	1.397683	0.003300	2280	1.335770	0.023500
2730	1.395133	0.003500	2270	1.335724	0.024600
2720	1.392815	0.003600	2260	1.335887	0.025700
2710	1.390660	0.003800	2250	1.336353	0.026800
2700	1.388440	0.003600	2240	1.337124	0.027600
2690	1.386041	0.003500	2230	1.338042	0.028100
2680	1.383746	0.004000	2220	1.339141	0.028400
2670	1.381745	0.004000	2210	1.340300	0.028200
2660	1.379559	0.004200	2200	1.341226	0.027500
2650	1.377626	0.004600	2190	1.342091	0.027000
2640	1.375627	0.004700	2180	1.342756	0.025700
2630	1.373859	0.005200	2170	1.343131	0.024600
2620	1.372064	0.005400	2160	1.343156	0.023200
2610	1.370363	0.005600	2150	1.342965	0.021900
2600	1.368531	0.006100	2140	1.342567	0.020800
2590	1.367170	0.006500	2130	1.342063	0.019400
2580	1.365554	0.006700	2120	1.341248	0.018400
2570	1.364168	0.007000	2110	1.340425	0.017300
2560	1.362525	0.007400	2100	1.339485	0.016500
2550	1.361507	0.007800	2090	1.338519	0.015500
2540	1.359877	0.007900	2080	1.337520	0.014900
2530	1.359150	0.008300	2070	1.336371	0.013800
2520	1.358609	0.008700	2060	1.335173	0.013400
2510	1.355256	0.004300	2050	1.333885	0.012500
2500	1.351934	0.009700	2040	1.332563	0.012100
2490	1.351689	0.010200	2030	1.331085	0.011500
2480	1.351231	0.010600	2020	1.329637	0.011200
2470	1.350015	0.011300	2010	1.328088	0.011000
2460	1.349239	0.011500	2000	1.326751	0.010900
2450	1.348098	0.012100	1990	1.325301	0.010800
2440	1.347195	0.012400	1980	1.323977	0.010700
2430	1.346060	0.012800	1970	1.322635	0.010800
2420	1.345115	0.013400	1960	1.321300	0.010400
2410	1.344019	0.013600	1950	1.319728	0.010500
2400	1.342971	0.014200	1940	1.318054	0.010200
2390	1.341745	0.014500	1930	1.316377	0.010700

Table 9. Continued

ν, cm^{-1}	n	k	ν, cm^{-1}	n	k
1920	1.314852	0.010700	1480	1.321672	0.055500
1910	1.313149	0.010900	1470	1.321925	0.054500
1900	1.311278	0.011100	1460	1.322119	0.054200
1890	1.309524	0.011800	1450	1.322243	0.052600
1880	1.307770	0.012100	1440	1.321887	0.052000
1870	1.306080	0.012900	1430	1.321687	0.051100
1860	1.304264	0.013200	1420	1.321289	0.050200
1850	1.302414	0.014000	1410	1.320889	0.049600
1840	1.300330	0.014500	1400	1.320621	0.048900
1830	1.298281	0.015500	1390	1.320211	0.047900
1820	1.296107	0.016400	1380	1.319399	0.047000
1810	1.293822	0.017300	1370	1.318989	0.046900
1800	1.291042	0.018500	1360	1.318587	0.045700
1790	1.288218	0.020200	1350	1.317960	0.044900
1780	1.285168	0.022300	1340	1.317267	0.044100
1770	1.282116	0.024900	1330	1.316680	0.043000
1760	1.278810	0.028200	1320	1.315317	0.041500
1750	1.275675	0.032500	1310	1.314118	0.041200
1740	1.272910	0.038100	1300	1.312892	0.040100
1730	1.271712	0.045100	1290	1.311696	0.039300
1720	1.272251	0.052300	1280	1.309875	0.038200
1710	1.274676	0.059100	1270	1.308416	0.037900
1700	1.278751	0.065400	1260	1.306591	0.037000
1690	1.283972	0.069400	1250	1.304947	0.036500
1680	1.289240	0.072300	1240	1.303073	0.036200
1670	1.294482	0.073800	1230	1.301760	0.035500
1660	1.299292	0.074300	1220	1.299728	0.034500
1650	1.303713	0.074100	1210	1.297600	0.033400
1640	1.307558	0.073100	1200	1.294621	0.032700
1630	1.310650	0.071600	1190	1.292104	0.032400
1620	1.312876	0.070000	1180	1.289382	0.032200
1610	1.314851	0.068900	1170	1.286675	0.031200
1600	1.316494	0.067300	1160	1.283102	0.031100
1590	1.317956	0.066100	1150	1.280088	0.031100
1580	1.319032	0.064500	1140	1.276212	0.030700
1570	1.319924	0.063200	1130	1.272978	0.031600
1560	1.320367	0.061800	1120	1.269582	0.031800
1550	1.320979	0.060900	1110	1.266716	0.031600
1540	1.321330	0.059600	1100	1.263114	0.031600
1530	1.321432	0.058300	1090	1.259447	0.029800
1520	1.321241	0.057700	1080	1.254172	0.029400
1510	1.321342	0.056900	1070	1.248688	0.027700
1500	1.321131	0.056300	1060	1.241968	0.027800
1490	1.321382	0.056100	1050	1.234997	0.026500

Table 9. Concluded

ν, cm^{-1}	\underline{n}	\underline{k}
1040	1.226898	0.026900
1030	1.218369	0.025900
1020	1.206256	0.024500
1010	1.192717	0.027000
1000	1.177938	0.030500
990	1.162323	0.035200
980	1.142904	0.042400
970	1.124056	0.055500
960	1.103478	0.071300
950	1.082775	0.092000
940	1.066611	0.126900
930	1.061058	0.158700
920	1.057951	0.190700
910	1.059931	0.223600
900	1.066702	0.258200
890	1.077110	0.284900
880	1.082934	0.315500
870	1.096018	0.354700
860	1.128786	0.403600
850	1.180581	0.421700
840	1.216470	0.416100
830	1.225892	0.405300
820	1.246525	0.449800
810	1.282934	0.446500
800	1.313818	0.454700
790	1.342507	0.457500
780	1.373392	0.454800
770	1.401880	0.456600
760	1.438969	0.452900
750	1.472501	0.435800
740	1.499955	0.414400
730	1.519955	0.392700
720	1.537012	0.369300
710	1.545142	0.344300

Table 10. Solid H₂O Optical Properties at 20°K

ν , cm ⁻¹	\underline{n}	\underline{k}	ν , cm ⁻¹	\underline{n}	\underline{k}
3700			3260	1.445524	0.469300
3690	1.190588	0.006400	3250	1.475075	0.457000
3680	1.190177	0.009900	3240	1.500433	0.443700
3670	1.185171	0.006800	3230	1.526854	0.429600
3660	1.180037	0.009600	3220	1.548814	0.408700
3650	1.173204	0.010400	3210	1.568938	0.390800
3640	1.166367	0.010200	3200	1.588236	0.372100
3630	1.156756	0.015800	3190	1.605619	0.346600
3620	1.152049	0.019700	3180	1.619442	0.325900
3610	1.143316	0.022100	3170	1.632847	0.300300
3600	1.136901	0.026500	3160	1.641196	0.273100
3590	1.125950	0.030700	3150	1.647790	0.250000
3580	1.115902	0.034300	3140	1.651583	0.222300
3570	1.105381	0.050000	3130	1.652494	0.198000
3560	1.098465	0.050900	3120	1.649911	0.173200
3550	1.087640	0.068400	3110	1.646282	0.151200
3540	1.078922	0.071400	3100	1.641083	0.130500
3530	1.071096	0.094900	3090	1.634084	0.107900
3520	1.061103	0.095000	3080	1.623124	0.089300
3510	1.055475	0.126200	3070	1.611662	0.073100
3500	1.053755	0.131200	3060	1.598854	0.059100
3490	1.037370	0.137400	3050	1.586082	0.047900
3480	1.020375	0.172700	3040	1.573300	0.039000
3470	1.022036	0.208600	3030	1.561417	0.031600
3460	1.027924	0.230000	3020	1.549432	0.025700
3450	1.039802	0.263800	3010	1.538979	0.022100
3440	1.048080	0.271900	3000	1.528947	0.018200
3430	1.049207	0.296500	2990	1.519987	0.016100
3420	1.060468	0.333700	2980	1.511594	0.014300
3410	1.083809	0.354600	2970	1.504630	0.013000
3400	1.105606	0.372900	2960	1.497887	0.011600
3390	1.124147	0.384700	2950	1.491902	0.010200
3380	1.145546	0.402800	2940	1.485204	0.008800
3370	1.167319	0.412200	2930	1.479823	0.009300
3360	1.182466	0.414700	2920	1.475397	0.009100
3350	1.197687	0.438300	2910	1.471571	0.007700
3340	1.222679	0.448500	2900	1.466825	0.006700
3330	1.250133	0.463400	2890	1.462300	0.005700
3320	1.273315	0.460300	2880	1.457582	0.005700
3310	1.299157	0.478200	2870	1.453947	0.005900
3300	1.325664	0.474300	2860	1.450215	0.005600
3290	1.354794	0.483900	2850	1.447258	0.006000
3280	1.386572	0.483400	2840	1.444230	0.005500
3270	1.418416	0.474100	2830	1.441315	0.005000

Table 10. Continued

ν , cm^{-1}	\underline{n}	\underline{k}	ν , cm^{-1}	\underline{n}	\underline{k}
2820	1.437951	0.004900	2380	1.368821	0.015300
2810	1.435402	0.005000	2370	1.367035	0.016400
2800	1.432456	0.004600	2360	1.363572	0.017900
2790	1.429643	0.004500	2350	1.364046	0.024000
2780	1.426843	0.005200	2340	1.369782	0.028800
2770	1.425043	0.005400	2330	1.372025	0.018800
2760	1.422998	0.005300	2320	1.368997	0.020900
2750	1.420881	0.004700	2310	1.367170	0.019300
2740	1.418056	0.004700	2300	1.365549	0.020700
2730	1.416189	0.005500	2290	1.364449	0.022200
2720	1.414377	0.005400	2280	1.364625	0.023300
2710	1.412514	0.005000	2270	1.363914	0.023300
2700	1.410244	0.005500	2260	1.363711	0.025000
2690	1.408556	0.005400	2250	1.363440	0.025200
2680	1.406878	0.006100	2240	1.363158	0.026200
2670	1.405176	0.005200	2230	1.362990	0.027600
2660	1.402979	0.006100	2220	1.364159	0.028900
2650	1.401584	0.006300	2210	1.365009	0.028800
2640	1.400256	0.006800	2200	1.365545	0.028400
2630	1.398522	0.006000	2190	1.366396	0.029300
2620	1.396480	0.007000	2180	1.366516	0.026900
2610	1.395522	0.007800	2170	1.365780	0.027600
2600	1.394123	0.007200	2160	1.366412	0.028500
2590	1.392723	0.008000	2150	1.367113	0.026700
2580	1.391247	0.008000	2140	1.367064	0.026700
2570	1.390100	0.008400	2130	1.366981	0.025100
2560	1.388571	0.008700	2120	1.365766	0.024200
2550	1.387615	0.009000	2110	1.365665	0.025000
2540	1.386124	0.009300	2100	1.365753	0.023800
2530	1.384924	0.009300	2090	1.364906	0.021700
2520	1.383631	0.010500	2080	1.363424	0.022400
2510	1.382643	0.009900	2070	1.362135	0.020500
2500	1.381103	0.011100	2060	1.361274	0.022500
2490	1.380504	0.011500	2050	1.360849	0.020600
2480	1.379466	0.011700	2040	1.359284	0.020100
2470	1.378310	0.011700	2030	1.357780	0.020700
2460	1.377336	0.012900	2020	1.356629	0.020000
2450	1.376339	0.012200	2000	1.355000	0.020400
2440	1.374769	0.013200	1980	1.351962	0.020200
2430	1.374202	0.014300	1970	1.350215	0.019600
2420	1.373104	0.013800	1960	1.348718	0.021000
2410	1.372200	0.015200	1950	1.347521	0.020800
2400	1.371427	0.015400	1940	1.346055	0.021500
2390	1.370839	0.015500	1930	1.344631	0.021800

Table 10. Continued

ν, cm^{-1}	n	k	ν, cm^{-1}	n	k
1920	1.343626	0.023000	1480	1.362398	0.066400
1910	1.341669	0.021900	1470	1.363023	0.076100
1900	1.340410	0.024800	1460	1.364225	0.072100
1890	1.339537	0.024200	1450	1.363598	0.068700
1880	1.337630	0.024200	1440	1.361686	0.077900
1870	1.335564	0.026300	1430	1.365501	0.071400
1860	1.334812	0.026900	1420	1.366666	0.080700
1850	1.333554	0.027800	1410	1.369901	0.070000
1840	1.331019	0.026900	1400	1.373324	0.080800
1830	1.329224	0.030500	1390	1.374442	0.063200
1820	1.327150	0.029800	1380	1.372282	0.072200
1810	1.324362	0.032000	1370	1.373345	0.066400
1800	1.323347	0.036400	1360	1.377148	0.068800
1790	1.322659	0.035100	1350	1.374372	0.058300
1780	1.318107	0.036300	1340	1.371176	0.061700
1770	1.315792	0.042000	1330	1.372769	0.065700
1760	1.315362	0.044700	1320	1.378791	0.060500
1750	1.311973	0.044100	1310	1.373384	0.051000
1740	1.306363	0.050600	1300	1.368617	0.055400
1730	1.305537	0.059800	1290	1.375149	0.064300
1720	1.305664	0.064600	1280	1.378045	0.045800
1710	1.304670	0.071300	1270	1.374179	0.047300
1700	1.307241	0.083900	1260	1.370600	0.042400
1690	1.315281	0.090900	1250	1.363474	0.035300
1680	1.324041	0.095200	1240	1.362759	0.051000
1670	1.332614	0.096100	1230	1.369774	0.038500
1660	1.338569	0.094200	1220	1.358424	0.025900
1650	1.342940	0.093700	1210	1.349902	0.035800
1640	1.349717	0.095000	1200	1.356225	0.044100
1630	1.354563	0.087800	1190	1.347786	0.014000
1620	1.353709	0.083100	1180	1.332293	0.036600
1610	1.354490	0.086700	1170	1.332901	0.041000
1600	1.356790	0.082700	1160	1.338570	0.044100
1590	1.359682	0.084000	1150	1.336647	0.038000
1580	1.360242	0.078600	1140	1.335012	0.038700
1570	1.360148	0.077800	1130	1.333158	0.038200
1560	1.359483	0.078400	1120	1.329720	0.031300
1550	1.359352	0.075400	1110	1.321090	0.032000
1540	1.359894	0.080800	1100	1.318805	0.037200
1530	1.363800	0.077800	1090	1.316825	0.033000
1520	1.363253	0.074900	1080	1.308353	0.028900
1510	1.363473	0.076500	1070	1.304622	0.037600
1500	1.365772	0.076300	1060	1.301123	0.031600
1490	1.368140	0.072600	1050	1.293653	0.027700

Table 10. Concluded

$\nu, \text{ cm}^{-1}$	\underline{n}	\underline{k}
1040	1.285554	0.035300
1030	1.274993	0.021500
1020	1.264823	0.042300
1010	1.258458	0.029100
1000	1.249005	0.041300
990	1.224899	0.023600
980	1.209704	0.059200
970	1.199161	0.060000
960	1.183929	0.068400
950	1.168755	0.100200
940	1.166223	0.109500
930	1.154340	0.130200
920	1.149868	0.152700
910	1.141908	0.170200
900	1.137685	0.198600
890	1.132458	0.223400
880	1.131016	0.256300
870	1.132482	0.297700
860	1.161455	0.349900
850	1.206045	0.375800
840	1.239501	0.366000
830	1.253306	0.377100
820	1.273714	0.389000
810	1.293143	0.396000
800	1.315654	0.407500
790	1.334696	0.410700
780	1.352420	0.418900
770	1.375062	0.437700
760	1.417817	0.449600
750	1.454988	0.434300
740	1.477747	0.412800
730	1.497449	0.414900
720	1.516547	0.388100
710	1.529164	0.387400